FACULTY OF SCIENCE
PALACKÝ UNIVERSITY IN OLOMOUC

Department of Experimental Physics

Master Thesis

Magnetic anisotropy of transition metal dimers supported by defective graphene

Author	Bc. Diana Václavková
Supervisor	doc. Mgr. Jiří Tuček, Ph.D.
Co-Supervisor	Mgr. Piotr Błoński, Ph.D.
Degree program	N1701 Physics
Field of study	Nanotechnology
Year	2018

Bibliographical identification

Author's first name and surname	Bc. Diana Václavková
Title	Magnetic anisotropy of transition metal dimers supported by defective graphene
Type of thesis	Master
Department	Department of Experimental Physics
Supervisor	Assoc. Prof., MSc. Jiří Tuček, Ph.D.
Year of presentation	2018
Number of pages	74
Number of appendices	0
Language	English
Abstract	The increasing requirements for higher speed, greater efficiency and increased data storage in electronic devices has spurred the interest in new structures with possible tailored magnetic properties. The most alluring structures are those with possible control of magnetism on the atomic scale. Such systems could later be used as the magnetic data storage devices where a bit with information would be stored in magnetic stable domains, if high magnetic anisotropy energy is present. This thesis focuses on the magnetic properties of transition metal dimer, consisted of iridum and cobalt atom, adsorbed on the single vacancy and nitrogen doped single vacancy graphene layer and their possible future applications in spintronics.
Keywords	Magnetic anisotropy, vacancies, doping, graphene, transition metals, spintronics

Bibliografická identifikace

Jméno a příjmení autora	Bc. Diana Václavková
Název práce	Magnetická anizotropie dimerů sestávajících se z přechodových kovů usazených do defektního grafenu
Typ práce	Diplomová
Pracoviště	Katedra experimentální fyziky
Vedoucí práce	doc. Mgr. Jiří Tuček, Ph.D.
Rok obhajoby práce	2018
Počet stran	74
Počet příloh	0
Jazyk	Anglický
Abstrakt	Neustálý nárůst požadavků pro ukládání a úschovu dat způsobil zájem o struktury s na míru připravenými magnetickými vlastnostmi. Nejvíce jsou žádané systémy, ve kterých je možno kontrolovat magnetické vlastnosti v atomovém měřítku. Struktury vykazující takovéto chování, by mohly být použity jako nová magnetická úložiště dat, kde bit informace je uložen v magneticky stabilních doménách.Další požadovaná vlastnost těchto struktur je vysoká magnetická anizotropní energie. Tento druh energie je zodpovědný nejen za stabilitu magnetického systému, ale zabraňuje také i možným ztrátám informace. Tato práce se soustředí na zkoumání magnetických vlastností systému, který se skládá z dimeru tvořeného z Ir a Co atomů, adsorbovaného na čistý a dopovaný grafén s jednou vakancí.
Klíčová slova	Magnetická anizotropie, vakance, dopování, grafen, přechodné kovy, spintronika

Declaration

I hereby state, that I have written this thesis myself under the supervision of Mgr. Piotr Błoński, Ph.D. and doc. Jiří Tuček, Ph.D. All used resources are listed under the section Bibliography.

In Olomouc, date .....

.....
Signature

I would first and foremost thank my co-supervisor Mgr. Piotr Błoński, Ph.D., for his invaluable guidance, enormous amount of patience and support throughout this thesis.

Further, I would like to thank my supervisor doc. Mgr. Jiří Tuček, Ph.D., whom I am very grateful for his insights and kind words. This thesis would not have been created without his help, support and the ability to push a project in the right direction.

I would also like to thank my friends and family for all their moral support and patience, especially David Harris for the help at the start of my thesis and Anders Dencker for his valuable language assistance.

Finally, I would like to thank the Internal Grant Agency of the Palacký University in Olomouc Project No. IGA_PrF_2018_021 the support is gratefully acknowledged.

Contents

Introduction

It is difficult to deny that scientific research is often seen as a bridge between satisfying a natural curiosity about the world and developing new technologies based on currently established knowledge. One of the fields that has particularly benefited from this connection is condensed matter physics, where countless number of naturally existing and human-fabricated specimen exist, which display a variety of fascinating phenomena. The motivation to investigate the properties of different materials and structures is constantly stimulated by novel findings in new and sometimes old, seemingly perfectly understood, systems.

At present, research efforts cover extremely broad range of topics, but the actual electronic devices are still relaying on silicon technology. It is a greatly appealing prospect to find alternative materials that would satistfy the increasing growth of requirements for higher speed, greater efficiency and larger data storage capabilities. Silicon substrates are no longer attractive, mainly due to low mobility of charge carriers and their poor compatibility with the elements of the 3d and 5d groups in integrated circuits. Another problem is the expensive fabrication of devices using silicon elements. [1] The rise in modern magnetic technologies has spurred intense research efforts aimed at improving our knowledge, especially about magnetic materials. Structures with tailored magnetic properties have attracted considerable attention because of the potential application in spintronics and high-density magnetic or magneto-optical data storage devices. [2]

Particularly, the control of magnetism at the atomic scale became desirable due to prospects of miniaturization of storage devices. [3, 4] The key parameter, relevant for the usability of magnetic systems as switchable magnets, is magnetic anisotropy energy (MAE).[5] Large value of MAE, characterizing an energetically stable structure, enables manipulation of the magnetic moment by an external electric field in ambient conditions. Such functionality is crucial for practical aspects of spintronics and quantum computation[6]. For room temperature operation, it is also essential to consider thermal fluctuations, which cannot overcome the strength of magnetic coupling.

Many commonly investigated nanostructures display MAE in the order of few meV, which is significantly smaller than thermal energy at room temperature (k_BT ≈ 30 meV for T = 296 K). [7] Therefore, it is important to achieve deep understanding of the mechanisms of magnetic coupling in small magnetic systems. Such knowledge could allow conscious tailoring of magnetic properties in small scale, and eventually lead to proposals and realisations of magnetic systems with sufficiently high MAE. From general wisdom, it is quite clear that strong magnetic anisotropy may be expected from atoms characterized by large value of spin and/or orbital momentum, especially in the presence of robust spin-orbit coupling.

One can imagine multiple candidates for systems exhibiting large value of MAE. Especially appealing are magnetic nanostructures, where the reduction of dimensionality introduces confinement effects, which often lead to enhancement of magnetic interactions. Another aspect of this problem is related to the flexibility of the choice of the atoms forming the magnetic system, which enables optimization of the magnetic properties to a considerable degree. From this point of view, transition metal (TM) clusters provide a solid platform suitable for testing of theoretical ideas, aiming to increase the value of MAE. [8] It is important to emphasize, that even the simplest forms of TM clusters may exhibit various magnetic properties. Some of them show large MAE value of 40-70 meV. [9] Other may exhibit even non-magnetic ground state. Given the diversity of possible magnetic configurations appearing in TM dimers, it is important to develop understanding of the factors that eventually determine value of MAE.

In simple terms, large magnetic moment is displayed by the 3d transition metal atoms, which often strongly interact through ferromagnetic coupling. However, these elements typically lack the strong spin-orbit coupling. Further on in the periodic table, the 4d and 5d elements reside, which, in their bulk form, are often found in non-magnetic configurations.[10] Nevertheless, reduction of dimensionality, realised for instance by formation of small mers based on 4d and 5d elements (such as dimers) often induces large intrinsic spin-orbit effects. For these reasons, it is far from obvious which TM clusters could be best candidates for large MAE systems. In such case, it is a good practice to turn to experimental data for guidance. Recent investigations of hybrid TM clusters, combining 3d elements with 4d or 5d elements, demonstrated exceptionally robust magnetic anisotropy. In this thesis, following the reasoning presented so far, IrCo dimers have been chosen as a test subject for first-principle calculations of the magnetic ground state. Cobalt and iridium are representatives of elements with partially filled 3d and 5d shells, respectively. Therefore, the undertaken study develops deeper understanding of fundamental mechanisms relevant for appearance of different magnetic configurations in TM clusters, providing at the same time a detailed characterization of a particular system, which can easily be

realised experimentally.[11, 12]

From practical point, it is important to take into account the impact of the substrate on the magnetic state of the considered IrCo dimer. Not only is the substrate coupling a factor that may influence the magnetic state of the dimer, but also is an inseparable aspect in many realistic systems, due to constraints imposed by the procedures of sample fabrication. In this regard, the basic question is whether the support will alter the magnetic state of the dimer and if, perhaps, induced changes could be beneficial for achieving higher magnetic anisotropy. Many types of substrates have been considered so far, including metallic materials (e. g. nickel or copper) and metal oxide layers. [13] High MAE in the system is not the only important parameter in order to obtain stable nanomagnetic structures. Another physical properties, such as the quantum number of the ground state and crystal field symmetry play an important role in the dynamics of magnetization, especially the magnetic lifetime.

Here, the case of IrCo dimer located over a single vacancy in graphene is investigated. Since the isolation of single carbon layers and demonstrating their remarkable electronic and mechanical properties, the possibility of marrying graphene with magnetism has been an intensely explored research topic, including both experimental and theoretical approaches. Many cases have been considered, such as edge magnetism or emergence of flat bands and therefore strong many-body interactions in ABC stacked graphite layers. Despite these efforts, magnetism in graphene is still an elusive phenomenon. Given the results obtained here for IrCo dimer supported by defective graphene, the inspection of such structures may be appealing for further discussion about inducing magnetic effects in thin graphite layers.

The Vienna $ab\ initio$ calculations, based of spin-polarized density function theory (DFT) implemented in Vienna simulation package, demonstrate the IrCo dimer can be effectively adsorbed onto the vacancy in graphene. The interplay between sp^2 hybridization of carbon atoms with spd hybridization in metallic atoms may have multiple consequences on the magnetic properties of the dimer. The calculations show that, independently on the initial position of the dimer, the IrCo complex becomes bonded onto the centre of the graphene vacancy. The strong binding of the 3d (cobalt) atom to the substrate stabilizes an out-of-plane alignment of the dimer, which is very important for achieving a high magnetic anisotropy. Due to the coupling with carbon atoms, spin and orbital momentum of the 3d (cobalt) atom are strongly quenched, but simultaneously weakening its binding with the 5d (iridium) atom. Consequently, iridium recovers its atomic character, which is characterized by larger spin and orbital anisotropy than would be displayed in the decoupled dimer configuration. The main conclusion of the presented study is that the IrCo dimer bonded onto a graphene vacancy maintains a large value of MAE and offers promise for obtaining graphene-based structures exhibiting stable magnetization.

1. Theoretical part

1.1. Theoretical background

The desire to describe the electronic structure of atoms, molecules and solids, have always been one of the main aspects of solid states physics and quantum chemistry. Unfortunately, the knowledge of the electronic configuration for new structures is not easy to obtain. The two main important properties of electrons in solids are particle/wave-like behaviour and the many-body interactions that are showing quantum mechanical correlations. Different theories and approximations have been developed in order to describe the state of electrons in atoms, molecules and solids which would give us a comprehensive understanding of the mechanisms behind. [14, 15] A concise overview of the historical advancement in understanding of quantum mechanical description of electrons, particularly electrons in solids, is given in this chapter.

1.1.1. Electronic structure

One of the first breakthroughs in the developement of the currently well-established concept of an electron happened in 1926, when the Austrian physicist Erwin Schrödinger described the hypothetical plane waves by the use of de Broglie relations. [16] The outcome of his work led to one of the most famous equations in physics, that has been given name after its discoverer, the time-dependent Schrödinger equation :

$$\mathrm{i}\hbar\frac{\partial}{\partial t}\psi(\vec{r},t) = \hat{H}\psi(\vec{r},t) \tag{1}$$

Since its proposal, the validity of Schrödinger's equation has been intensely debated in scientific community. Even though the time-dependent Schrödinger equation constitutes a foundation of modern quantum physics, in most cases its use is impractical because of the relativistic formulation that it contains. Schrödinger himself later postulated the non-relativistic approximation for more accessible usage. In this new form the equation is being used frequently to this day in quantum chemistry and theoretical calculations due its computational power.

The wave function $\Psi(\vec{r},t)$ in equation 1 describes the state of the particle in momentum space and the Hamiltonian, $\hat{H}$, describes the kinetic and potential energy of the particle. When the Hamiltonian for a single particle is considered in form:

$$\hat{H} = \hat{T} + \hat{V} = -\frac{\hbar}{2m}\vec{\nabla}^2 + V(\vec{r},t) \tag{2}$$

then, the equation 1 can be used and the non-relativistic time-dependent single particle Schrödinger equation will take a form:

$$\mathrm{i}\hbar\frac{\partial}{\partial t}\psi(\vec{r},t) = \left[-\frac{\hbar}{2m}\vec{\nabla}^2 + V(\vec{r},t)\right]\psi(\vec{r},t). \tag{3}$$

The Hamiltonian can be written in $N-$dimensions, as followed:

$$\hat{H} = \sum_{i=1}^{N}\frac{\hat{p_i}^2}{2m_i} + V(\vec{r}_1,\vec{r}_2,...,\vec{r}_N,t) = -\frac{\hbar^2}{2}\sum_{i=1}^{N}\frac{1}{m_i} + V(\vec{r}_1,\vec{r}_2,...,\vec{r}_N,t). \tag{4}$$

The corresponding Schrödinger equation then reads:

$$\mathrm{i}\hbar\frac{\partial}{\partial t}\psi(\vec{r}_1,\vec{r}_2,...,\vec{r}_N,t) = \left[-\frac{\hbar}{2}\sum_{i=1}^{N}\frac{1}{m_i}\nabla_i^2 + V(\vec{r_1},\vec{r_2},...,\vec{r_N},t)\right]\psi(\vec{r}_1,\vec{r}_2,...,\vec{r}_N,t). \tag{5}$$

Unfortunately, the equation 5 does not always have a simple solution. It is possible, in certain cases, to separate the formula into two parts, making it easier to solve. Treating the equation in such a way will lead to the time-independent Hamiltonian. The solution for such approach describes standing waves that represent the stationary states in the system (so called orbitals). The time independent Schrödinger equation can not only simplify the solution but can also be helpful in solving the corresponding time dependent equation.

A useful method for obtaining the desired time independent Schrödinger equation is the mathematical method of variable separation. By applying this approach to the many-body Hamiltonian, the Schrödinger equation will take the form:

$$E\psi(\vec{r}_1,\vec{r}_2,...,\vec{r}_N)=\left[-\frac{\hbar}{2}\sum_{i=1}^{N}\frac{1}{m_i}\nabla_i^2+V(\vec{r_1},\vec{r_2},...,\vec{r_i},\vec{r_j},...\vec{r_N})\right]\psi(\vec{r}_1,\vec{r}_2,...,\vec{r}_N). \tag{6}$$

The main postulate of quantum mechanics then states that the state of a particle is fully described by its time dependent wave function. The next step in fully describing the electron structure is understanding of the Copenhagen interpretation of quantum physics. [17] This approach provides that the physical interpretation of the squared wave function as the probability density, which can be written as:

$$|\psi(\vec{r}_1,\vec{r}_2,...,\vec{r}_N|^2 d\vec{r}_1 d\vec{r}_2...d\vec{r}_N \tag{7}$$

Looking at the equation 6, one has to notice that the exchange in-between two particles in their positions should be considered. It is obvious that in the case of total probability density the outcome does not depend on the position exchange, which can be represented by the following equation:

$$\psi(\vec{r_1},\vec{r_2},...,\vec{r_i},\vec{r_j},...\vec{r_N})=\psi(\vec{r_1},\vec{r_2},...,\vec{r_i},\vec{r_j},...\vec{r_N}). \tag{8}$$

Another thing that has to be recognized when calculating the electronic structure for the case of position exchange is that two possible schemes can happen, depending on the particle properties. The first possible scenario can be described by the symmetrical wave function, where there will not be any observable changes. Such a way corresponds to bosons (particles with integer or zero spin). The second possible scheme is that due the position exchange, there will be change of the sign in front of the wave function, which is usual for the case of fermions (particles with half integer spin). Such wave function follows the Pauli exclusion principle, stating that in an atom or molecule, no two electrons can have the same four electronic quantum numbers, noted with n, l, m, s. The first number, n, describes the electron energy level of an electron and is called the principal quantum number. The second is called azimuthal quantum number l, or aslo known as the orbital quantum number. The number representing the specific orbital is the magnetic quantum number m. Last is the spin projection quantum number, giving the spin value of the electron within the orbital, noted with s.[18]

- **Born - Oppenheimer approximation**

  Except of position exchange, many other possible processes that can happen in the systems have to be considered. Important thing that has to be taken in account is also the environment which is surrounding the space described by the Schrödinger equation and corresponds to the wave function. All atom and molecule systems deal with charge particles that are present in the space surrounding given system .That is why it is necessary to consider such forces when calculating properties of given structures.[19] By looking at Schrödinger equation for single electron in Coulomb potential field, the equation then can be written in a form of:

$$i\hbar\frac{\partial}{\partial t}\psi(\vec{r})=\left[-\frac{\hbar^2}{2m}\vec{\nabla}^2-\frac{e^2}{4\pi\epsilon_0}\cdot\frac{1}{|\vec{r}|}\right]\psi(\vec{r}). \tag{9}$$

  Using the equation 6, general Schrödinger equation for many-body system consisted of N electrons can be acquired.

$$E_i\psi_i(\vec{r}_1,\vec{r}_2,...\vec{r}_N,\vec{R}_1,\vec{R}_2,...\vec{R}_N)=\hat{H}\psi(\vec{r}_1,\vec{r}_2,...\vec{r}_N,\vec{R}_1,\vec{R}_2,...\vec{R}_N) \tag{10}$$

  Equation 10 describes a system that has N electrons and M cores. This equation is however, valid only when one neglets the external magnetic and electric fields and their possible effects on the structure. At first glance, it can be seen how challenging the finding of the solution for the described system might be [20].

  That is why physicists have been trying to come up with new ways on simplifying the equation and finding easier solution. The first approximation allowing such smoother computation is the Born-Oppenheimer approximation. For its simplicity and computational power, it has been widely used in past years. This approach still plays a key role in electron structure calculations [21].

  The Born-Oppenheimer approximation is based on the fact that the mass of the nucleus is 10^3 times larger than the mass of electrons. Even if a light nucleus is considered, the mass of proton

is still 3000 times greater than the mass of an electron. By this knowledge it can be assumed that electrons are moving particles in the field created by stationary nucleus. Such a creative thought allowed the possible separation of the movement of electrons and nuclei [22, 23].

This simplified approach allows the negligence of certain members of the Hamiltonian which eventually means that the description of nuclei system can be neglected as well. The part of the equation, describing the repel of nuclei, is considered as constant for a given structure. This leaves only the electron Hamiltonian to be calculated. The solution gives the electron wave function, describing the dynamics of electrons. The most important thing to note is that the movement of electrons is strongly dependent only on the spatial coordination of electrons, which can be expressed by:

$$\hat{H} = -\frac{1}{2}\sum_{i=1}^{N}\nabla_i^2 - \sum_{i=1}^{N}\sum_{k=1}^{M}\frac{Z_k}{r_i k} + \sum_{i=1}^{N}\sum_{j>1}^{N}\frac{1}{r_i j}. \tag{11}$$

It is essential to realise that this approximation fails for systems where the multiple of the potential surface energy are close to each other in energy or crossing each other. The dissociative adsorption of molecules on metal surfaces is another example of when this approximation breaks down. The reason behind the failing in the mentioned systems can be found in the part of the equation describing the electron - electron interactions. This term involves the quantum effects that are connected to electrons and their quantum behaviour that can be expressed as:

$$\frac{1}{2}\sum_{i\neq j}\frac{e^2}{|r_i - r_j|}. \tag{12}$$

Electrons belong to the group of fermions, and so they have to follow the Pauli repulsion principle. The Pauli principle demands the electron wave function to be anti-symmetrical with respect to the position exchange of any two electrons. It can be written in the form of:

$$\Phi(x_1, ..., x_i, ..., x_j, ..., x_N) = -\Phi(x_1, ..., x_i, ..., x_j, ..., x_N). \tag{13}$$

To meet such requirements the Slater determinants are used as main computational tool. They meet up with the conditions through an approximate linear combination of Hartree products, which are the non-interacting electron wave functions. Slater determinants will take a form:

$$\psi_0 \approx \phi_{SD} = (N!)^{-\frac{1}{2}} \begin{vmatrix} \chi_1(\vec{x}_1) & \chi_2(\vec{x}_1) & \dots & \chi_N(\vec{x}_1) \\ \chi_1(\vec{x}_2) & \chi_2(\vec{x}_2) & \dots & \chi_N(\vec{x}_2) \\ \vdots & \vdots & \ddots & \vdots \\ \chi_1(\vec{x}_N) & \chi_2(\vec{x}_N) & \dots & \chi_N(\vec{x}_N) \end{vmatrix} \tag{14}$$

where the lines correspond to the electrons and columns give the information about orbital spin.

- **Hartree-Fock formalism**

  The next step in solving the Schrödinger equation occurred with the concept of determining the correlation energy. It is undermined by the rule that the many-body wave function needs to contain $3N$ variables. It is known that solids are made out of approximately $N \cdot 10^{23}$ electrons and that is why the solution in this way was practically impossible.

  Hartree-Fock approximation was the next step in searching for a better solution. The Hartree-Fock method gives much more precise results and is most of the time used as a main computational tool in modern quantum chemistry. Another useful property of this approximation is its usage for materials that have defects in their lattice or for scenarios with adsorption on surface. The electron structure of isolators can also be studied thanks to this new approach.

  This method uses Slater determinant for the approximation of wave function for the ground state of N electrons. Such an approach guarantees the electron description that is following the Pauli principle[24]. The next step is then to find the best possible approximation of the wave function, that would lead to the final Hartree-Fock energy, given by:

$$E_{HF} = \langle\psi_0|\hat{H}|\psi_0\rangle = \sum_a \int \chi_a^*(1)(-\frac{1}{2}\nabla^2 - \frac{Z_A}{r_{iA}})\chi_a(1)dx_1 \tag{15}$$

$$+\frac{1}{2}\sum_{ab} \int \chi_a^*(1)\chi_a(1)r_{12}^{-1}\chi_b^*(2)\chi_b(2)dx_1dx_2 \tag{16}$$

$$-\frac{1}{2}\sum_{ab} \int \chi_a^*(1)\chi_b(1)r_{12}^{-1}\chi_b^*(2)\chi_a(2)dx_1dx_2. \tag{17}$$

The first of the terms, given by the equation 15, describes the kinetic and potential energy for the attraction to the nuclei of a single electron. The other two terms, 16 and 17, characterize purely electron presence. The first one (equation 16) expresses the Coulomb term and the latter (equation 17) defines the exchange term which arises from the antisymmetric nature of the Slater determinant.

After few simplifying steps, the Hartree-Fock equation can be re-written into its more known form:

$$f|\chi_a\rangle = E_a|\chi_a\rangle \tag{18}$$

The main problem in the Hartree-Fock method is that it completely neglects correlations between electrons with same spin. The further progress in theoretical calculations was made with newly proposed way how to get the energy of the system, the density functional theory. [25, 26].

1.1.2. Density functional theory (DFT)

The previous chapter shows how to solve the Schrödinger equation by using different approximations. All mentioned ways so far have one thing in common. The fundamental property they share is the wave function which represents the many-body electron system. As soon as the wave function is known, the energy of the system and other properties can be calculated. This approach works well for smaller systems, unfortunately even these computations are still very complex and also time demanding. Every one of the discussed approximations until now fails when a structure that consists of more than 100 atoms is investigated.

Density functional theory differs from aforementioned methods because instead of using wave function it uses electron density as a central variable. The advantage lies in the reduction of dimensions of the given problem. In the case of Hartree-Fock method, the solution is strongly dependant on $3N$ spatial variables. In the case of DFT, the density is always only 3 dimensional. Thanks to this property, density functional theory can be applied on much larger and more complex systems of atoms [27, 28].

- **Thomas Fermi model**

  The first people who considered the idea of the energy being explained by electron density were Thomas and Fermi in early 1920's. Their model was based on the assumption that the kinetic energy of electrons is derivative from the quantum statistical theory which foundations are based on the uniform electron gas [29, 30].

  The problem being overlooked in this theory is the approach to the electron-nuclei and electron-electron interactions. In this model, both of the interplays are taken only from the point of classical physics. This causes the Thomas-Fermi Model to break down when trying to describe shell core structures. It also cannot explain the existence of molecules. Nonetheless, this model is very important in the development of theoretical calculations because of the significant insight, that the energy can be calculated only from electron density [31].

  The concept was further explained in the years 1964 and 1965. In these years two main papers that established the foundations for the density functional theory known today were published. The physicists Hohenberg, Kohn and Sham have shown that the ground energy state is the functional of the density ground state and that both of these cases can be found by the minimisation of the energy with the respect to density, that is if the functional is known [32].

In the second paper they published a possible way of assembling the density from non-interacting orbitals - the so called Kohn-Sham wave function, which led to the foundations of the new density functional theory - that are Kohn-Sham equations [33].

- **Hohenberg-Kohn theorems and Kohn-Sham equations**

  Hohenberg-Kohn formalism is based on two main theorems:

  1. Theorem: For any system of interacting particles in an external potential $v_{ext}(r)$, the potential can uniquely be determined except for a constant, by the ground state particle density $n_0(r)$.

  2. Theorem: A universal functional for the energy $E(n)$ in the terms of the density $n(r)$ can be denoted, valid for any external potential $v_{ext}(r)$. For any particular $v_{ext}(r)$, the exact ground state energy of the system is the global minimum value of this functional, and the density $n(r)$ that minimizes the functional is the exact ground state density $n_0(r)$.

  These theorems are the mathematical proof that the energy ground state is functional of electron density. Kohn-Sham equations and theorems, allowing to simplify DFT calculations, are based on the theorem that defines the process of calculations.

  3. Theorem: For each interacting system A with energy functional, there exists a non-interacting system B, described by the Hamiltonian:

$$\hat{H} = \hat{T}_B + \hat{V}_B \tag{19}$$

  with an appropriate V_B, which yields the same ground state density

$$n(\vec{r}) = n_B(\vec{r}). \tag{20}$$

  Following the Hohenberg-Kohn theorems the energy is then defined as:

$$E(n) = T_s(n) + \int v_{ext}(\vec{r}) n(\vec{r}) d\vec{r} + \frac{1}{2} \int \frac{n(\vec{r}) n(\vec{r'})}{|\vec{r} - \vec{r'}|} d\vec{r} d\vec{r'} + E_{xc}(n). \tag{21}$$

  First part in the equation 21 is the kinetic energy, second expression is the energy from the external potential. Third formula represent classical electrostatic energy (Hartree energy) of an electron. The last part is the already mentioned exchange correlation energy which contains all the many-body effects in the system. Using the variational principle for minimizing the functional energy with the respect to one particle (normalization process), the following Kohn-Sham equation is obtained:

$$\left\{ -\frac{\hbar}{2m} \nabla^2 + v_{ext}(\vec{r}) + v_H(\vec{r}) + v_{xc}(\vec{r}) \right\} \psi_i(\vec{r}) = \epsilon_i \psi_i(\vec{r}) \tag{22}$$

  where the exchange-correlation potential v_{xc} is derivative functional from the exchange-correlation potential:

$$v_{xc}(\vec{r}) = \frac{\delta E_{xc}\left[n(\vec{r})\right]}{\delta n(\vec{r})}. \tag{23}$$

  The energy ground state is then given:

$$E = \sum_i^N \epsilon_i + E_{xc}\left[n(\vec{r})\right] - \int v_{xc}(\vec{r}) n(\vec{r}) d\vec{r} - V_H - V_{nucl-nucl}. \tag{24}$$

  It is important to know that in order to use Kohn-Sham equations, the correct value for E_{xc} functional has to be known. The exact form of this energy is has not been established. For this

reason, different approaches are considered in order to get the best possible approximation for the exchange energy.

The Figure 1 shows all the functionals, from Hartree approximation to the exchange -correlation functional, that are the best to explain the exchange energy.

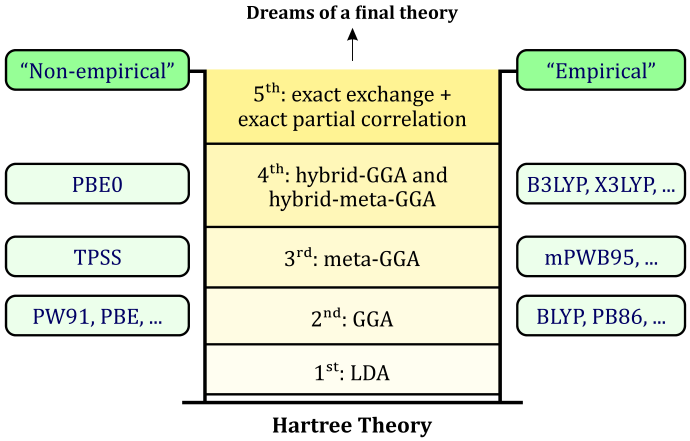

Figure 1 | Scheme of "Jacob's ladder" of exchange-correlation functionals proposed by J. P. Perwed. Reprinted with permission from [44].

1.1.3. Exchange-Correlation Approximations

The quality and efficiency of Kohn-Sham equations depends mainly on the choice of the functional exchange correlation energy form.

The approximation is the simplest way how to guess unknown distribution of the exchange-correlation energy in Kohn-Sham equation. The main principle lies in the assumption that the energy E_{xc} can be locally approximated by the summation of exchange energy E_x and the correlation energy E_c of the electrons in space of same density.

- **Local density approximation (LDA)**

  Local density approximation is the method for calculating the exchange energy E_x. It takes in account the electronic distribution of an infinite number of electrons, that are moving in an infinite volume in space. This space is defined by the uniform distribution of a positive charge. Such system is well known and is called the uniform electron gas. In the case of molecules, the exchange functional is same in every point of the space just like it would be in the case of free electron gas of the same density in the same position [34, 35]. The energy of LDA functional is then given by:

$$E_{xc}^{LDA}[\rho] = \int \rho(\vec{r})\epsilon_{xc}[\rho(\vec{r})]d\vec{r}. \tag{25}$$

  The ϵ_{xc} is the exchange correlation energy per electron in a uniform electron gas. For this case the exchange correlation energy is split into a separate parts that are the exchange and correlation energies. The exchange energy for uniform gas was derived by Dirac and takes the form of:

$$E_x^{LDA}[\rho] = -\frac{3}{4}\left(\frac{3}{\pi}\right)^{\frac{1}{3}} \int \rho^{\frac{4}{3}}(\vec{r})d\vec{r}. \tag{26}$$

  The local spin density approximation ($LSDA$) is another extension for the LDA calculations for systems, that involve spin polarization or the so call open-shell systems [36, 37].

  LDA is a method relying only on the density in the particular point. With this approach, the outcomes that are expected to be in a good agreement with real systems are good vibration

frequencies, the equilibrium of calculated structures and also suitable dipole moments. Theoretically, LDA is valid only in systems where the electron density varies slowly. However, in real life the LDA calculations have shown to provide exact solutions even for highly inhomogeneous systems [32].

Numerous other methods have been developed in order to achieve better results for the value of the exchange correlation energy. Another main group of these approximations is based on the use of the density gradient as the main foundation for the calculations - so called non local or generalised gradient approximations [38, 39].

- **Generalised gradient approximation (GGA)**

  The main difference between the GGA and LDA is that the energy functional correlation energy depends on the density, defined as $\delta\rho(\vec{r})$ in addition to the density defined by the equation:

$$E_{xc}^{GGA}[\rho] = \int F_{xc}(\rho, \delta\rho)d\vec{r}. \tag{27}$$

  The F_{xc} varies for different functionals. Similarly like in the case of LDA, the exchange correlation energy is split into two separate parts, the correlation and exchange energy [40, 41].

- **Hybrid functional methods**

  There also exist the hybrid methods that cover all the truly non-local effects. These mechanisms are based on the adiabatic connection method (ACM)[42]. They all are based on the equation that is expressing the exchange correlation energy:

$$E_{xc} = \int_0^1 \langle\phi(\lambda)|V_{xx}|\phi(\lambda)\rangle d(\lambda) \tag{28}$$

  where λ is the extent of inter electronic interactions ranging from 0 (none) to 1 (exact).

  The homogeneous electron gas is a system of N electrons in the volume V with homogeneous positive background charge. This keeps the system neutral. If we consider taking N as the limit where: $N \to \infty$ and $V \to \infty$ with the relation that $\frac{N}{V} = n = const.$ then we can get an exact value for the E_x in this model as:

$$E_x = -\frac{3}{4}\left(\frac{3}{\pi}\right)^{\frac{1}{3}} \int d(\vec{r})n^{\frac{4}{3}}(\vec{r}) \tag{29}$$

  Unfortunately the correlation energy can be analytically found only for limit cases of either high or low densities. Using the Monte-Carlo techniques it has been calculated and parametrized as the function of n [43].

1.1.4. Plane waves and pseudopotentials

A set of base wave functions are almost always necessary in order to solve the electron Schrödinger equation. Essentially, all electron calculation methods today rely on the expansion of the unknown wave function into set of basis functions. There are many different ways of choosing the correct set of basis, such as Gaussian functions, localised atomic like orbitals or plane waves [45]. In the last case, this approach is used in DFT calculations the most. The eigenvalues can be expressed as:

$$\psi_{n\vec{k}}(\vec{r}) = \sum_G c_{n\vec{k}}(\vec{G}) \times \frac{1}{\sqrt{\Omega}} e^{\mathbf{i}(\vec{k}+\vec{G})\cdot\vec{r}} \tag{30}$$

where $c_{n\vec{k}}$ are the expansion coefficients of the wave function in a plane wave basis $e^{\mathbf{i}(\vec{k}+\vec{G})\cdot\vec{r}}$ and $\vec{G}$ are the reciprocal lattice vectors. Bloch wave function is defined by the $\vec{k}$ and the pre-factor $\frac{1}{\sqrt{\Omega}}$ preserves the normalization of the wave function.

Most physical properties of solids are mostly dependent on the structure of valence electrons rather than the structure of electrons located in the inner orbitals. Meanwhile, the deep inner electrons described by the plane wave basis sets needs a great amount of basis functions for corresonding description. Regardless, the fact that the inner electrons are not as important when it comes to the information about the physical properties of the structure, the computational time that is needed for the calculations is larger than for those in valence orbitals. For this reason, another approximation, that replaces the strong ion potential with weaker pseudopotential, is needed [46].

The pseudopotential (PS) method is based on two main assumptions. First lies in the fact that in almost any system it is possible to identify a set of the so-called core orbitals. Second part is connected to the valence orbitals. The valence orbitals show oscillating behaviour which is caused mainly due to Pauli exclusion principle. In pseudopotential approximation the original atoms that form a given chemical system are modified by removing core energy levels and enforcing the Pauli exclusion principle via repulsive pseudopotential. Such approach allows to get rid of the distortions of the atomic valence orbitals and allows efficient application of plane wave basis set expansion. A schematic representation of pseudopotential formalism is represented in Figure 2.

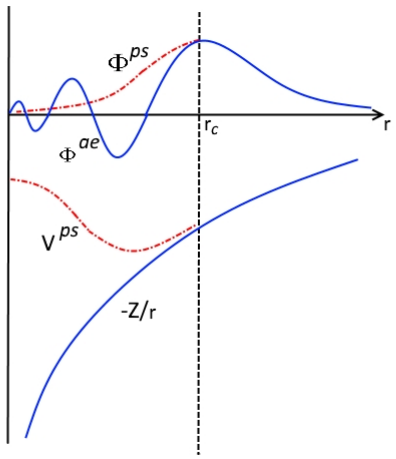

Figure 2 Scheme of pseudopotential and corresponding pseudo wavefunction. A nodeless pseudo wave function Φ^{ps} (red line)matches with all electron wavefunction Φ^{ae} (blue line) at cut-off radius r_c. This introduces a much softer pseudopotential V^{ps} compared to all electron potential $V^{ae} \sim -Z/r$. Reprinted with permission from [47].

The most common form of a pseudopotential is then given by:

$$V_{ps} = \sum_{lm} |Y_{lm}\rangle V_l(r) \langle Y_{lm}| \tag{31}$$

where Y_{lm} are the spherical harmonics.

1.1.5. The projector augmented wave (PAW) method

In the past decades, the electron structure calculations have contributed to our understanding of solids and their properties. Most calculations use the local density approximation that the density functional theory benefits from. As mentioned before, the DFT can describe the ground state of the non interacting electrons, which can be recognised in the effective potential. Many different approaches exist to solve the one particle Schrödinger equation. They can be separated into three main groups.

The first group is formed of the linear methods, which are based on two main pillars, the augmented plane wave method(created by Andersen) and the Korring-Kohn-Rostock methods. The second group are pseudopotentials methods, that stand on the norm-conserving $ab\ initio$ pseudopotentials developed by Hamann, Schluter and Chiang. The third class of methods are using the Gaussians basis sets for the array and are predominantly used in chemistry [48].

When pseudopotential method is combined with plane wave basis set, such arrangement shows a huge advantage in the calculations when compared to other methods. This consolidation allows us to simplify the computations due to lower performance is needed.

The wave functions describing the structure state differ depending on which part of the space they describe. Wave functions characterizing the space close to the core are oscillating due the strong core potential. At the other hand wave functions that represent the space closer to the bonds are smooth. These different states of wave functions cause the main problem when it comes to describing the electron structure. PAW approach treats this problem in such a way that the wave functions are separated into two parts. First part is concerning the core sphere where are partial wave expansions and the second part contains an envelope of wave functions that is defining the space outside the core sphere.

Bloch then transformed these ideas into pseudo-Hilbert space to reduce the problem with oscillation and formulated the projector augmented wave method [49, 50].

The foundation of this method lies in fast transfer of pseudo-wave functions $|\tilde{\phi}_i\rangle$ with the linear transformation τ into the true all-electron wave functions $|\phi_i\rangle$.

$$|\phi_i\rangle = \tau|\tilde{\phi}_i\rangle \tag{32}$$

It is also necessary to modify the nodal structure of the all-electron wave function in the core region which is smooth beyond r_c. Transformed Kohn-Sham equations can be then expressed as:

$$\tau^\dagger H\tau|\tilde{\phi}_i\rangle = \tau^\dagger\tau|\tilde{\phi}_i\rangle\epsilon_i, \tag{33}$$

where $|$ describes the Hermitian adjoint. The transform operator is defined as:

$$\tau = 1 + \sum_R \tilde{\tau_R}. \tag{34}$$

It has to be ensured that outside the augmentation region, each pseudopotential wave function can be expressed into pseudopotential partial waves, which can be done by:

$$\tilde{\psi} = \sum_i |\tilde{\phi}_i\rangle c_i, \tag{35}$$

where c_i is a constant. Then it can be assumed that each arbitrary pseudopotential wave function can be expressed by using pseudopotential partial waves as:

$$\tilde{\psi}(r) = \sum_{i\in R} \tilde{\phi}(r)\langle\tilde{p_i}|\tilde{\psi}\rangle \tag{36}$$

where the set of projector functions $|\tilde{p_i}\rangle$ must satisfy the completeness condition:

$$\sum_i |\tilde{\phi}_i\rangle\langle\tilde{p_i}| = 1. \tag{37}$$

So that the one-center expansion $\sum_i |\tilde{\phi}_i\rangle\langle\tilde{p}|\tilde{\psi}\rangle$ of PS wave functions is identical to the PS wave function $|\tilde{\psi}\rangle$ itself. Which implies that the expression can be written with the Dirac delta function, δ_{ij}, as:

$$\langle\tilde{p_i}|\tilde{\phi_j}\rangle = \delta_{ij}. \tag{38}$$

In conclusion, the linear transformation can take form of:

$$\tau - 1 + \sum_i \left(|\phi_i\rangle - |\tilde{\phi}_i\rangle\right)\langle\tilde{p_i}|. \tag{39}$$

This transformation then describes the the valence wave functions and fictitious pseudo-wave functions can be established. The all-electron wave function can then be obtained from pseudo-potential wave function by:

$$|\psi\rangle = |\tilde{\psi}\rangle + \sum_i \left(|\phi_i\rangle - |\tilde{\phi}_i\rangle\right)\langle\tilde{p_i}|\tilde{\psi}\rangle. \tag{40}$$

It can be seen that only three unknown variables determine the transformation. The all-electron partial waves, obtained by radially integrating the Schrödinger equation of the atomic energy for a set

of energies and orthogonalization to the core states. Then one pseudo-potential partial wave function, that collides with corresponding all-electron partial wave outside the augmentation region for each all-electron partial wave. And at the end for each projection function and for every pseudo-potential partial wave that is localized outside the augmentation region and that subjects to the equation number 38.

Pseudowave functions are then variation of quantum in PAW methods and can be expressed with the plane waves in the form of:

$$\tilde{\psi_{i,k}}(r) = \sum_{G} C_{i,k+G}\, e^{\mathbf{i}(k+g)r}. \tag{41}$$

Outside the core region are the pseudo-potential wave functions with good agreement with the all-electron wave functions, but the deviation near the nuclei is significant. Which is the reason that the partial waves were introduced.

1.1.6. Relativistic density functional theory

After the discovery and successful adaptation of the non-relativistic DFT in theoretical calculations, new problems have raised. It was proven that relativistic effects could play an important role in studied structures and without including them into the calculations the results could show different behaviour of the systems from what is being observed in realistic systems. That is why a further development of the traditional DFT was necessary in order to fully understand the behaviour of structures. The relativistic effects influence the electronic and magnetic behaviour and many other properties of structures.

Principles of relativistic quantum theory

The foundations of relativistic density functional theory (RDFT) were first written by Rajagopal and Callaway who formulated the relativistic generalization of Hohenberg-Kohn theorem. It has been done shortly after the succesfull usage of DFT, however the RDFT was used years later. In the case of non-relativistic density functional theory the variable playing the key role is the ground density state. In the case of relativistic density functional theory, the main variable is the ground state four current density j^{μ}. The j^{μ} is the variable that determines the many-particle ground state ϕ [51].

The ground state of many-body problem and consequently the ground energy state E_{tot} can be understood as the unique functional j_{μ}. Further minimization of the functional E_{tot} with the respect to j_{μ} sets up a way of establishing correct ground state four current. Once this result is obtained, it can be inserted into the E_{tot} and the correct ground state is acquired. In other words, first the the solution of finding energy for many-body system is gathered and is further transformed into finding adequate functional $E_{tot}(j)$. In order to get such suitable functionals, it has been shown that the orbital-dependent treatment of kinetic energy is mandatory for the reproduction of many fundamental quantum mechanical properties. One way of achieving such situation is to consider new, auxiliary, non-interacting system, which ground state four current is same like for the cause of our interacting system. [52] And so new possible ways of separating the total energy of interacting system into four main components are achieved. The kinetic energy T_S, the coupling to external fields energy E_{ext}, direct (Hartree) energy E_h and the exchange correlation energy functional $E_{xc}(j)$ which contain all the complicated many-body properties then can be gathered. Following steps require the minimization of E_{tot} with the respect to the single-particle states of auxiliary system. Such treatment will then give the single particle equations of RDFT, that were first written by Rajagopal and MacDonald and Vosko [53, 29].

The biggest difference between DFT and relativistic DFT is in the presence of infinite zero point energies and ultraviolet divergences. For example the finite vacuum correlations like vacuum polarisation and Casimir energy are shown in both fundamental quantities, the four current and the total energy. Such problems have to be treated with suitable re-normalization processes, that fully rely on the re-normalization vacuum Greens functions of quantum electrodynamics (QED).

- **Relativistic Optimized Potential Method**

  It is important to realise that the power of RDFT lies in the fact that the relativistic local density approximation $(RLDA)$ xc-functional depends mainly on the density, more than on full four current. This property allows to find new direct treatment for magnetization effects such as the

spin-degree of freedom. MacDonald and Vosko as well as Ramana and Rajagopal first proposed the formalism, where the spatial coordinates of j_μ are replaced by the magnetization density m.

However this, so-called collinear, treatment is imperfect. The orientation in the collinear treatment is limited only along one direction. The problem rises from the fact that this approach fails in the case of systems where the imperfect treatment of the electronic self-interaction happens. This problem can be solved by the use of new density functionals, where the E_{xc} is allowed to be orbital-dependent, which spreads the idea behind the kinetic energy T_S to the xc-functional. Such solution is called the optimized potential method (OPM) and uses density functionals of corresponding xc-potentials. This technique has attracted considerable interest after it was shown that the OPM allows an exact treatment of the exchange in RDFT [54, 55].

Relativistic Hohenberg-Kohn theorem

The Born-Oppenheimer approximation is used for the case of determining the ground density state and the properties of systems at their ground state. [56] The electrons are communicating with each other via phonons and they lie in the field of an external static potential, in the four vector form V^μ. Such system is then described by the Lagrangian:

$$\mathcal{L} = \mathcal{L}_e + \mathcal{L}_\gamma + \mathcal{L}_{int} + \mathcal{L}_{ext} \tag{42}$$

where the $\mathcal{L}_e$ denotes the Langragian of noninteracting fermions,

$$\mathcal{L}_e(x) = \frac{1}{4}\{\left[\hat{\bar{\psi}}(x), \left(ic\bar{\partial} - mc^2\right)\hat{\psi}(x)\right] + \left[\hat{\bar{\psi}}(x)\left(-ic\bar{\partial} - mc^2\right), \hat{\psi}(x)\right]\} \tag{43}$$

and where the $\mathcal{L}_\gamma$ is the Lagrangian of noninteracting photons:

$$\mathcal{L}_\gamma(x) = -\frac{1}{16\phi}\hat{F}_{\mu\nu}(x)\hat{F}^{\mu\nu}(x) - \frac{\lambda}{8\phi}(\partial_\mu \hat{A}^\mu(x))^2 \tag{44}$$

and $\mathcal{L}_{int}$ and $\mathcal{L}_{ext}$ provide the interaction between fermions and photons as well as between the fermions and the external potential:

$$\mathcal{L}_{int}(x) = -e\hat{j}^\mu(x)\hat{A}_\mu(x) \tag{45}$$

$$\mathcal{L}_{ext}(x) = -e\hat{j}^\mu(x)\hat{V}_\mu(x) \tag{46}$$

The operators $\hat{\psi}(x)$ and $\hat{A}_\mu(x)$ are the fermion and photon field operators, $\hat{F}_{\mu\nu}(x)$ is the electromagnetic field tensor and $\hat{j}^\mu(x)$ is the fermionic current density. [57]

Relativistic Kohn-Sham equations

Just like for the DFT, the relativistic Kohn-Sham equations are needed when describing how to bring together the density from the non-interacting system. The relativistic variant of these equations and theorems guarantee the formal existence of a density functional description of relativistic systems. Unfortunately, it does not give any information about how to construct the crucial functional $E_{tot}\,[j]$. [58]

Explicit approximations to $E_{tot}\,[j]$ can be derived by the usage of variety of methods. The most important approach starts with a study of the homogeneous electron gas. For such described system the energy functional is known in the form of a simple function of the gas density. This functional can then be extended in a systematic procedure by inclusion of inhomogeneity corrections which depend on the gradients of the density. If this approach is utilized for the complete energy functional one ends up with relativistic (extended) Thomas–Fermi models.[59]

As in the non-relativistic context, however, these models have found very limited use due to the fact that they omit important quantum mechanical properties, because they neither reproduce atomic shell structure nor do they lead to molecular binding.

1.2. Magnetism

Magnetism and magnetic properties of magnets have attracted much attention already in the ancient Greece and China due the ability of pulling iron based materials towards themselves in long distances [60]. Today it is well known that magnetism is related to many-body phenomena. The origin of which can be explained with non-relativistic quantum physics.

Magnetic properties of materials are derived from their magnetic states. The magnetic state of a system has atomic origin and is mainly given by the state of electrons. From magnetic point of view, every atom can be characterized by its magnetic moment $\vec{\mu}$. There are three main contribution to the total magnetic moment of an atom. The first one is the orbital movement of electrons around the nucleus of the atom along given path (orbital). Second contribution comes from the inner magnetic moment - the spin of electron. The last part is from the external magnetic field that is affecting the movement of electrons around the nucleus.

The magnetic moment $\vec{\mu}$ that is corresponding to one electron is then given as:

$$\vec{\mu} = \gamma \vec{L} \tag{47}$$

where the $\vec{L}$ is the momentum vector and the γ is a constant known as the gyromagnetic ratio.

The total magnetization can be calculated as sum of all magnetic moments of all atoms divided by the total volume of material.

$$\vec{M} = \frac{\sum_{i=1}^{n} \vec{\mu_i}}{V} \tag{48}$$

If an external field of the magnetic induction $\vec{B}$ is applied on an atom, which direction is different than the one of the external field, the magnetic moment of an atom will tilt to the direction of external field in given angle Θ and starts the precession movement , as shown in the Figure 3.

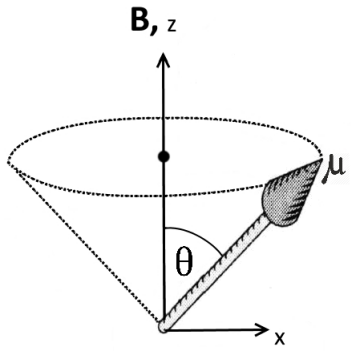

Figure 3 Scheme of the precession of the electron around the external field direction. Reprinted with the permission from [60].

A formation of a local magnetic moment and the interactions within the structure are the necessary conditions for the existence of a magnetic order in the system.

Atoms consists of one and more electrons. Electrons occupy different energy levels called orbitals. When an orbital is filled, the structure shows no total momentum. However in the case of partially filled electron orbitals, electrons can arrange in such way that to total spin and orbital moment is nonzero. The spin and orbital moment are bonded through weak bond, which origin lies in the spin-orbit coupling.

- **Spin-orbit coupling interaction**

  Spin-orbit interactions can be looked at like the perturbation states with defined angular, L, and spin S momentum, defined by quantum numbers. The angular momentum makes an electron behave like a circulating electric current. This leads to a magnetic moment with an associated magnetic field. The magnetic moment from the electron's spin interacts with the magnetic field from its orbital motion. Such contact results in a spin-orbit coupling interaction. It is determined by the charge on the atomic nucleus, which depends on the atomic number Z. For the

light atoms, the spin-orbit interaction is weak and the individual spins are stronger than the spin-orbit coupling. The Scheme that is applied for such configurations is known as the Russell-Sunders coupling. An important rule for finding the lowest-energy configurations for the electrons in a partially filled shell was formulated by the German physicist Friedrich Hund. In the case of heavy atoms however, the Russell-Saunders coupling scheme fails. In heavy atoms the spin and orbital angular moments are strongly coupled and the spin-orbit coupling becomes a strong force affecting the system, which is described by the $j - j$ coupling scheme.[61]

So far the situation described was for the case when magnetic moments in an atom are isolated and cannot interact with each others. In real situations however, there exists different interactions between the magnetic moments of atoms themselves and also between the magnetic moments and electric potentials of the surrounding space. The magnetic interactions support magnetic ordering in materials. The magnetic interactions compete against thermal fluctuations that are the cause of a chaotic ordering of magnetic moments in systems. Every material exhibits critical (transition) temperature, noted as T_C (Curie temperature) and T_N (Néel temperature), respectively. Above these temperatures, the thermal fluctuations dominate and the material shows paramagnetic behaviour. When under the blocking temperature, the magnetic interactions rule over the structure and the system exhibits magnetic ordering.

- **Crystal field and Jahn-Teller effect**

  In the case when the atoms form a solid, the Coulomb interaction of the electronic charges distribution $\rho_0(\vec{r})$ with the surrounding charges in the crystal must be considered. This phenomena is called the crystal-field interaction. A crystal field is an electric field that originates in neighbour atoms in the crystal lattice. Neighbouring orbitals are considered as negative point charges, which size and effect depends on the symmetry of the system. The biggest contribution comes mainly from p orbitals and d orbitals. Depending on the symmetry of the system, different degenerated states are possible.[61]

  Not only the surrounding of an atom can effect the symmetry of system. Magnetic properties of elements can cause the changes of the structure energy levels itself. Such scenario can happen in systems where it is energetically preferred to break the symmetry and deform the structure of the lattice in order to even the energies of electrons in orbitals. This is known as the Jahn-Taller effect. This effect is then a geometric distortion of a non-linear system that reduces/disturbs its symmetry which leads to change of the energy. The deformation can increase or lower energy of certain orbitals. This effect does not apply for structures with filled or no electrons in orbitals. However for the case of partially filled orbitals, Jahn-Taller effect plays a key role because it can lead to lowering the total energy.

When it comes to transition metal compounds, the spin-orbit interaction effects are much more weaker in the comparison to its crystal field effect. That causes breaking the symmetry of the charge density of the transition metal in the presence of neighbours point charge atoms.

1.2.1. Magnetic interactions

Materials with half filled d or f orbitals generally exhibit magnetic order up to room temperatures. Fundamental property of ferromagnets such as Fe, Co or Ni is their exhibition of spontaneous magnetization. However, recent reports have been showing the evidence that also in structures with no electrons on d and f orbitals, magnetism can occur.

Universally, the Hamiltonian of many-body system is not only time and spatial but also all particle spin dependent. The complete behaviour of the electrons spin and orbital angular moments, determined by the orbital movement, is describing the magnetism in the system. The mechanism behind the arise of feromagnetism was explained by Heisenberg with the use of Pauli exclusion principle. The effective Coulomb repulsion for a pair of electrons with parallel spins is then weaker than the one in case of electrons with anti-parallel spins - such synergy is known as the exchange interaction.[60]

- **Exchange interactions**

  Exchange interactions play key role in the long distance magnetic ordering. Its origin lies in the electrostatic interactions of same point charges.

In quantum mechanics the spin moment is described by the expectation value of the spin operator S_z. The orbital moment can be calculated from the expectation value from angular momentum operator L_z in the presence of spin-orbital coupling. If these two variables are known, the magnetic behaviour is then defined by the exchange interaction in-between spins. There are two possible arrangements of the spins in the structure. First of them is parallel, aleading to the manifestation of ferromagnetism, and the second is anti-parallel or so called antiferromagnetism.[60]

There exist different ways and methods on how to investigate the magnetic properties of materials. For example the X-ray magnetic circular dichroism, which is an experimental method that can obtain the orbital moments of the system. The $ab\ initio$ DFT can describe the magnetic properties not only for volume materials, the surface of the structures but even for less dimensional structures - such as the 2D systems.

The orbital exchange interaction is describing the surface molecular magnetic interactions. The exchange integral, that is part of the Heisenberg model can be obtained from $ab\ initio$ simulations. What must be considered is the total energies in the system, such as:

$$H = -\frac{1}{2}\sum_{ij} J^{ij}\vec{s_i}\vec{s_j} \tag{49}$$

where the J^{ij} is the exchange integral and s is the i^{th} spin vector.

Spin dipole interations
Spin dipole moment is another important aspect used to describe the magnetic structures. Its origin lays in the spin density, that is mainly being caused by effects of the crystal field and by spin orbital interactions. In the case of heavy earth elements the spin orbital interactions are much more stronger than when compared to their crystal field. That is also why the creation of bands is weaker and the structures behave like free ions.

Another important property after the spin-orbit coupling are the dipole-dipole interactions. These two phenomenons are conditional for the explanation of the origin of ferromagnetism in 2D systems, such as ultra-thin films.[60]

- **Dipolar interactions**

  Magnetic dipolar interactions are considered when two different magnetic dipols $\vec{\mu_1}$ and $\vec{\mu_2}$ that are distant by r are interacting with each others. This effect depends on the distance r and the different guidelines of the vectors. This interaction is very weak and dominates when temperatures are close to a few mili Kelvins. That is why such interaction cannot be responsible for magnetic ordering in most magnetic materials.

However the problem with explaining the magnetism within the non-relativistic quantum theory is the undertaking of the free energy of the system that is not dependent on the direction of magnetization (the isotropic case). This property is a direct contradiction to the results from experiments, showing that the magnetizations generally lies in preferable directions with the respect to the crystal axis and it also depends on the shape of the structure when considering finite samples. Such effects that have to be taken in account when trying to describe the magnetism of the system are over-all important parts for the magnetic anisotropy.

1.2.2. Magnetic anisotropy energy

Magnetic anisotropy energy (MAE) is a very important subject that refers to the dependence of the magnetic properties on the direction in which they are measured. The type of magnetic anisotropy affects properties such as magnetization and hysteresis curves in magnetic materials. That is one of the main reasons why the nature of the magnetic anisotropy is an important factor in determining magnetic materials for a particular application.[62]

The magnetic anisotropy in thin films has two mechanisms that are responsible for its occurrence. First it can be explained as result of the magneto-crystalline anisotropy. Such anisotropy is a result of the magnetization that aligns itself along a preferred crystallographic directions. The inner free energy of system is lowest for a spontaneous spin quantization axis, also known as easy axis, compared to the other, hard axis. The energy required to rotate the the spin system of a domain from

one direction to the other is defined by the energy that is needed to overcome the spin-orbit coupling. Magneto-crystalline anisotropy is intristic to the material.[62]

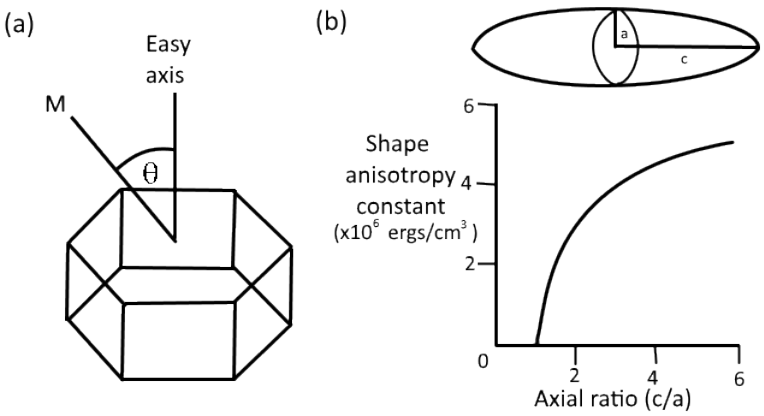

Figure 4 Magnetic anisotropy energy. (a)Angle between the magnetization direction in the material and the easy axis that is preferred in materials such as cobalt.(b)Shape anisotropy constant. Reprinted with permission from [60].

The magneto-crystalline anisotropy however fails to describe samples with no preferred orientation of its grains like in the case of polycrystalline structures. The second mechanism that can explain the MAE is shape anisotropy, shown in the Figure 4. Strain anisotropy and interface anisotropy can also be significant in some materials.[62]

1.3. Graphene

Carbon is one of the most fundamental materials on the planet and the foundation of organic chemistry. It is a non metallic chemical element with the letter C in periodic table. The name is derived from the Latin *carbo*, which means charcoal or ember. Carbon can be found in the abundance in the universe, such as in the stars, suns, comets and in the atmospheres of other planets. Because of its ability to bond to both electronegative and electronpositive elements, carbon excels above others. No other material offers such a diversity of systems that show an unlimited number of different structures with an equally large variety of physical properties. The whole family of structures that are based on carbon purely are called carbon allotropes. [63]

The most often appearance of carbon is in the form of nuclide carbon 12C, described by the atomic number 6. It consists of 4 valence electrons that can bond to itself or to other elements without limits through single bond (with energy roughly (~350 kJ mol^{-1})), double (~610 kJ mol^{-1}), or triple (~840 kJ mol^{-1}) bonds. [65, 66] The valence state is responsible for three main types of hybridization that is sp, sp^2 and sp^3 depending on the number of σ bonds in the structure, as shown in the scheme diagram: 5

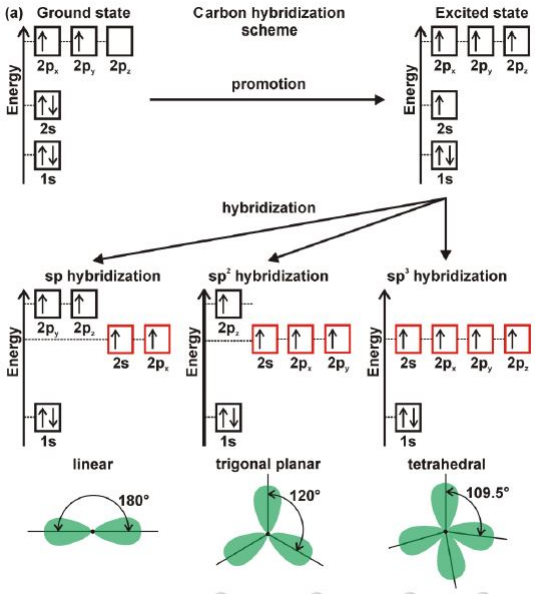

Figure 5 Schematic description of sp, sp^2, and sp^3 hybridization in carbon with illustration of bonding structure. Reprinted with permission from [64].

With the improvement of the knowledge and our understanding in the field of nanotechnology, there has been discovered many different structures that are purely based on carbon atoms. The unique and distinctive properties that can be observed in these structures allow us to separate them into two main classes.[**?**]

The first class is based on the dependence of the dominant covalent bonds in the structure, created between carbon atoms. This set can be divided into two subgroups. First group are graphene nanostructures containing only the sp^2 hybridization. Second group are carbon nanostructures, that contain mixed hybridization states (both sp^2 and sp^3). [68]

Second class is sorting carbon structures accordingly to the geometries. Depending on the sizes of their dimensions, these allotropes can be divided into 4 main groups:

1. 0D structures – Nanostructures from this group have all their dimensions in the region of nanometres such as fullerenes and quantum dots.

2. 1D structures – Nanostructures belonging to this group have one dimension greater than 100 nanometres, such as nanotubes or nanostrings.

3. 2D structures – Two dimensions of the structures are greater than 100 nanometres, such as graphene.

4. 3D structures – All dimensions are in the region above 100 nanometres, for example nano crystals.

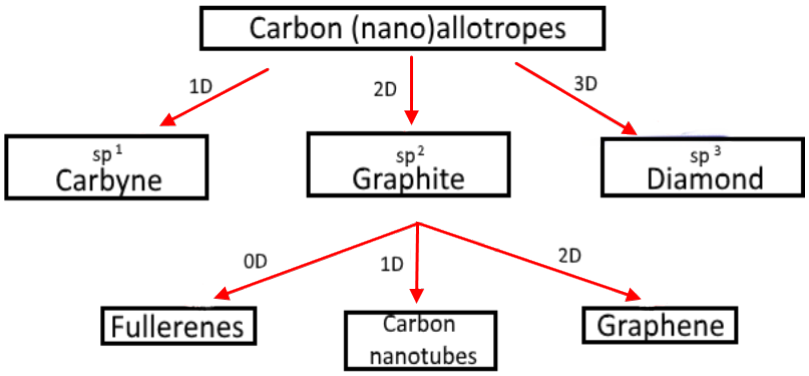

Figure 6 | Graph showing classes of carbon nanoallotropes with most known members of the groups.

The element carbon is widely distributed in the nature in its two main allotropic modifications, diamond (clear electrical insulator and one of the hardest materials on Earth) and graphite (greasy electrical conducting dark material), in the Figure 7

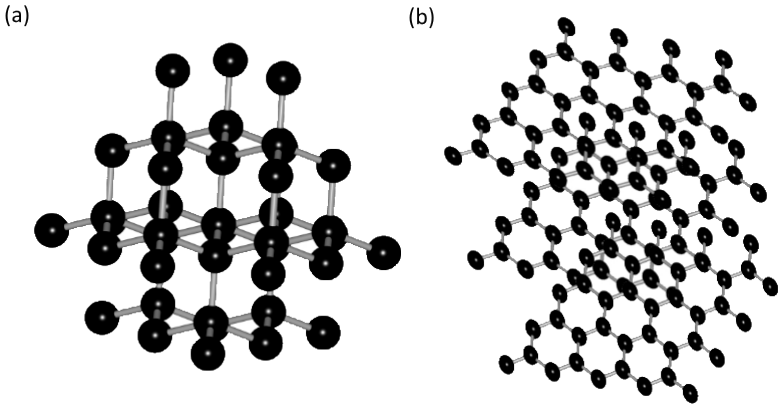

Figure 7 | Alignment of carbon atoms in the diamond (a) and graphite (b) allotropes.

There are many carbon nano allotropes and their derivates, where the main representatives are shown in the Figure6, that are interesting not only for possible engineering applications in spintronic but also for bioengineering, drug delivery or in the combination with other chemical compounds in electronics. [69]

Graphene

Graphene – a two-dimensional (2D) allotrope of carbon atoms – plays an important role since its discovery in 2004. For the discovery of this two dimensional structure was given a Nobel price for Physics in 2010 to its discovereres Andre Geim and Konstantin Novoselov. Graphene is the foundation for understanding the electronic properties in the carbon allotropes. It is a single layer of carbon atoms arranged in a honeycomb structure made of hexagons. [70]

The structural flexibility of graphene is reflected in its electronic properties. The σ bonds between carbon atoms (separation by 1.42 Å), that are created due the sp^2 hybridization between one s orbital and two p orbitals, lead to a trigonal planar structure. The σ band is responsible for the robustness of the lattice structure in all allotropes. Due to the Pauli principle, these bands have a filled shell and form a deep valence band. The unaffected p orbital, which is perpendicular to the planar structure, can bind covalently with neighbouring carbon atoms, leading to the formation of a π band. Since each p orbital has one extra electron, the π band is half filled. [71]

Half-filled bands in transition elements have played an important role in the physics of strongly correlated systems. Their strong tight-binding character gives them a property that causes the Coulomb energies to be large which leads to strong collective effects. The magnetism and insulating behaviour exist due to the correlation gaps. Stacking can change the electronic properties considerably and the layering structure can be used in order to control the electronic properties.[72, 73]

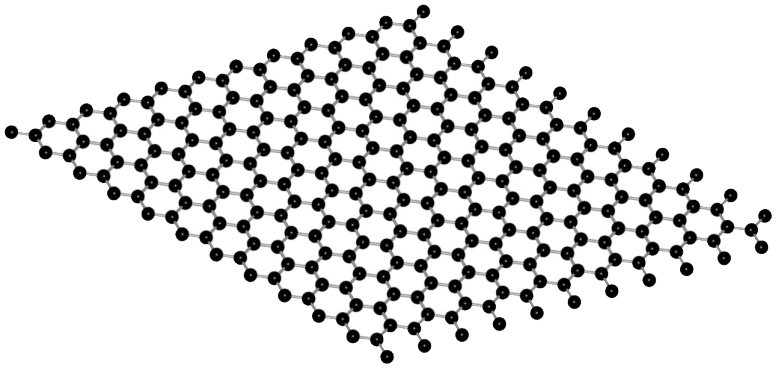

Figure 8 | Scheme of graphene layer.

Low energy excitations are massless, chiral, Dirac fermions. The Dirac fermions move with a speed v_f, which is 300 times smaller than the speed of light c. If subjected to magnetic fields, new interesting aspects show, such as the anomalous integer quantum Hall effect.

Another interesting feature of Dirac fermions is their insensitivity to external electrostatic potentials thanks to the Klein paradox, that is, the fact that Dirac fermions can be transmitted with probability 1 through a classically forbidden region.

One of the most unique property of graphene is the fact that the conductive and valence bands are connected in two points of the reciprocal space, K and K'. This is due the hexagonal symmetry of the crystal lattice. Without any doping, the valence band is fully occupied up to these Dirac points, causing the conductive band to be empty. After applying voltage to the graphene plane the width of the conductive band can be adjusted from 0 to 0.25 eV.

Graphene structure can be divided into two equivalent triangular sub-lattices, sub-lattice A and B, as shown in the picture 9.

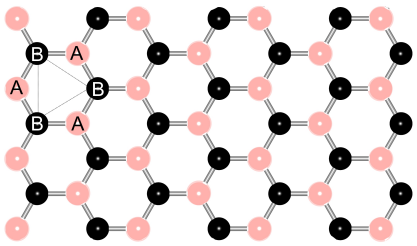

Figure 9 | Schematic of graphene sub-laticces A and B.

It is well known that the graphite is an ideal diamagnetic material. However when defects are introduced to its crystal lattice, spontaneous magnetization can be observed. For example in the porous graphite, where hexagonal holes occur, spontaneous magnetization has been observed in most cases. Its origin is strongly dependent on the size and arrangement of the holes.

Recent studies and experiments shown that materials on sp based materials could exhibit magnetic behaviours. In 1990^{th} it has been proven that such materials show magnetism, however the contribution from sp bonds is lacking the strength to stabilize magnetism through the structure. That is why new ways of imprinting magnetism in sp based materials were needed.[66]

1.4. Inducing magnetism in graphene

The thought of imprinting magnetic and electronic properties of graphene in order to gain suitable material for electronic devices was firstly proposed after the use of electrons and ions irradiation of the carbon materials. Pure graphene is metal and due to the p orbital combination it is believed to be non magnetic. However when different distortions are introduced to the graphene layer magnetism can be detected in the structure.

1.4.1. Vacancies in graphene lattice

Vacancy defect removes one p_z orbital from the π-system of graphene. P_z orbital is eliminated together with the knocked-out carbon. The single atom p_z vacancies have a particularly profound effect on the electronic structure of ideal graphene. Elimination of one atom from one of the sublattices introduces a zero-energy state in the complementary sublattice and the quasi-localized states appear.[68]

In the case of single vacancy, the carbon atoms surrounding the empty space create a weak bond, caused by the Jahn-Teller effect. That shows a very strong exchange splitting and contributes 1 μ_B to the total magnetic moment of the defect. However the magnetic moment is highly unlike to occur at room temperatures.[74]

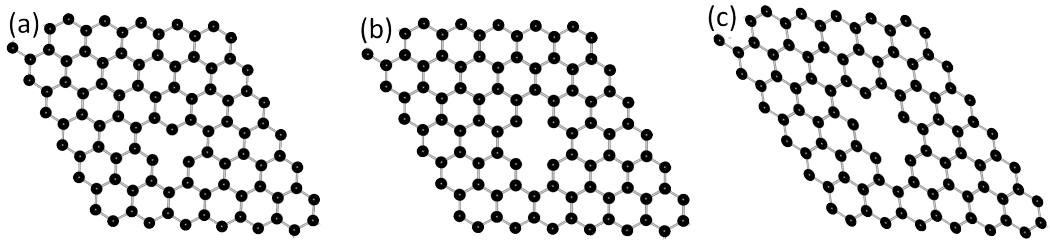

Figure 10 | Different types of vacancies in graphene. (a) single-vacancy, (b) double-vacancy and (c) multiple vacancy.

It has been said that the graphene lattice can be viewed as two inequivalent triangular sub-lattices that have different spin populations of carbon atoms (labelled A and B). When defects are produced in the A lattice, only the p_z orbitals of carbon atoms in the B sub-lattice contribute to the quasi-localized states, and vice versa. These states extend over several nanometres around the defect and the magnetic moments can make a ferromagnetic (FM) coupling.

1.4.2. Substitutional doping by heteroatoms

Vacancies are not the only way how to bring magnetism into the graphene sheet. Doping graphene by different substitutional atoms has attracted much attentions due the possible applications for new materials for Li-ion batteries, field-effect transistors or for example electrochemical biosensing.

Two types of carriers atoms can bring to the structure, holes or electrons, we talk about either the p- or n- doped systems. The doping changes the electronic and magnetic properties such as the width of the band gap which, as can be seen in the Figure 11. Most common dopants are boron for the p-type and nitrogen as the n-type carrier. Other, often used choices, are the phosphor, sulphur and oxygen.

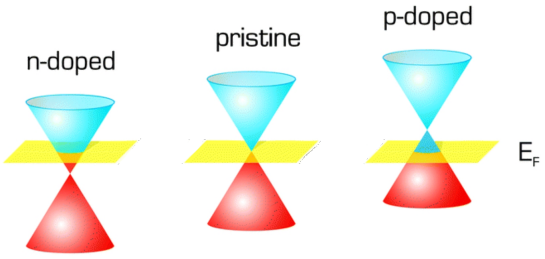

Figure 11 | Changes in the band gap of graphene layer when doping graphene with n- and p-dopant, respectively.

Substitutional doping of graphene by nitrogen atoms has particular advantages due the similar atomic size. The nitrogen one more electron, compared to the carbon atom, affects the graphene electric conductivity. There are four possible groups of nitrogen atoms that are considered in the doping of graphene - graphitic, pyrrolic, pyridinic and adsorbed.[75] First one is the graphitic. In this case the extra electrons adds up to the π electrons close to the Fermi level of graphene. Stoner magnetism can occur when the roaming electrons occupy narrow bands at the Fermi level. Pyrrolic doping belongs to the second groups and it has been shown that for this type of doping, the magnetism decreases. The last two groups, the pyridinic and adsorbed doping have also a considerably lower effect on inprinting the ferromagnetism (FM) in the structure. However for all the cases, the concentration of nitrogen atoms in the structure is a key factor, affecting strongly the manifestation of the magnetism in graphene layer. [75]

When nitrogen atoms are present around a vacancy in graphene layerit has been observed, that larger macroscopic magnetic signals can occur as compared to a standalone carbon vacancy. The π orbitals of the atoms around the border regions of graphene and nitrogen are localized and are responsible for the magnetism. Nitrogen doped graphene has also shown potential for stabilising several atomic species. Such different electronic and magnetic behaviours of nitrogen doped vacancies under external elements adsorption provides a very valuable method to manipulate the magnetism of the structure.

1.4.3. Edge confinement

A novel approach on how to imprint magnetic properties into the sp based materials is by confining the structure spatially. Three main classes derived from graphene are up to this day recognised: (a) graphene nanoribbons (GNRs), (b) graphene nanoflakes and (c) graphene quantum dots. The magnetism in these structures strongly depends on its shape.

The electronic and magnetic properties of graphene nanoflakes and graphene quantum dots have been broadly studied in the past and only graphene nanoribbons are further discussed. Graphene nanoribbons are graphene layers terminated in one direction with a specific width. The geometric structures of GNRs are shown in Fig 12

Two types of edges of a graphene nanoribbons plane are recognized when considering the electronic structure of micro-graphite: a phenanthrene (or armchair) edge and an acene (or zigzag) edge, Figure 12. Narrow and long graphene nanoribbons with zigzag edges feature a sharp peak in the density of states at the Fermi energy. Such a peak is not observed in the case of bulk graphite. Unsaturated valence bonds at the boundaries of graphene flakes are filled with stabilizing elements: these stabilizers are theoretically considered to be hydrogen atoms. Graphite nanoribbons for example have an extremely high density of states at the Fermi level, which leads to paramagnetism and (for a certain packing) to antiferromagnetism. [76]

Zigzag-type nanoribbons are always metallic. A specific feature of the zigzag GNRs is the appearance of a pair of almost flat bands on the Fermi energy. These bands create a sharp peak in the density of states at the Fermi level in the region where the π and π^* bands of 2D graphite contact each other. The charge density in the flat band state is strongly localized on the zigzag edge sites. In the case of the zigzag type strips, a ferrimagnetic structure is possible.[77]

The experimental and theoretical calculations reveal that all such GNRs are semiconductors with an energy gap. For armchair GNRs, the width of a graphene nanoribbon characterizes the energy gaps. Similarly, the energy gaps can be fitted for zigzag GNRs, using the width of a zigzag nanoribbon

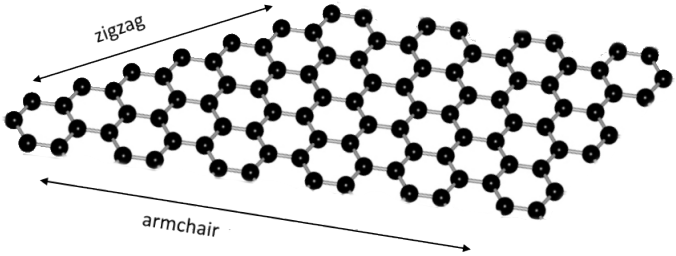

Figure 12 Edge confinement at graphene layer with the zigzag and armchair edge configuration.

in angstroms. The most important thing is that edge states lead to the appearance of magnetic order in zigzag nanoribbons. Such spin polarization system has ferromagnetic FM coupling on the same edges, while anti-ferromagnetic (AFM) coupling between the two challenge edges.

1.4.4. Functionalization

The doping of atoms into the layer of graphene is not the only way how to create magnetic moments in the system. It has been observed that by bonding/adsorbing different atoms or whole compounds onto graphene layer, the properties of the structure will rapidly change. The advantage of this approach are the strong exchange interactions that support the magnetic ordering in the graphene layer. The self-sustainable magnetism has been observed in the functionalized graphene layers up to room temperatures, such as the $C_{18}\,(OH)_{1.8}\,F_{7.2}$. [79] There are two main types of functionalization.

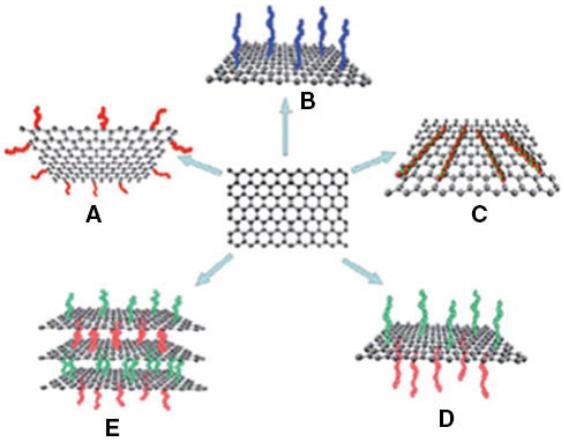

Figure 13 Different possible function groups with different bonding to the structure. (A) Scheme of molecules bonded to the edges of graphenelayer. (B) Scheme of molecules bonded to only one side and (D) shows bonding to both sides of graphene plane. (C) Scheme od molecules bonded along the graphene layer and (E) shows possible novel structures based on graphene functionalization. Reprinted with permission from [80].

First is the case when strong covalent bond (chemisorpiton) occurs and the second group contains the groups of molecules that are poorly bonded to the graphene surface by weak van der Waals interactions (physisorption). The covalent functionalization bring with it great changes not only to the structure but also in the properties of the material. In the case of weak van der Waals forces the situation is completely different. There are no significant changes in the graphene layer, but it can lead to more stable structures.

2. Computational part

2.1. Computational details

The electronic structure calculations and structural optimizations described here were investigated by employing the Vienna *ab initio* simulation package (VASP) [82, 83]. The results based on DFT as implemented in the VASP perform an iterative solution of the Kohn-Sham equations within a plane-wave basis and by the use of periodic boundary conditions. Different types of basis set containing plane waves were considered. Main computations discussed further have set maximum kinetic energy 600 eV. For result precision and fairness, calculations were also done for 400 eV and 500 eV. A semi-local functional in the generalized gradient approximation and the spin-interpolation proposed by Vosko *et al.* are used to describe electronic exchange correlation and spin-polarization.[43] The use of a semi-local functional is known to be essential for the correct prediction of the ground state of the ferromagnetic 3d elements. The Brillouin zone was sampled using different sets of Γ-centred *k*-point mesh. In the case of maximum kinetic energy 400 eV the 6×6×1 *k*-point mesh was used, for 500 eV the 9×9×1 and 11×11×1 Γ-centred *k*-point mesh for the kinetic energy 600 eV, with a Gaussian smearing of 0.02 eV.

The PAW method is used to describe the electron-ion interactions. The PAW approach produces the exact all-electron potentials and charge densities without elaborating the non-linear core-corrections, which is particularly important for magnetic elements.[50] Spin-orbit coupling has been implemented in VASP by Kresse and Lebacq.[85] Calculations including spin-orbit coupling have been performed in the non-collinear mode implemented in VASP by Hobbs *et al.*[83] and Marsman and Hafner.[86] The Kohn-Sham equations with the relativistic effective potential have been solved self-consistently. Geometric, electronic and magnetic degrees of freedom were relaxed simultaneously without any constraint until the change in total energy between successive iteration steps is smaller than 10^{-6} eV. Alternatively, the magnetic force theorem (non-self consistent calculations (nsc)) has been used to confirm/disprove the MAE, obtained from the self consistent calculations.

For each system described in this work, two sets of calculations were performed. First the calculations have started with a scalar-relativistic (SR) mode. The geometry has been optimized by a static relaxation using a quasi-Newton method, starting from different initial locations and configurations of the dimer, until the forces on all atoms were less than 25 meV/Å. The energetically most stable and favourable position of the dimer was found by structures relaxation without symmetry constraints. In the second step, the configurations resulting from the scalar-relativistic calculations were used to initialize the calculations including spin-orbit coupling, allowing only for the relaxation of electronic and magnetic degrees of freedom. To determine the magnetic anisotropy for each configuration of the dimer on graphene, a set of self-consistent calculations with different initial orientations of the magnetic moments were performed. The magnetic anisotropy energy was calculated as the difference in the total energies calculated for the easy and hard magnetic axes.

2.2. Structural models

Two structural models were used. First one contains a dimer adsorbed on top of a single vacancy graphene (SVGraphene). Second model is created of SVGraphene layer where the carbon atoms near the vacancy are replaced with the nitrogen atoms, creating the nitrogen doped single vacancy graphene (N-SVGraphene) sheet.

The SVGraphene-dimer complex is represented by a periodically repeated unit cell containing 47 C atoms in the graphene layer and the dimer is consisted of one Co atom and one Ir atom. For the case of N-SVGraphene, there is 44 C atoms and 3 N atoms in total and the dimer is again created of one Co and one Ir atom. The structural models are shown in the Figure 14.

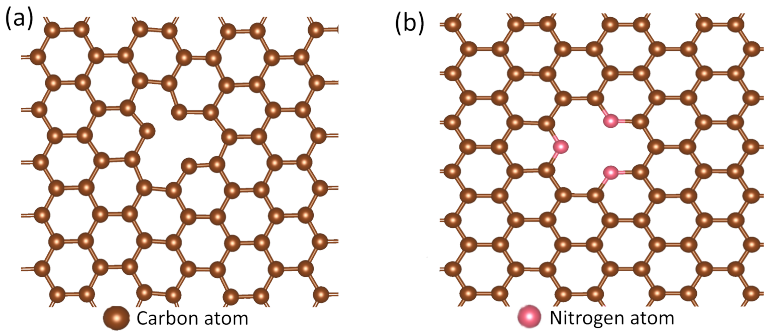

Figure 14 | (a) The model of SVGraphene sheet and (b) the model of the N-SVGraphene layer.

The electronic structure of the graphene layer is modified in both cases. The case of missing carbon atom in the graphene layer is well known and the changes in properties of such structure can be seen in the density of states (DOS). Comparison of the DOS of the free-standing graphene layer where the states close to the Fermi level show characteristics for the linear dispersion relations - with the SVGraphene DOS is shown in the Figure 15 (a).

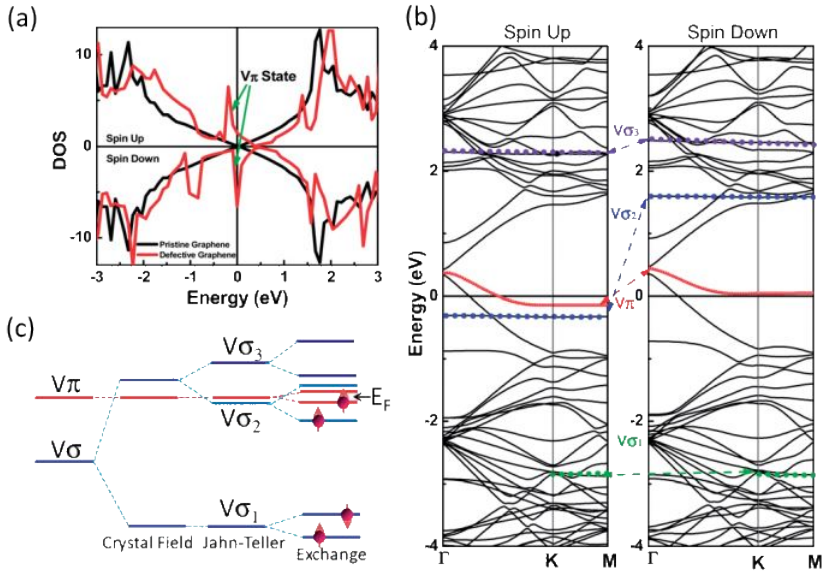

Figure 15 | (a) The DOS of pristine graphene and graphene with one vacancy. (b) Band structure splitting of graphene with one vacancy. (c) Scheme of band splitting for V_σ and V_π states. Reprinted with permission from [87].

The missing carbon atom causes the rise of a localized state V_π in the midgap surrounding, when compared to the energy of pure graphene which is zero in the region. Due the crystal field and Jahn-Teller distortion the localized state is split into $V_{\sigma 1}$, $V_{\sigma 2}$ and $V_{\sigma 3}$ states, as can be seen in the Figure 15 (b).

In the case of N-SVGraphene the comparison for DOS of SVGraphene from the calculations with the DOS of N-SVGraphene is presented in the Figure 16. The electron doping coming from the N atoms causes the Diract point in the graphene band structure to shift slightly above the Fermi level and a small energy gap appears at the high symmetric *k*-point.

The nitrogen atoms contribute to the localized state V_π via the p orbitals, Figure 17. Obtained results are found to be in a good agreement with available experimental and theoretical findings. [88]

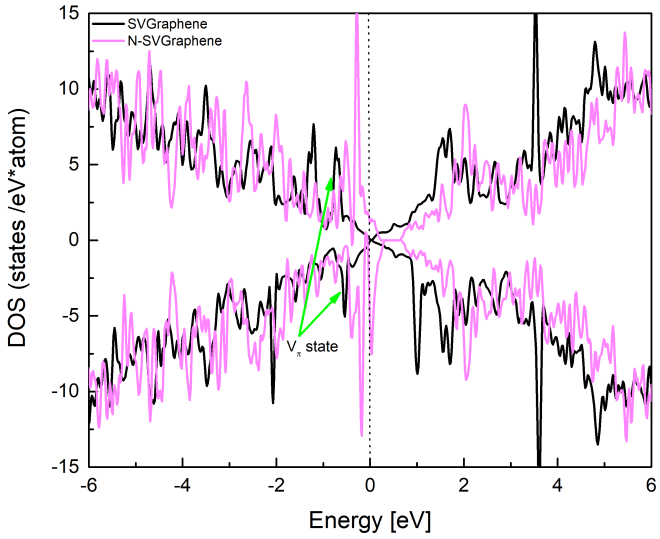

Figure 16 DOS comparison for the SVGraphene and N-SVGraphene sheet. Dashed line shows the Fermi level.

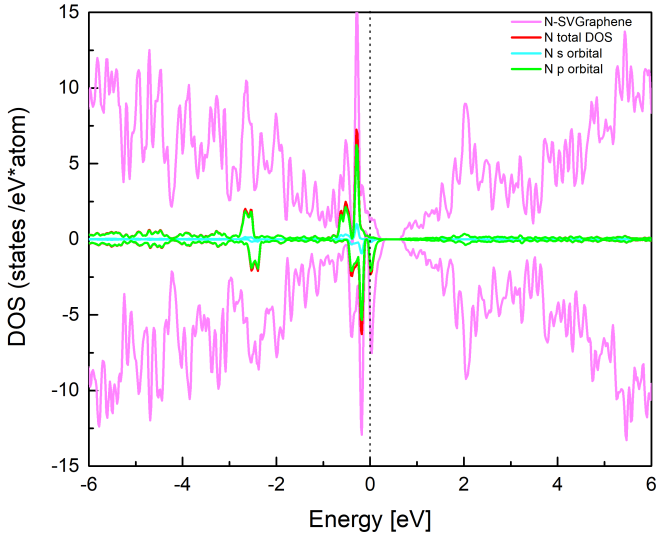

Figure 17 Total and local DOS for N-SVGraphene and the nitrogen atoms. Dashed line shows the Fermi level.

The energy that defines the interaction energy of the dimer with the graphene defective sheet is defined as the total energy of the IrCo/SVGraphene complex, $E_{IrCo-graph}$, minus the energy of the clean graphene layer, E_{graph}, and the total ground state energy of the dimer in the gas-phase, E_{IrCo}:

$$E_{int} = E_{IrCo-graph} - E_{graph} - E_{IrCo} \tag{50}$$

Dimer, with an initial geometry determined for free cluster in earlier calculations, was placed on top of the graphene layer around created vacancy. Two possible configurations are further discussed: an upright dimer with either the 3d or 5d atom bonded to the graphene and the N-doped vacancy, respectively.

2.3. Scalar - Relativistic calculations

2.3.1. Graphene layer with CoIr dimer bonded to the single vacancy graphene layer

Co down

The initial positions and final relaxed structure of the dimer adsorbed on the graphene in the case of the Co atom bound to the C atoms in graphene layer are shown in Figure 18. The dimer binds in an upright configuration through the Co atom in the centre of a vacancy.

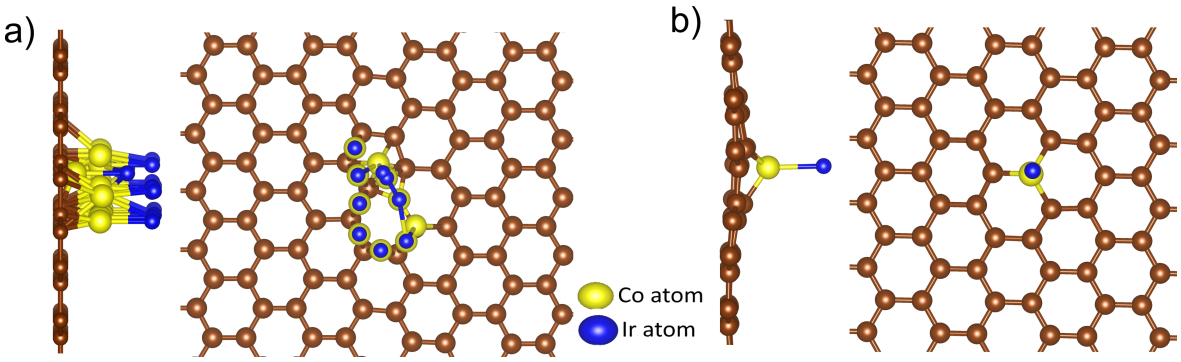

Figure 18 CoIr dimer with Co atom bound to the defective graphene sheet. The initial positions are shown in the panel (a) and the final position after relaxation is shown in the panel (b).

The calculations for the free dimer show a spin moment of 3.68 μ_B, with a bond length of 2.08 Å in the gas-phase. On graphene, the Co-Ir distance is 2.24 Å, which is slightly larger than the dimer length in the gas-phase. The relaxed C-C distance in a pristine graphene layer is 1.41 Å, which is in a very good agreement with the one from the SR calculations, which varies from 1.40-1.42 Å, depending on the position of the C atom in the structure. The shorter distances are showing carbon atoms surrounding the vacancy. The distance between the C atoms that are bonded to the Co atom is of 1.78 Å. The Co atom lies above the average level of the buckled C layer. The higher positioned Ir atom is 3.52 Å above the graphene layer. Calculated distances are somewhat in agreement with other theoretical calculations [89].

The binding energy of graphene with the dimer in this configuration is 5.72 eV/dimer. The system is characterised by the total magnetic moment of 1.6 μ_B. The spin moment of Ir atom is 1.59 μ_B and Co atom shows only 0.03 μ_B. The C atoms that are directly connected to the Co atom are showing small magnetic moments (0.01 μ_B). However the further from the vacancy, the lower the changes are and the magnetic moments on the furthest positioned C atoms in the graphene layer remain unchanged, when compared to the pristine case.

The effect of binding the dimer onto the graphene layer on the electronic and magnetic properties of the whole system can be seen in the overlaps of their electronic density of states with the eigenstates of the graphene layer.[91]. Figure 19 shows the spin-polarized DOS of the adsorbed CoIr dimer in comparison with the SVGraphene. In the DOS of the SVGraphene the pronounced V_π states can be seen. For this case these states are slightly shifted towards lower energies.

The local DOS of the 3d and 5d atoms are presented as well. The totat local DOS of Ir atom contributes to the total DOS, mainly for lower energies. The total local DOS of Co atom has minor contribution, compared to the one of Ir atom. The most pronounced input strengthens the region for lower energies around Fermi level. A sharp relatively large peak appears at the Fermi level, suggesting higher magnetic behaviour. The contribution to this state comes mainly from the Ir atom.

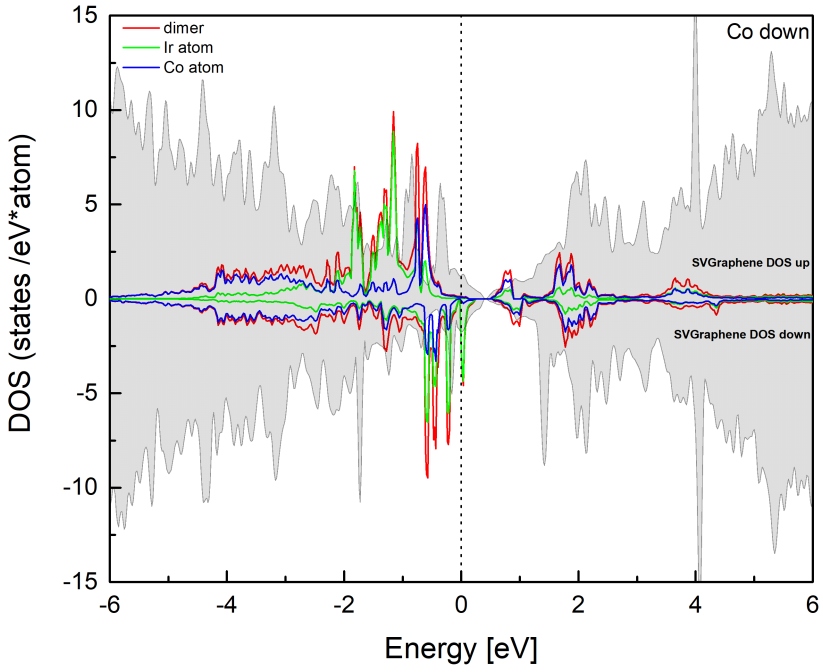

Figure 19 | Spin-polarized scalar-relativistic total and local DOS for CoIr dimer and total single vacancy graphene DOS. Dashed line shows the Fermi level.

In addition, a flat (parallel) adsorption configurations were also examined for the CoIr dimer. The relaxation processes led to a similar configuration where the dimer was positioned in the middle of the vacancy. The dimer remained connected with the graphene layer through the Co atom with the Ir atom holding a certain angle with the graphene plane. However these configurations were energetically disfavoured and not considered in further studies in this thesis.

Ir down

Second configuration considered in the calculations for the dimer was the case of Ir atom bound to the graphene layer (the Co and Ir atoms were switched in the primary set-up). The initial positions and conclusive relaxed structure can be seen in the Figure 20. The position for the dimer was again preferred in the centre of the vacancy in an upright configuration. The Ir atom remained bonded to the C atoms in the graphene plane and Co atom stayed in perpendicular position, with small rotation from the dimer axes.

Scalar-relativistic calculations show the Ir-Co distance to be 2.38 Å , which is again slightly larger than the dimer length in gas-phase as well as in the case for the CoIr dimer discussed above. The C atoms surrounding the vacancy migrated closer to the centre of the position of missing atom, which corresponds with previous theoretical and experimental investigations. The distance between the graphene layer and the Ir atom is 1.92 Å, making the Ir atom stand again above the level of C atoms. The higher positioned Co atom in the dimer, is 3.85 Å above the graphene layer. The distances for this configuration are larger than for the previous case.

The binding energy of graphene with the dimer being 6.88 eV/dimer, which is bigger than for the previous setup. The magnetic behaviour of this configuration is showing higher total magnetic moment, that is 1.83 μ_B, where the Ir atom contributes with 0.08 μ_B and Co atom with 1.97 μ_B. C atoms that are directly connected to the Ir atom show double magnetic spin moment of 0.02 μ_B than for the previous case, however situation remains same for the further C atoms from the vacancy and the graphene layer magnetic state remains unchanged as well.

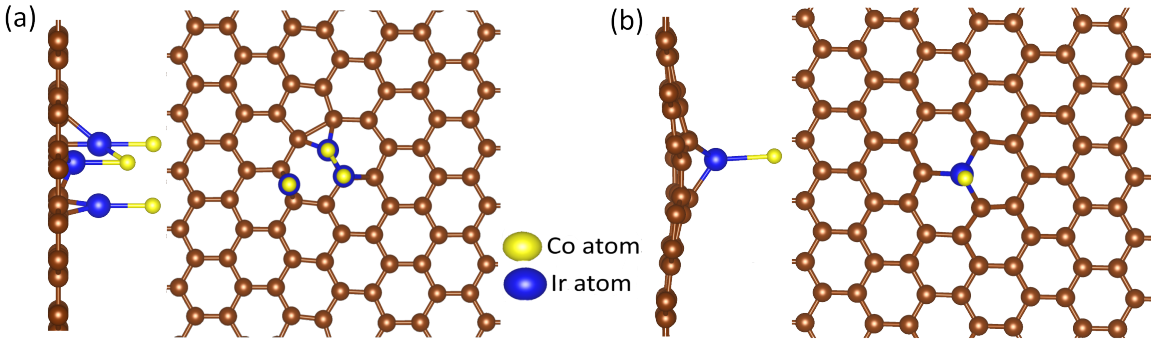

Figure 20 | IrCo dimer with Ir atom bound to the graphene sheet. The initial positions are shown in the panel (a) and the final position after relaxation is shown in the panel (b).

The Figure 21 presents the total and local DOS for the IrCo dimer with comparison to the SV-Graphene layer. There is an important contribution to the total DOS from Co atom, which lies on the Fermi level in the form of a sharp peak. The region around the Fermi level shows two significant peaks. All these states come from the Co atom. Just like for previous formation, the total DOS is strong for lower energies. In total, the DOS contribution is lower for this configuration with the respect to the previous case.

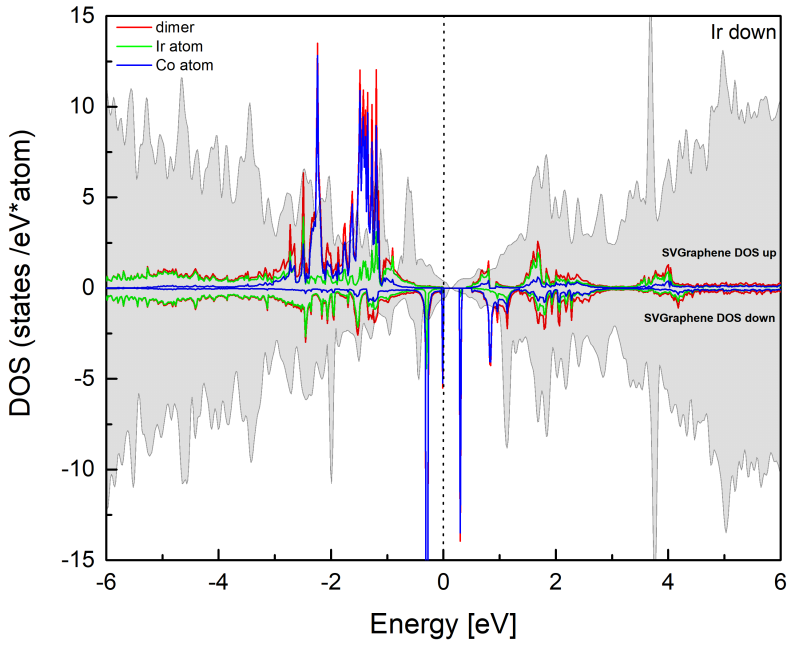

Figure 21 | Spin-polarized scalar-relativistic total and local DOS for IrCo dimer and total single vacancy graphene DOS. Dashed line shows the Fermi level.

A parallel adsorption configurations were examined as well. The Co atom migrated above the level of Ir atom, showing that the upright configuration is again preferred. However the relaxations led to configurations energetically less stable than all previous cases and were not further studied.

For transition metal homoatomic dimers, it have been already demonstrated that the nature of the eigenstates in the vicinity of the Fermi level can explain the change in magnetic properties and the variation of the MAE. [81]. Previous results also show the eigenvalue spectra of IrCo dimers supported by graphene layer. [91] In this work the authors shown that the large MAE in the system is caused by the difference in single occupied δ_d^* level which is split under the SOC.

2.3.2. N doped graphene layer with IrCo dimer to the graphene layer

The same process was used in the calculations for the IrCo dimer adsorbed on nitrogen doped SV-Graphene.Two main configurations of the dimer are further considered. First one is the case for Co atom bound to the nitrogen atoms surrounding the vacancy. The second is for the Ir atom bound to the nitrogen doped vacancy.

Co down

The initial positions and relaxed structure of the CoIr dimer positioned perpendicular to the graphene layer with the Co atom bonded to the N atoms in graphene are shown in Figure 22. For this configuration the dimer relaxed in all cases to the centre of the vacancy and remained in the upright configuration. The binding energy for the dimer on N-SVGraphene is 4.12 eV/dimer. This energy is slightly smaller than the one for undoped SVGraphene layer with CoIr and IrCo dimer, respectively. The distance between atoms of the dimer when adsorbed on the N-SVGraphene layer is 2.12 Å, which is similar with the length of the dimer in the gas-phase.

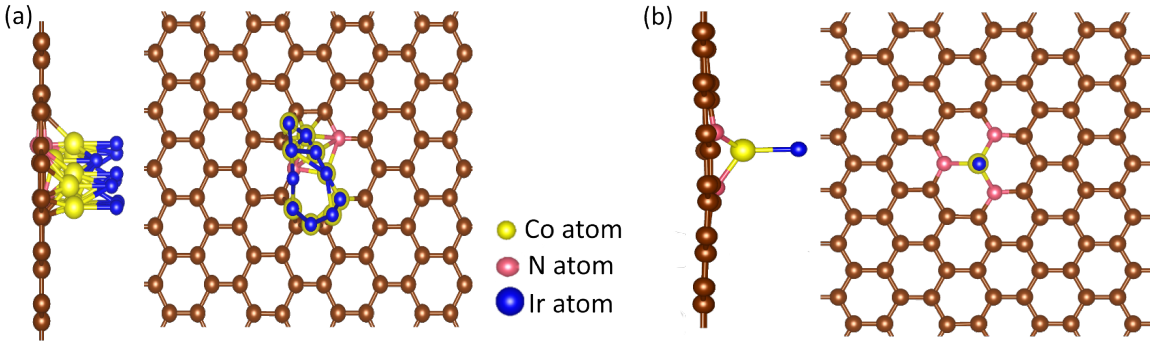

Figure 22 IrCo dimer with Ir atom bound to the N doped graphene sheet. The initial positions are shown in the panel (a) and the final position after relaxation is shown in the panel (b).

The relaxed C-C distance in the N doped graphene layer is around 1.45 Å, which is in a very good agreement with the calculated distance for the single vacancy graphene and pristine graphene layer. The length between doped N atoms with the C atoms in plane is 1.34 Å. In this case the nitrogen atoms surrounding the vacancy, did not migrate to its centre and moved out of it. The distances for the N atoms bonded to the Co atom are 2.1 Å. Such length is showing higher positioned Co atom than for the undoped cases. For both examples, the Co atom is above the average level of graphene plane. The Ir atom is 3.8 Å above the graphene plane in this configuration.

The magnetic behaviour of the structure is described by the magnetic moment of 1.07 μ_B with the contribution from Co atom of the size 0.38 μ_B and 0.72 μ_B from Ir atom. The magnetic moments of N atoms are almost 0 and the same values are exhibited by the C atoms in graphene layer.

The effect of the support on the electronic and magnetic properties of the system are different due doped nitrogen atoms in the graphene single vacancy. The Figure 23 shows the spin-polarized DOS of the N-SVGraphene and the adsorbed CoIr dimer on top. The total and local DOS of the 3d and 5d atoms are presented as well. The effect of nitrogen contribution to the total DOS is lowered when the dimer is present in the structure. However the configuration of CoIr dimer on the N-SVGraphene layer shows occurrence of well pronounced states in the region of Fermi level. The contribution for total DOS is similar for both of the transition metal atoms. In the energy region from -1 to 0 eV the dominance of Ir atom is shown. The DOS results are supporting the calculated magnetic moments for the structure.

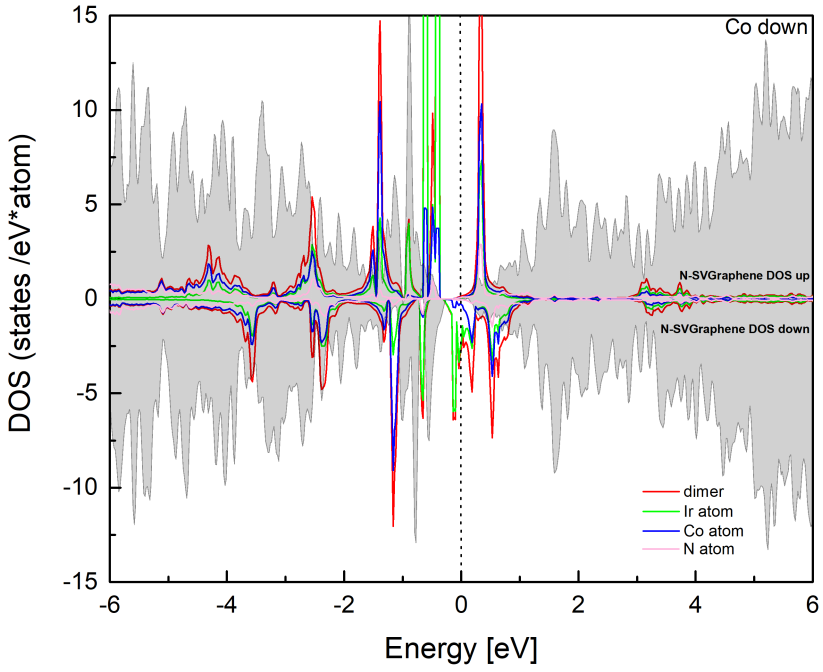

Figure 23 | Spin-polarized scalar-relativistic total and local DOS for CoIr dimer and total single vacancy graphene DOS. Dashed line shows the Fermi level.

Flat adsorption of different dimer positions were inspected as well. After the relaxation processes, the final configuration led to the same situation as the one for upright calculations. The ground energies of these systems were disfavoured and the systems were not considered in further steps.

Ir down

For the second configuration, the initial positions and relaxed structure of the dimer with the Ir atom bound to the N atoms in SVGraphene are shown in Figure 24. As can be seen from the Figure 24, the preferred position of the dimer is again for all cases in the middle of the vacancy. The binding energy for the N-SVGraphene with the dimer is 3.59 eV/dimer. This energy is similar to the previous case.

Scalar-relativistic calculations show that the length of the dimer is 2.19 Å, which is again, very similar to the length in the gas-phase. The distance of N atoms bound to the edges of the vacancy migrated away from its centre, causing the length of the C-N to be 1.37 Å. The bond length between the C atoms remained unchanged to the one of pure graphene layer. Ir atom is positioned 2.02 Å above the level of graphene and the distance of the Co atom from its substrate is 2.19 Å. The distances for this configurations are the shortest out of all described configurations.

The system exhibits magnetic moment of -1.59 μ_B, where the Ir atom shows magnetic moment -1.87 μ_B. The contribution of the Co atom to the total magnetic moment is 0.16 μ_B, which is minor, when compared to the input of Ir. C atoms that are connected to the N atoms show in this configuration slightly higher magnetic moments, that are 0.03 μ_B. However the rest of the C atoms in the system have magnetic moments close to zero and the magnetic state remains unchanged as well.

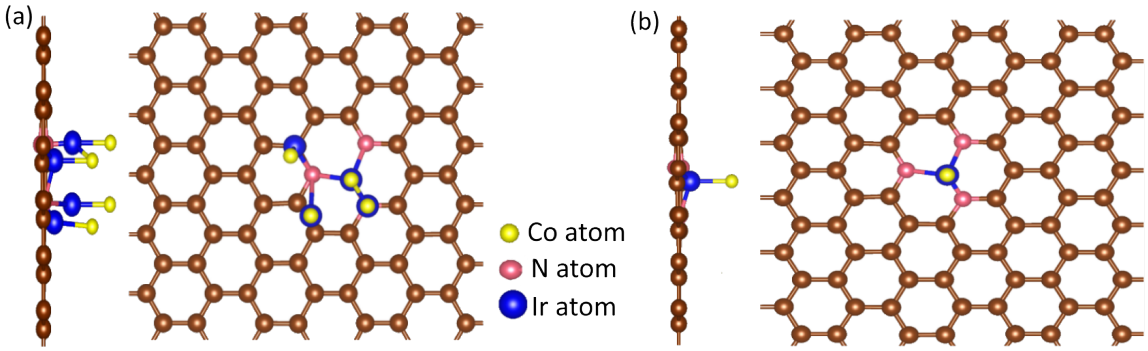

Figure 24 | IrCo dimer with Ir atom bound to the N doped graphene sheet. The initial positions are shown in the panel (a) and the final position after relaxation is shown in the panel (b).

The Figure 25 shows the spin-polarized DOS of the nitrogen doped single vacancy graphene and the total and local DOS of the adsorbed IrCo dimer. The results are showing very different properties than for the previous case. The contribution of the Co atom rules over the smaller one of the Ir atom. However, there is a significant peak on the Fermi level, which is suggesting the great magnetic response of the system, which is further discussed in the spin-orbital section.

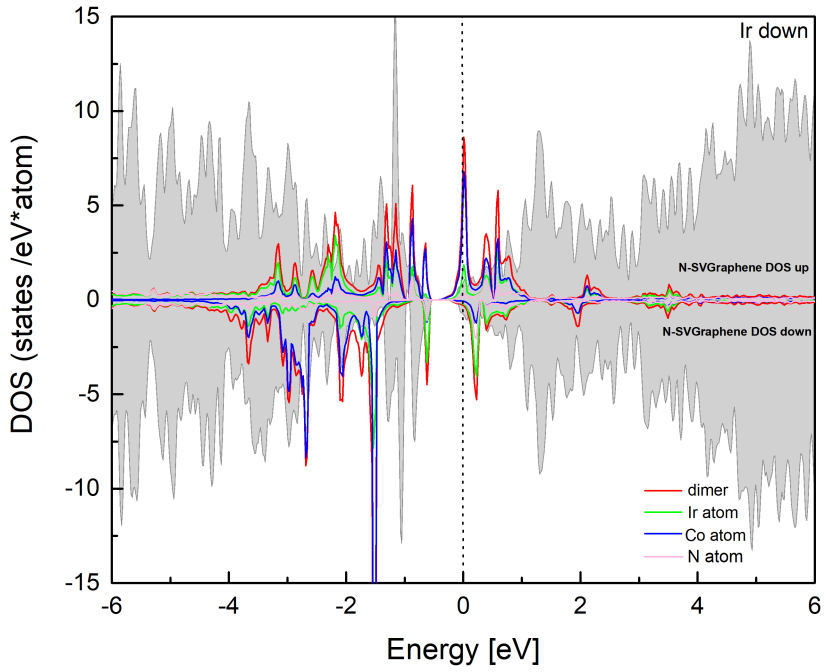

Figure 25 | Spin-polarized scalar-relativistic total and local DOS for IrCo dimer and total single vacancy graphene DOS. Dashed line shows the Fermi level.

In this case, the parallel adsorption of the dimer was also considered. The relaxation calculations led to complicated results, with different final positions, that were mostly physically impossible. That is why these systems were not studied further.

2.4. Spin-Orbital coupling and relativistic calculations

Calculations inluding the SOC have been performed for the stable ground-state configuration with different initial orientations of the magnetic moments. The alignments of the orientation were either with the dimer axis and so perpendicular to the defective graphene layer (along *z* direction) or perpendicular to the dimer and parallel to the defected graphene sheet (*x* and *y* directions).

2.4.1. Graphene layer with IrCo dimer bonded to the graphene layer

The MAE for the energetically most favourable configurations of the dimer/defective graphene complex is defined as the difference between the total energies calculated for easy and hard axis orientations of the magnetization. The values of MAE obtained in calculations with different cut-off energy for the dimer adsorbed on the SVGraphene are summarized in the Figure 26.

For the dimer with Ir atom bound to the SVGraphene layer, the MAE is weak and remains almost unchanged, regardless of the value cut-off energies and *k*-point mesh setup. However the situation is different for the case when the Co atom in the dimer is bound to the SVGraphene. The value of MAE is large for this configuration. Further is discussed only the setup of 600 eV energy cut-off with 11×11×1 *k*-point mesh.

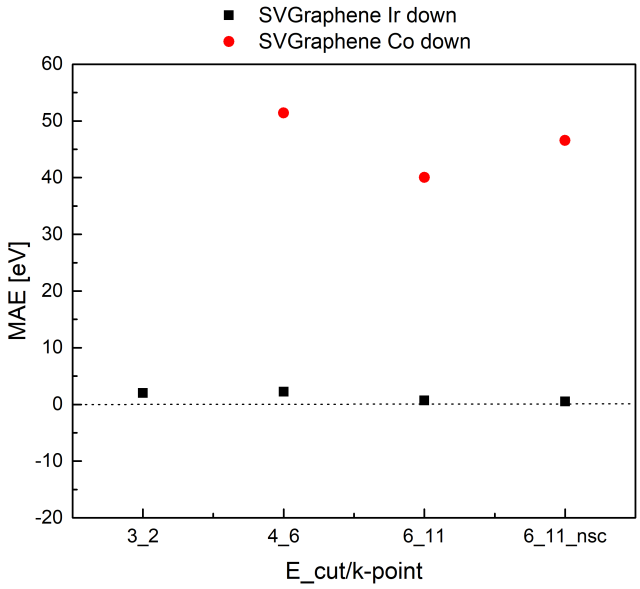

Figure 26 Overview of the calculated values of MAE for different energy cut-off and different *k*-point mesh setup. The first number tells the cut-off energy and second the *k*-point mesh choice.

Co down

The scalar-relativistic calculations for the CoIr dimer in the gas-phase predict a spin magnetic moment of 3.68 μ_B, with the Ir atom contributing with 2.07 μ_B and Co atom 1.61 μ_B. On the defective graphene the spin moment of the entire dimer-substrate complex with Co binding to the C atoms around vacancy differs.

The Table 1 presents the spin and orbital moments and anisotropies together with the MAE for the CoIr dimer in the scalar-relativistic (SR) and in the SOC calculations. For the SR calculations it can be seen that the total spin magnetic moment is reduced. Calculations including SOC strongly affect the magnetic moments of both atoms.

Calculations predict an easy magnetization direction perpendicular to the substrate and parallel to the dimer axis. From the Table 1, it can be seen that the rotation of the magnetization from easy to hard direction leads to a transition from a high moment (m_L = 1.7 μ_B) to a low moment (m_L = 0.7 μ_B), which is confirmed by the strong orbital anisotropy.

Structure	SR	Perpendicular SOC			In-plane SOC			Anisotropies		MAE
	m_S	m_S	m_L	m_{tot}	m_S	m_L	m_{tot}	δm_S	δm_L	
Co down	1.59	1.44	1.70	3.14	1.29	0.70	1.99	0.15	1.00	40.03

Table 1 The spin (m_S) and orbital (m_L) moments and the spin (δm_S) and orbital (δm_L) anisotropies, together with the calculated magnetic anisotropy energy of the CoIr dimer on the SVGraphene layer. All magnetic moments are given in μ_B. The magnetic anisotropy energy is given in meV.

Details of the local spin and orbital moments for the dimer atoms adsorbed on the defective graphene layer are shown in the Figure 27. The relativistic computations shown the spin and orbital moments different than those characterizing the free dimer. The orbital moment of Co atom in particular is nearly completely quenched by the interaction with the substrate. The Ir atom for the perpendicular magnetization shows enhanced both spin and orbital moment.

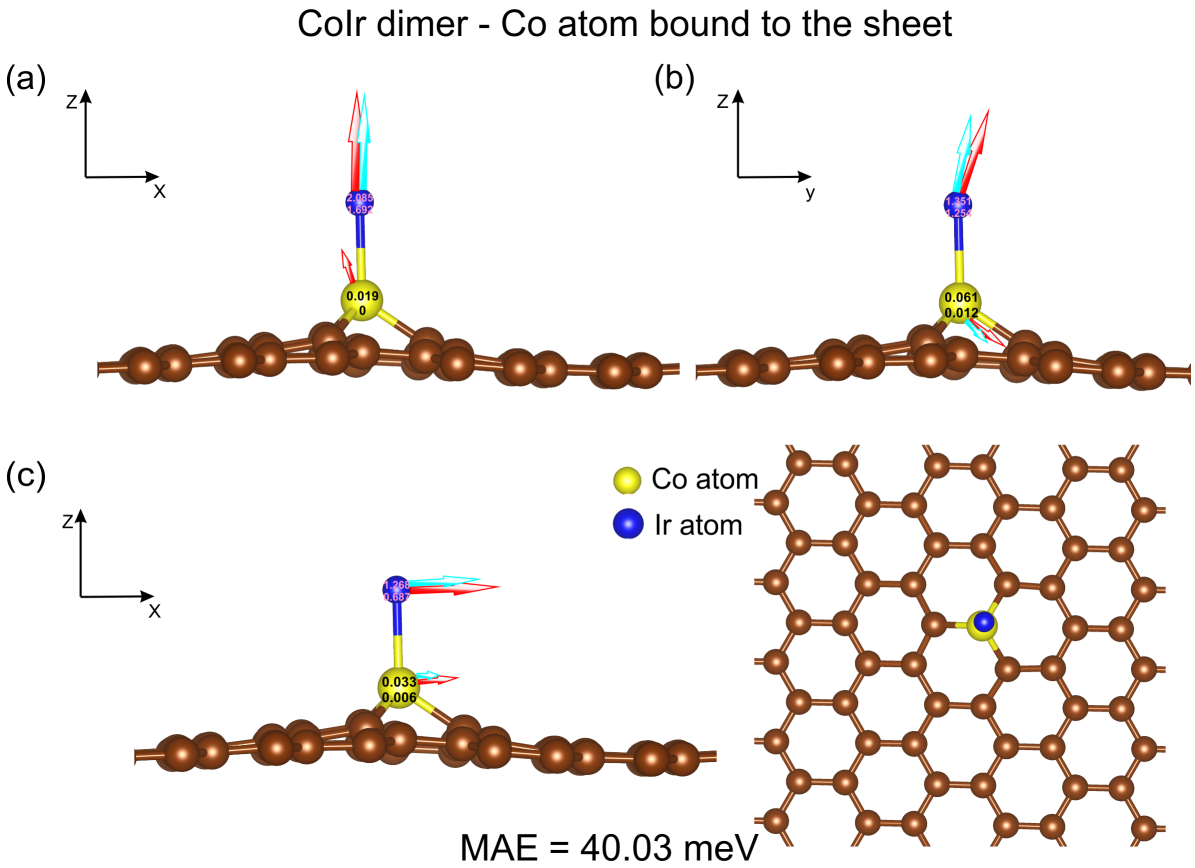

Figure 27 Magnetic structure of CoIr dimer supported on a graphene layer in the stable upright configuration. The different magnetization direction is displayed. The panels (a), (b), (c) demonstrate magnetisation along *x*, *y*, *z* directions, respectively. The magnetic anisotropy energy is listed underneath. Red (blue) arrows show the spin (orbital) magnetic moments. The numbers give the total spin (upper number), and orbital (lower number) magnetic moments in μ_B. Top view is shown in the inset in panel (c). The length of the arrows corresponding to the orbital momentum was multiplied by a factor of 10 for better visibility of vector orientation.

The MAE is 40.03 meV/dimer, which is in good agreement with previous theoretical works [87]. The orbital anisotropy, which is dominated by the contribution from Ir atom is the main factor determining the MAE of the CoIr dimer.

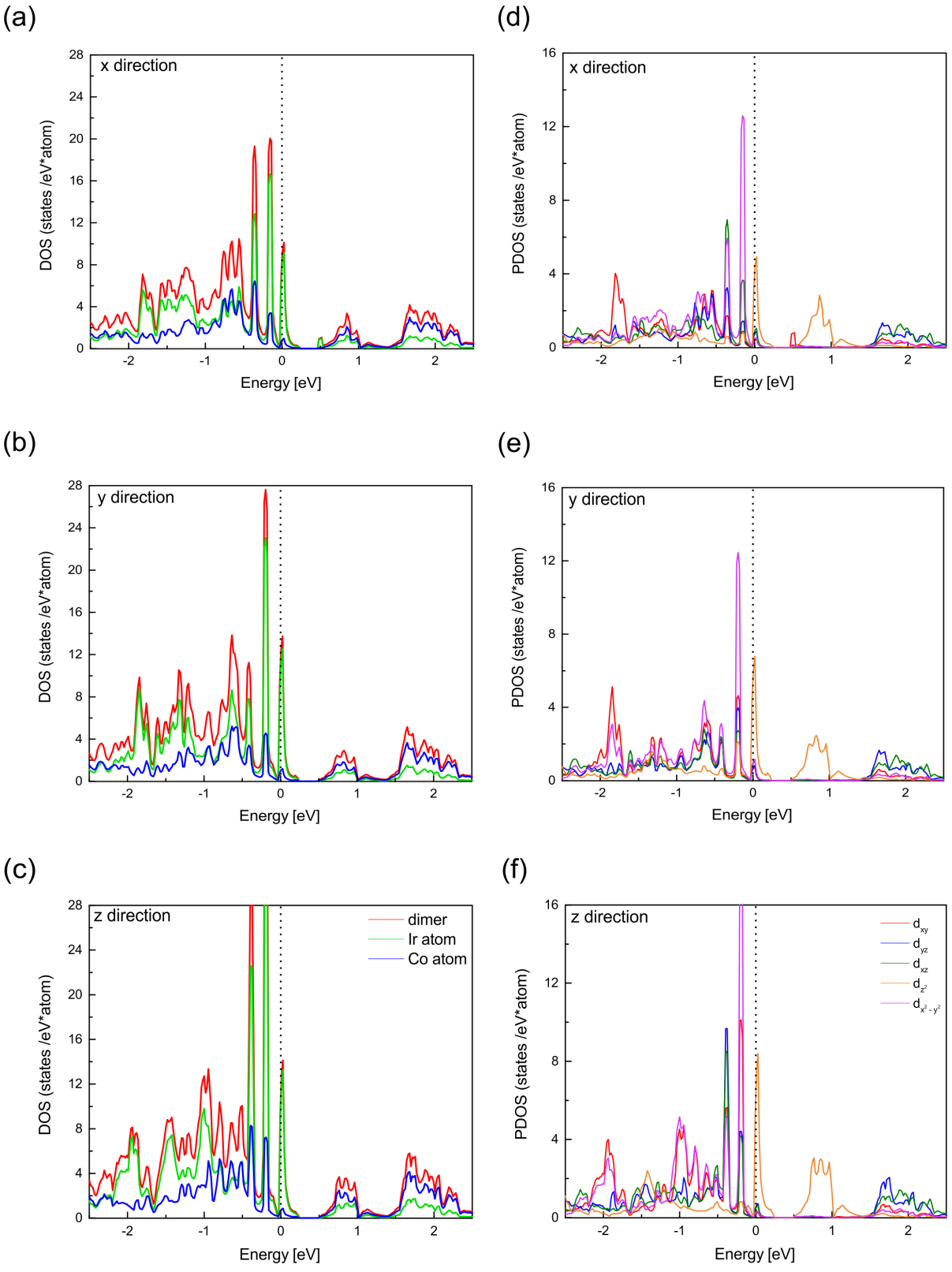

Figure 28 The Figure shows the total, side decomposed (panel (a), (b), (c)) and partial d-band (panel (d), (e), (f)) electronic DOS for CoIr dimer adsorbed on the SV-Graphene layer, calculated including SOC for different magnetization directions. For the magnetization parallel to the support and perpendicular to the dimer (along the *x* and *y* axis) the DOS are shown in the panels (a), (d), and (b),(e). For the magnetization perpendicular to the support and parallel to the dimer axis (along the *z* axis) are in the panels (c), (f). Dashed line shows the Fermi level.

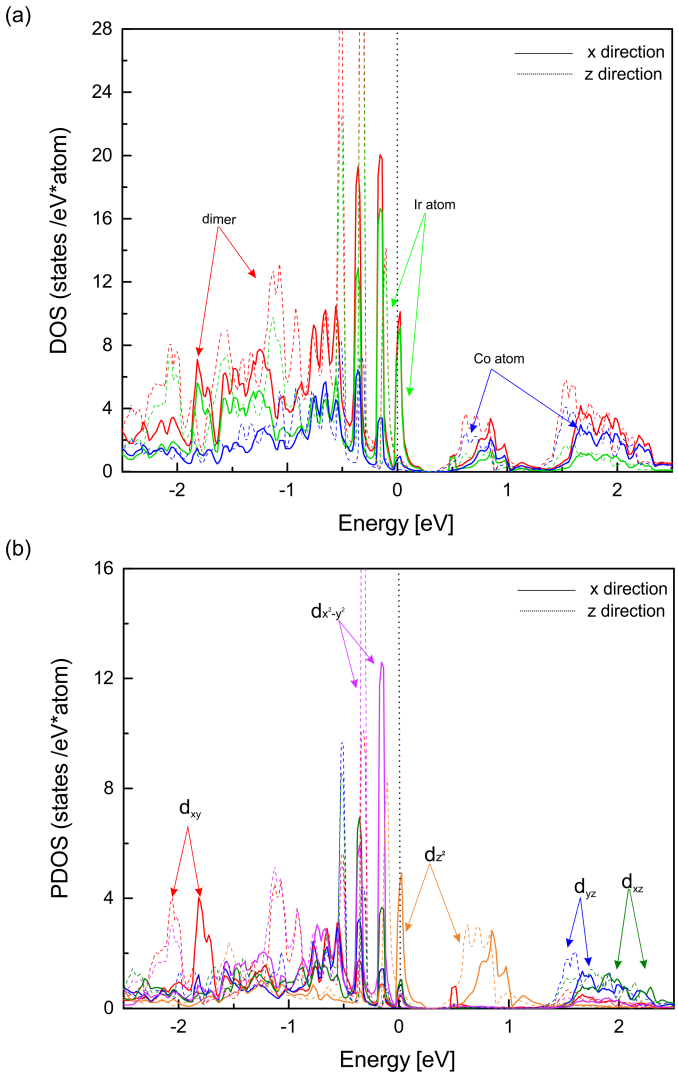

Figure 29 Comparison of the total, site decomposed (panel (a)) and partial d-band (panel (b)) electronic DOS for the CoIr dimer adsorbed on the defective graphene layer, for magnetization perpendicular to the support (*z*- direction, dash lines) and for magnetization parallel to the support (along the *x*-direction, full lines). Dashed perpendicular line shows the Fermi level.

It has been demonstrated that the nature of the eigenstates in the local area of the Fermi level can explain the different values of the MAE [9]. Also, it has been shown that the same argument can be used in order to explain the effects of the interaction with the substrate and so be responsible for the variations of the MAE [89]. It is argued that a weak force is created by forming chemical bonds between the d orbital states of the transition metal atom and the sp^2 hybrid states of the C atoms. The eigenstates of the 3d and 5d atoms undergo a bonding/anti-bonding splitting which leads to their broadening due to the hybridization with the substrate orbitals.[89]

To understand the forces for the development of the MAE in the system the total DOS and mainly partial d-band DOS of the transition metal atoms, close to the Fermi level and is plotted for the different direction of magnetization. The relativistic total and site-decomposed DOS of the adsorbed CoIr dimer are shown in the Figure 28 in the left column. The right column shows the partial d-states DOS (PDOS) calculated for magnetization along the *x*, *y* and *z* direction.

The decomposed partial d-states DOS on the dimer are split into three groups, δ_d (d_{xy}, $d_{x^2-y^2}$), π_d(d_{xz}, d_{yz} and σ_d(d_{z^2}). For the CoIr dimer adsorbed on the SVGraphene the most important point is the change in the occurrence of the δ_d partial DOS upon a change in the magnetization direction; for better comparison the *x* and *z* directions are presented in the Figure 29. This input comes mainly from the Ir atom. For the magnetization parallel to the graphene layer the partial DOS shows a peak at the Fermi level, coming from the σ_d contribution, which is for the perpendicular magnetization shifted towards the lower energies. For the perpendicular magnetization the SOC splitting gives rise in the

δ_d, while the π_d and σ_d states remain almost unaffected by the change in the direction of magnetization.

Ir down

In the case of Ir atom bound to the SVGraphene, the SR calculations for the whole complex reveal same spin magnetic moment, like for the case of Co atom bound to the defective graphene, that is 1.59 μ_B. The Table 2 shows the spin and orbital moments and anisotropies for the IrCo dimer as well as the MAE calculated for this system.

The calculations show that the easy magnetization direction is perpendicular to the graphene and parallel to the dimer axis. In comparison with previous configuration, there is a substantial change in the value of the orbital moment, which is almost 6 times lower for the perpendicular magnetization direction. The rotation of the magnetization from easy to hard axis changes very little the moments, which is also supported by both the spin (δm_S = 0) and orbital (δm_L = 0.03) anisotropy.

Structure	SR	Perpendicular SOC			In-plane SOC			Anisotropies		MAE
	m_S	m_S	m_L	m_{tot}	m_S	m_L	m_{tot}	δm_S	δm_L	
Ir down	1.59	1.83	0.27	2.10	1.83	0.24	2.07	0.00	0.03	0.69

Table 2 The spin (m_S) and orbital (m_L) moments and the spin (δm_S) and orbital (δm_L) anisotropies, together with the calculated magnetic anisotropy energy of the IrCo dimer on the SVGraphene layer. All magnetic moments are given in μ_B. The magnetic anisotropy energy is given in meV.

To further investigate the magnetic properties of the system, the local spin and orbital moments for the transition metal atoms adsorbed on the SVGraphene are displayed in the Figure 30. The calculations including the spin-orbit coupling demonstrate large spin moments on the Co atom. As can be seen from the Figure, the contribution from Ir atom is very small. The spin moment of Ir atom is nearly completely quenched and the orbital moment is almost equal to zero. Unlike the previous case however, the alighment of the spin and orbital moments are non-collinear, which can explain the very small value of magnetic anisotropy. The MAE is only 0.69 meV/dimer for this configuration.

In order to probe the MAE value further, the total, local and partial DOS of the dimer adsorbed on the SVGraphene layer are shown in the Figure 31. The relativistic total and local DOS of the dimer and its atoms are presented in the left column. The partial d-states DOS for the different magnetization orientation are displayed in the right column of the Figure. Small peak appears at the Fermi level, that is caused by the σ_d states. The Co atom contributes most to the total DOS of the dimer.

To compare the changes of inputs caused by the different magnetization direction, the results for *x* and *z* computations are shown in the Figure 32. When the magnetization is perpendicular to the substrate, the partial DOS shows that the SOC splitting adds to the δ_d and σ_d states. However, the changes in the density of states are very small, which as well explains the negligible MAE in this system. The π_d states remain unchanged.

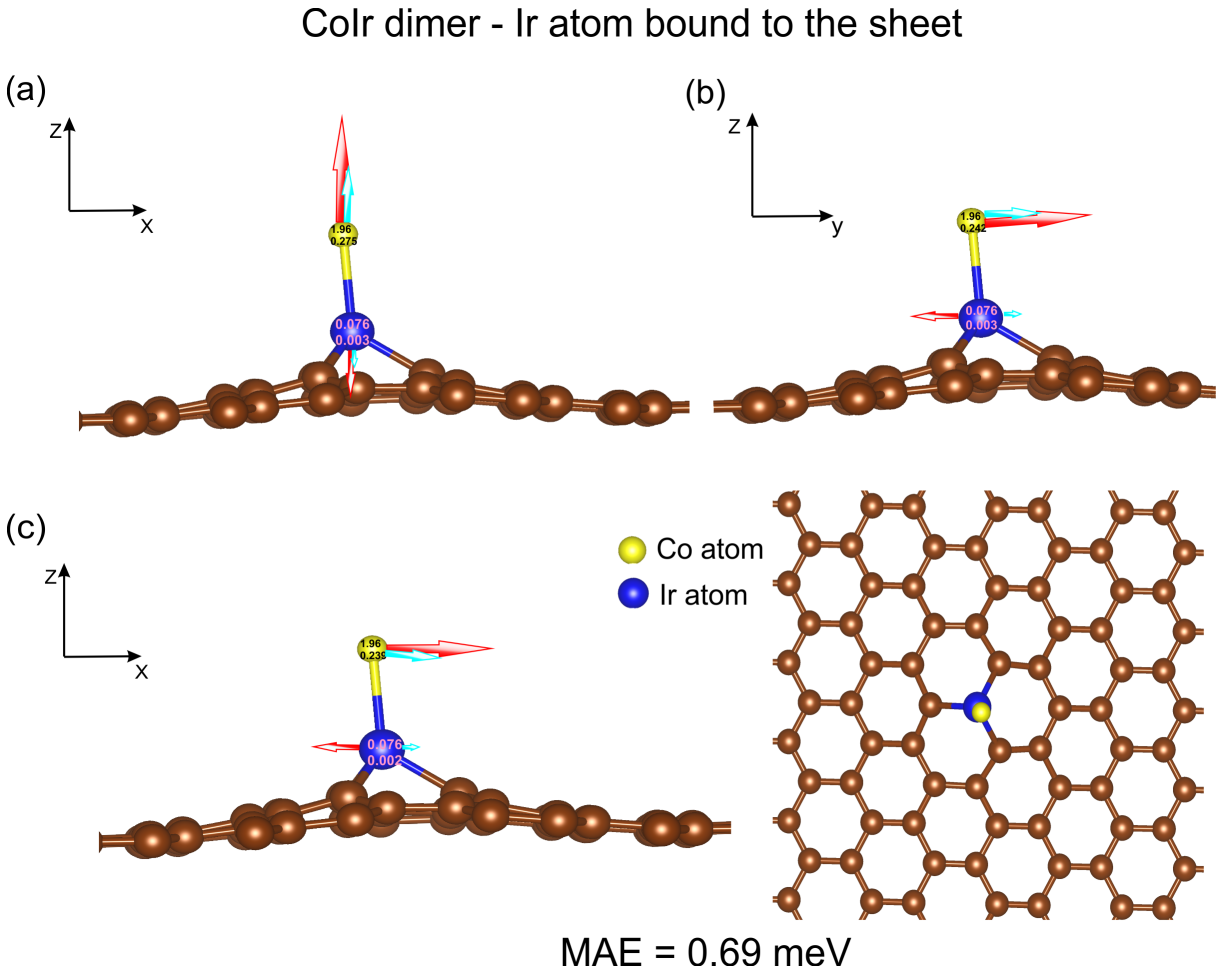

Figure 30 Magnetic structure of IrCo dimer supported on a graphene layer in the stable upright configuration. The different magnetization direction is displayed. The panels (a), (b), (c) demonstrate magnetisation along *x*, *y*, *z* directions, respectively. The magnetic anisotropy energy is listed underneath. Red (blue) arrows show the spin (orbital) magnetic moments. The numbers give the total spin (upper number), and orbital (lower number) magnetic moments in μ_B. Top view is shown in the inset in panel (c). The length of the arrows corresponding to the orbital momentum was multiplied by a factor of 10 for better visibility of vector orientation.

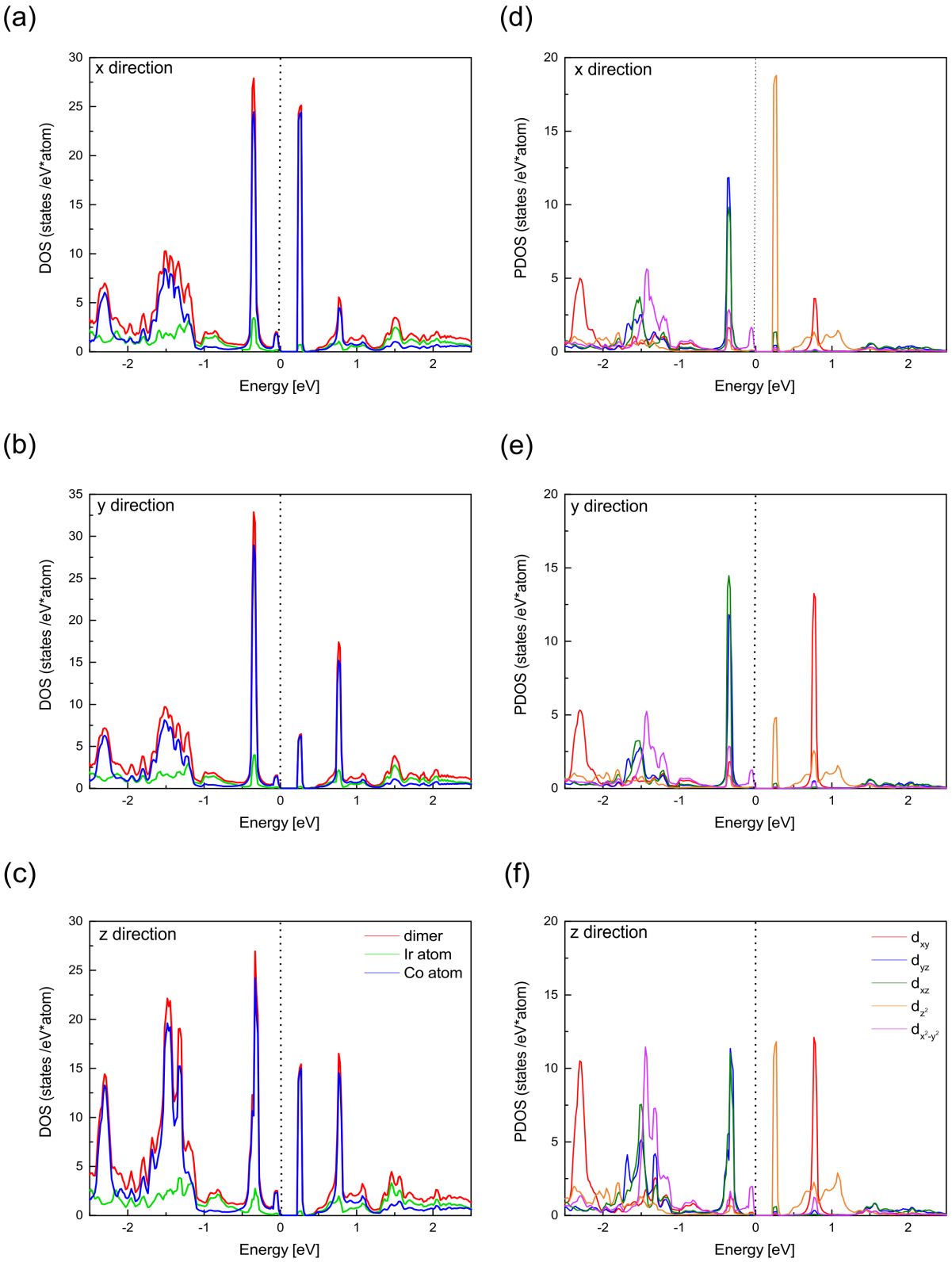

Figure 31 The Figure shows the total, side decomposed (panel (a), (b), (c)) and partial d-band (panel (d), (e), (f)) electronic DOS for CoIr dimer adsorbed on the SV-Graphene layer, calculated including SOC for different magnetization directions. For the magnetization parallel to the support and perpendicular to the dimer (along the *x* and *y* axis) the DOS are shown in the panels (a), (d), and (b),(e). For the magnetization perpendicular to the support and parallel to the dimer axis (along the *z* axis) are in the panels (c), (f). Dashed line shows the Fermi level.

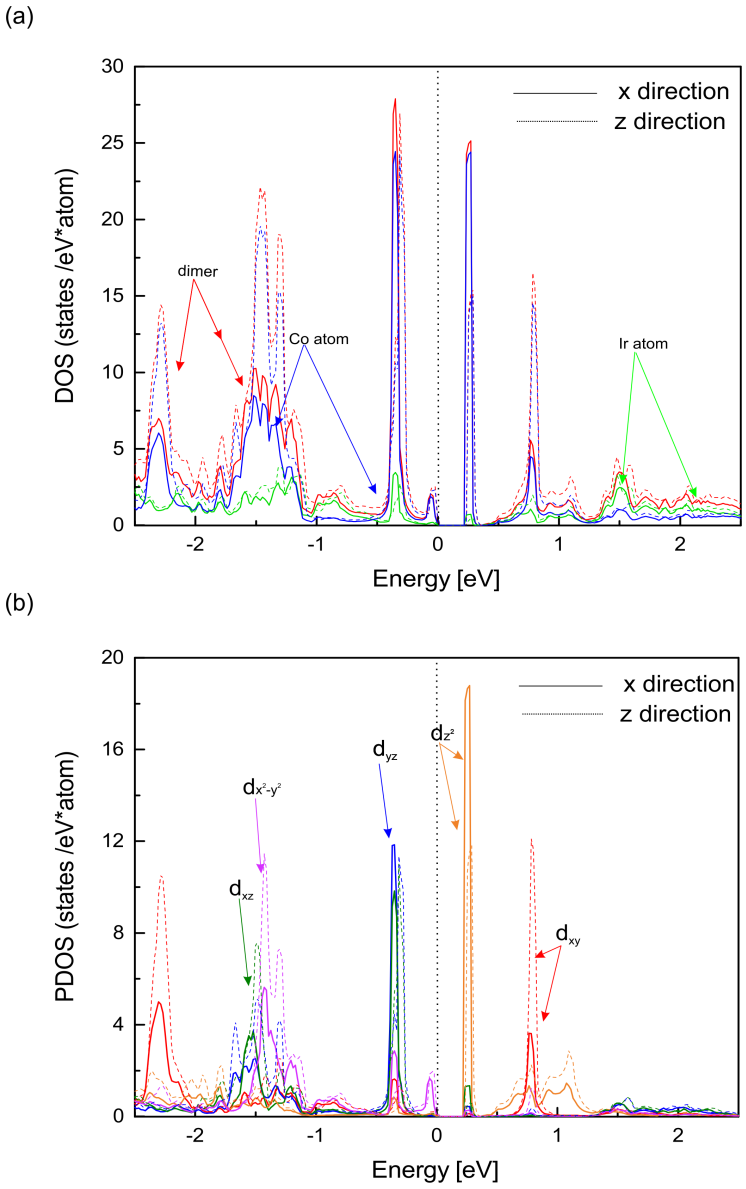

Figure 32 Comparison of the total, site decomposed (panel (a)) and partial d-band (panel (b)) electronic DOS for the IrCo dimer adsorbed on the defective graphene layer, for magnetization perpendicular to the support (*z*- direction, dash lines) and for magnetization parallel to the support (along the *x*-direction, full lines). Dashed perpendicular line shows the Fermi level.

2.4.2. N doped graphene layer with IrCo dimer to the graphene layer

For the system with nitrogenized single vacancy in the graphene layer same process was applied. The calculations for the given configuration were run for multiple energy cut-off and *k*-point mesh as well as the force theorem was applied in order to confirm the computational results. In addition, calculations with 500 eV cut-off energy and 9×9×1 *k*-point mesh were run in order to compare with results published in [87], where a double nitrogen doped vacancy in graphene layer was considered.

The values of MAE acquired from the relativistic calculations are presented in the Figure 33. The computations with nitrogen doped single vacancy show similar values of the MAE, which are either around 40 meV for the case of Ir atom bound to the N-SVGraphene, or around 10 meV for Co atom bound to the substrate. However for the Ir bound to the graphene layer the situation varies rapidly. The calculations show that the MAE for the setup 6_11 is around 300 meV. However the force theorem, where the system aligns accordingly to the preferable the magnetization, shows that the MAE is similar to the rest of measurements. That can be explained with the fact that the the magnetization direction causes changes in the whole complex and leads to de-magnetization of the system (6_ 11). The setup of 600 eV energy cut-off with 11×11×1 *k*-point mesh is further discussed.

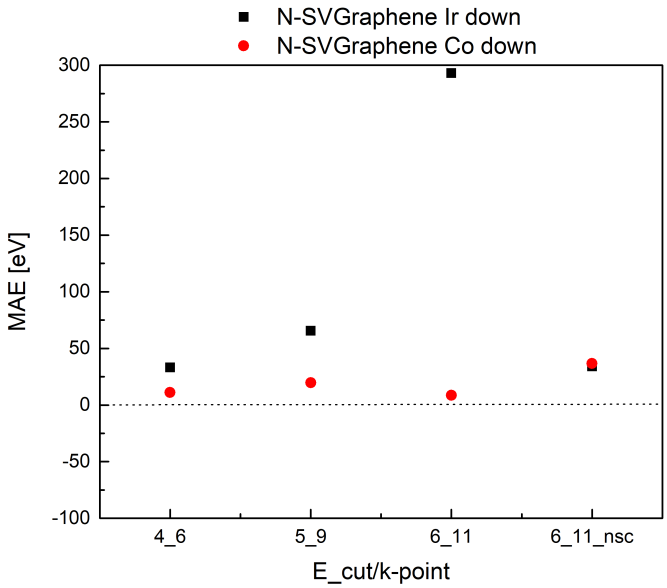

Figure 33 Overview of the calculated values of MAE for different energy cut-off and different *k*-point mesh setup.

Co down

The scalar-relativistic calculations for the dimer/N-SVGraphene complex show a spin moment of 1.59 μ_B. In comparison with the free standing dimer, the total magnetic moment is twice lower. The SR and SOC calculation results are summed up in Table 3. It presents the spin and orbital moments and spin and orbital anisotropies and the MAE for this system. For the relativistic calculations, the magnetic moments of both atoms are again strongly affected.

Structure	SR	Perpendicular SOC			In-plane SOC			Anisotropies		MAE
	m_S	m_S	m_L	m_{tot}	m_S	m_L	m_{tot}	δm_S	δm_L	
Co down	1.59	1.36	0.91	2.28	0.71	0.12	0.83	0.66	0.79	8.58

Table 3 The spin (m_S) and orbital (m_L) moments and the spin (δm_S) and orbital (δm_L) anisotropies, together with the calculated magnetic anisotropy energy of the CoIr dimer on the N-SVGraphene layer layer. All magnetic moments are given in μ_B. The magnetic anisotropy energy is given in meV.

The calculations predict an easy magnetization direction perpendicular to the substrate and parallel to the dimer axis. The Table 3 reveals that the rotation of the magnetization from easy to hard direction leads to a transition from a high spin and orbital moment (1.59 μ_B and 1.36 μ_B, respectively) to a low moments (0.71 μ_B and 0.12 μ_B, respectively), which is also confirmed by the strong spin and orbital anisotropy, δm_S = 0.66 μ_B and δm_L = 0.79 μ_B, respectively.

Details of the local spin and orbital moment for the dimer atoms adsorbed on the N-SVGraphene are shown in the Figure 34. The calculations including spin-orbit coupling reveal that unlike the undoped case, the contribution from the atoms is somewhat similar for the spin moments. However the orbital moment of Co atom is again nearly completely quenched by the interaction with the substrate. The Ir atom exhibits large spin and orbital moments for the perpendicular magnetization.

The different magnetization directions show collinear alignment of the magnetic moments. The MAE for this configuration is 8.58 meV. When compared with the results from [90], they obtained MAE 8 times larger. Calculations for the same setup, used in the article, however with only single vacancy, predict MAE of 20 meV. The double vacancy seems to be responsible for higher magnetic response of the system.

Further investigation of the magnetic properties of the CoIr/N-SVGraphene complex are done by the total, local DOS of the dimer and the partial d-band DOS of the transition metal atoms. The Figure 35 shows that the most pronounced contribution to the total DOS comes from the Ir atom, especially in the region of the Fermi level. Significant peak appears at the Fermi level for all the directions of magnetization.

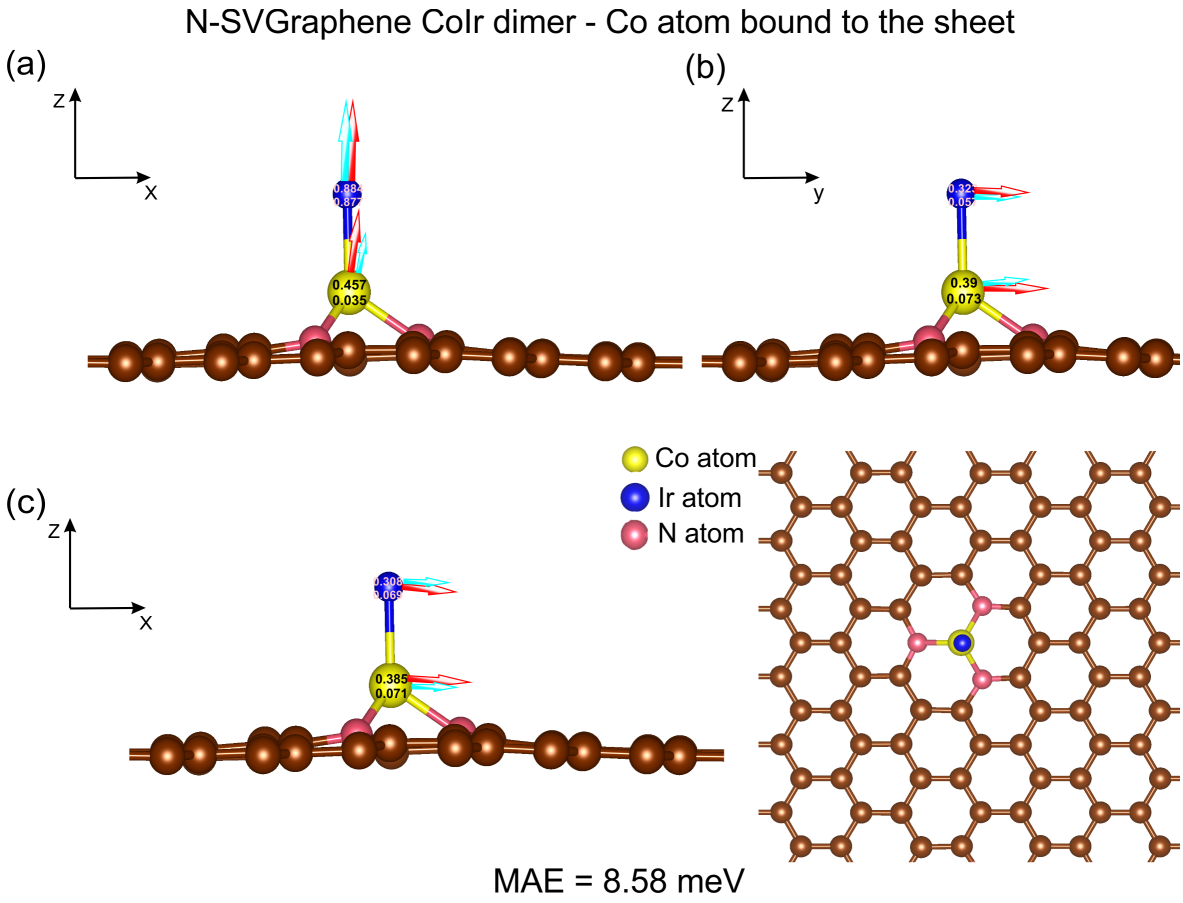

Figure 34 Magnetic structure of CoIr dimer supported on the N doped graphene layer in the stable upright configuration. The different magnetization direction is displayed. The panels (a), (b), (c) demonstrate magnetisation along x, y, z directions, respectively. The magnetic anisotropy energy is listed underneath. Red (blue) arrows show the spin (orbital) magnetic moments. The numbers give the total spin (upper number), and orbital (lower number) magnetic moments in μ_B. Top view is shown in the inset in panel (c). The length of the arrows corresponding to the orbital momentum was multiplied by a factor of 10 for better visibility of vector orientation.

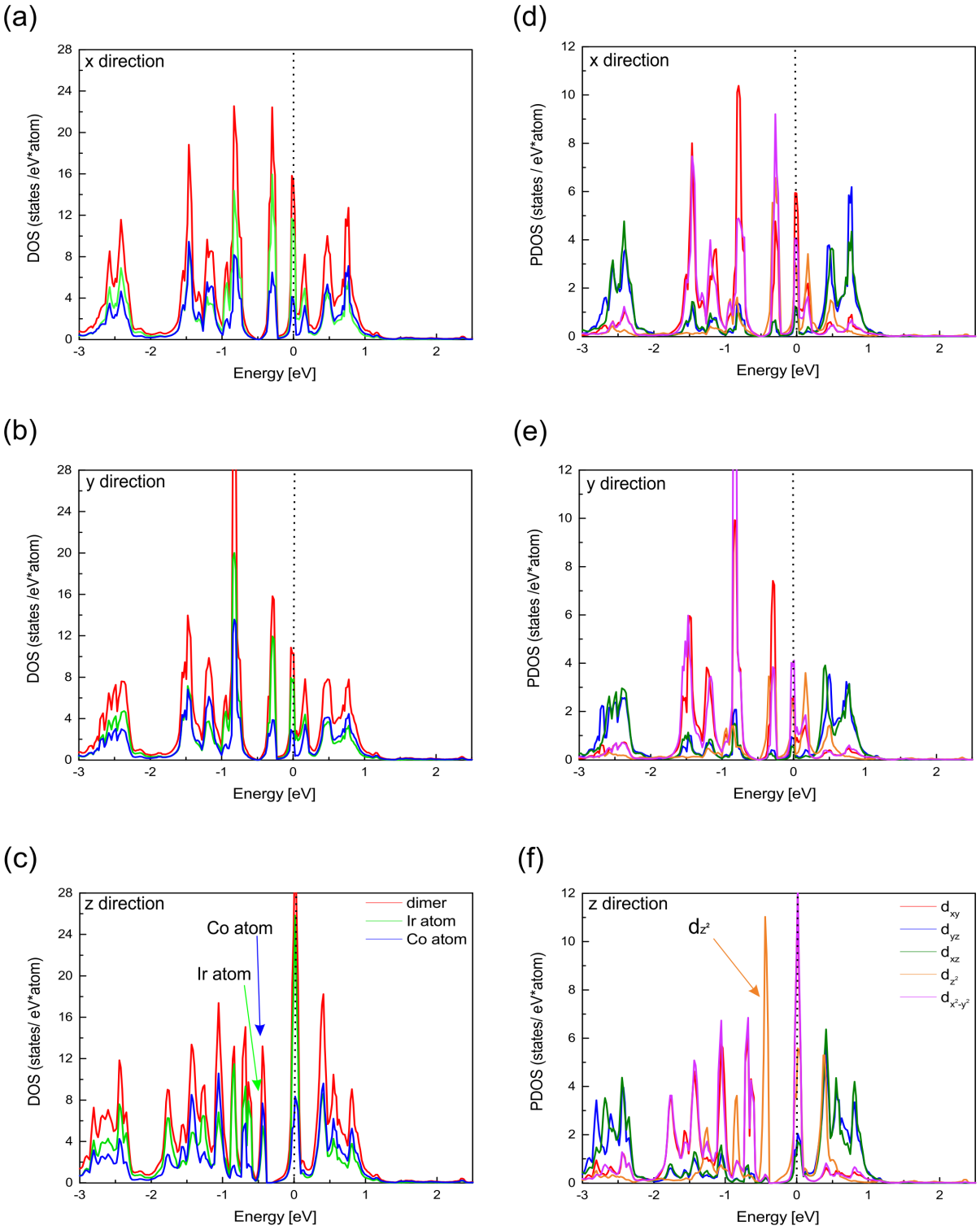

Figure 35 The Figure shows the total, side decomposed (panel (a), (b), (c)) and partial d-band (panel (d), (e), (f)) electronic DOS for CoIr dimer adsorbed on the N-SVGraphene layer, calculated including SOC for different magnetization directions. For the magnetization parallel to the support and perpendicular to the dimer (along the *x* and *y* axis) the DOS are shown in the panels (a), (d), and (b),(e). For the magnetization perpendicular to the support and parallel to the dimer axis (along the *z* axis) are in the panels (c), (f). Dashed line shows the Fermi level.

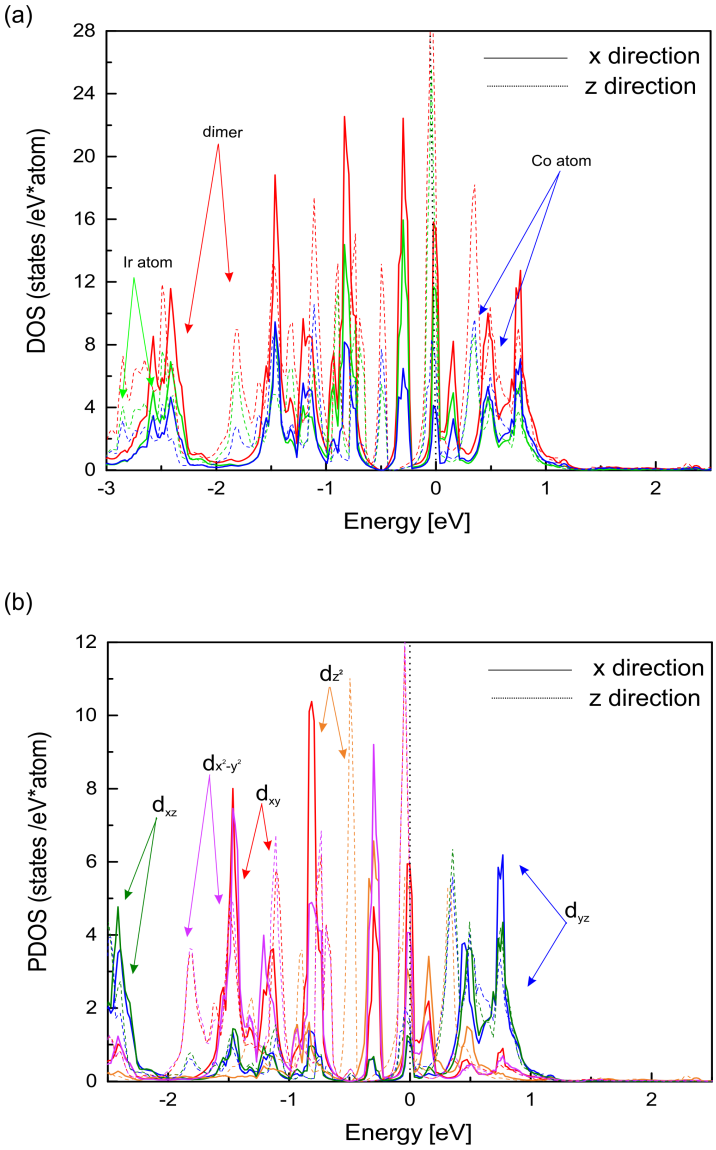

Figure 36 Comparison of the total, site decomposed (panel (a)) and partial d-band (panel (b)) electronic DOS for the CoIr dimer adsorbed on the N-SVGraphene layer, for magnetization perpendicular to the support (*z*- direction, dash lines) and for magnetization parallel to the support (along the *x*-direction, full lines). Dashed perpendicular line shows the Fermi level.

The comparison of the partial d-band DOS, displayed in the Figure 36, shows that the main input to the DOS states comes from the d orbitals of the dimer atoms. The high peak, appearing at the Fermi level is caused by the δ_d states. From the Figure, it is observed that the δ_d states change in the occurrence upon the change in the magnetization direction. The π_d and σ_d states remain mostly unchanged. Another important difference is the downshift of some peaks, mainly of the δ_d states. This transition shows the change in the occupations and accordingly the change of spin state. That is another reason for the relatively large MAE calculated for this system.

Ir down

The situation of the Ir atom bound to the N-SVGraphene is the most elusive out of all the described results. The SR calculations predict a magnetic moment of 1.59 μ_B. However the relativistic calculations show increase of the magnetic moment, shown in the Table 4. The structure exhibits great spin and orbital moments.

The easy magnetization direction is predicted to be perpendicular to the N-SVGraphene layer and parallel to the dimer axis. The Table shows that the rotation of the magnetization from easy to hard direction leads to a transition from a high moment to a low moment, which corresponds with the strong spin and orbital anisotropies, that are for this case higher than 1 μ_B.

Structure	SR	Perpendicular SOC			In-plane SOC			Anisotropies		MAE
	m_S	m_S	m_L	m_{tot}	m_S	m_L	m_{tot}	δm_S	δm_L	
Ir down	1.59	1.64	1.20	2.84	0.30	0.07	0.37	1.34	1.13	293.04

Table 4 The spin (m_S) and orbital (m_L) moments and the spin (δm_S) and orbital (δm_L) anisotropies, together with the calculated magnetic anisotropy energy of the IrCo dimer on the N-SVGraphene layer. All magnetic moments are given in μ_B. The magnetic anisotropy energy is given in meV.

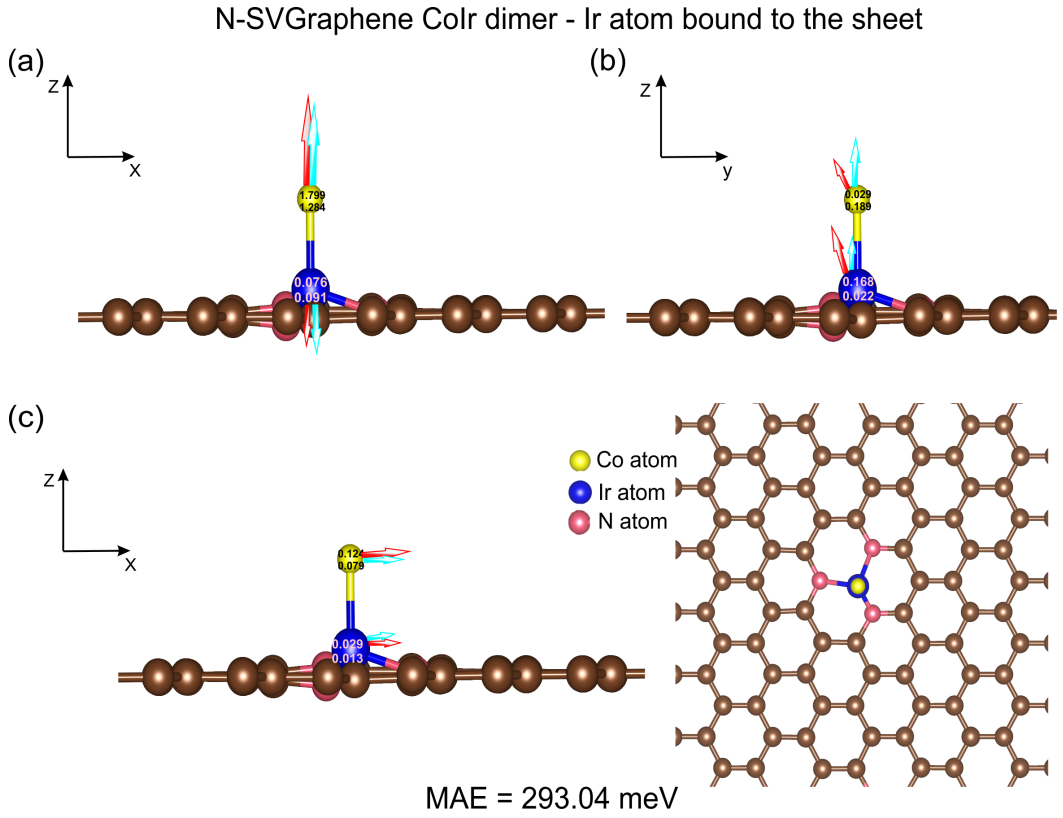

Figure 37 Magnetic structure of IrCo dimer supported on the N-SVGraphene layer in the stable upright configuration. The different magnetization direction is displayed. The panels (a), (b), (c) demonstrate magnetisation along *x*, *y*, *z* directions, respectively. The magnetic anisotropy energy is listed underneath. Red (blue) arrows show the spin (orbital) magnetic moments. The numbers give the total spin (upper number), and orbital (lower number) magnetic moments in μ_B. Top view is shown in the inset in panel (c). The length of the arrows corresponding to the orbital momentum was multiplied by a factor of 10 for better visibility of vector orientation.

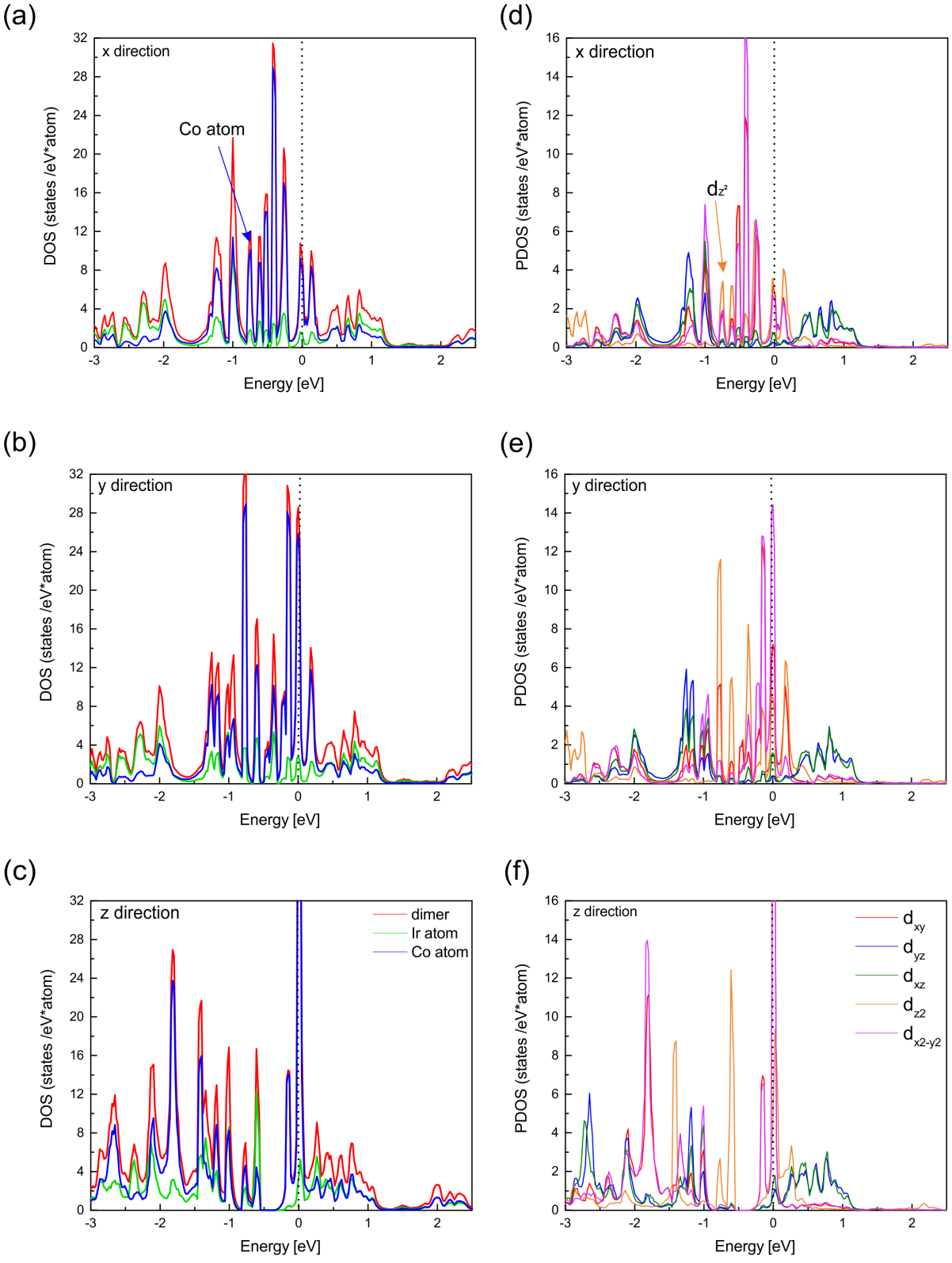

Figure 38 The Figure shows the total, side decomposed (panel (a), (b), (c)) and partial d-band (panel (d), (e), (f)) electronic DOS for IrCo dimer adsorbed on the N-SVGraphene layer, calculated including SOC for different magnetization directions. For the magnetization parallel to the support and perpendicular to the dimer (along the *x* and *y* axis) the DOS are shown in the panels (a), (d), and (b),(e). For the magnetization perpendicular to the support and parallel to the dimer axis (along the *z* axis) are in the panels (c), (f). Dashed line shows the Fermi level.

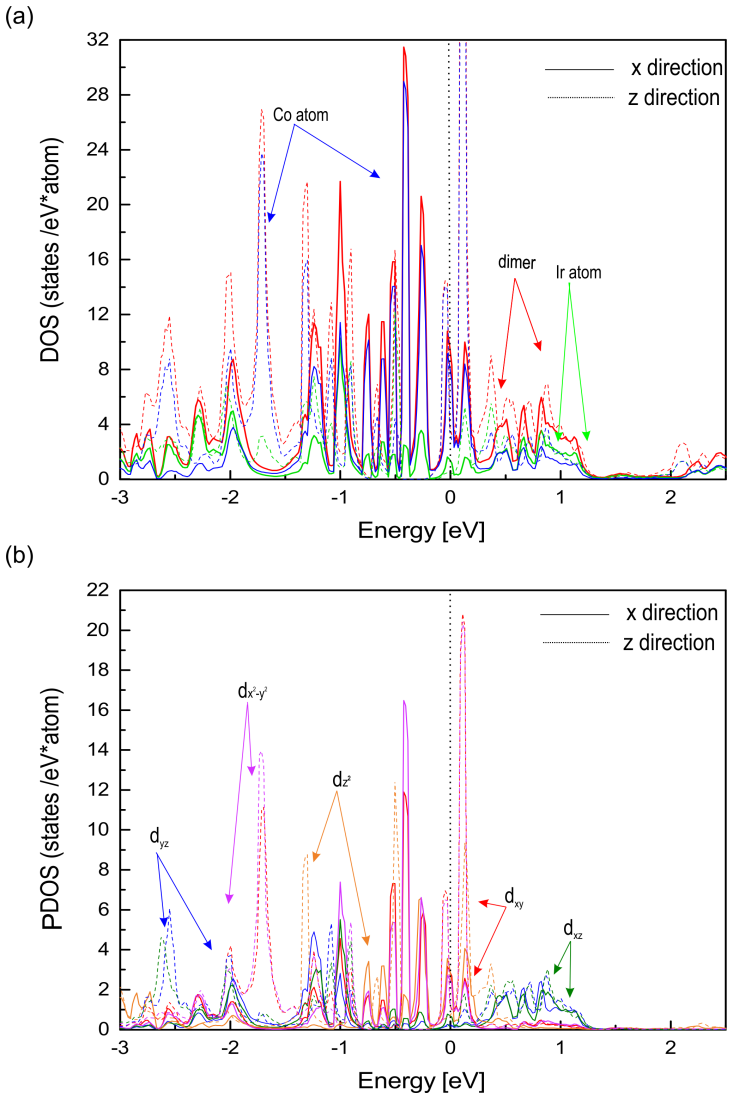

Figure 39 Comparison of the total, site decomposed (panel (a)) and partial d-band (panel (b)) electronic DOS for the CoIr dimer adsorbed on the N-SVGraphene layer, for magnetization perpendicular to the support (*z*- direction, dash lines) and for magnetization parallel to the support (along the *x*-direction, full lines). Dashed perpendicular line shows the Fermi level.

The contribution from the dimer atoms as well as their spin and orbital moments are presented in the Figure 37. As can be seen in the Figure 37, the main contribution to the magnetic moments comes from the Co atom. The spin and orbital moments of the Ir atom are almost completely quenched and are of insignificant value when compared to these of the Co atom. Another interesting situation occurs for the magnetization direction being perpendicular to the substrate. The spin and magnetic moments of the atoms are non-collinear, unlike for the parallel magnetization direction. Regardless that, the calculations for this system predict giant magnetic anisotropy (MAE = 293.04 meV).

The Figure 38 shows the total and local DOS states for the atoms of the dimer. Significant peak appears at the Fermi level for the y and mainly z magnetization direction. Like for the spin and orbital moments, the Ir atom contributes for the most part to the total DOS. When looking at the Figure 39 the changes in the occurrence of the d-states partial DOS upon a change in the magnetization direction are quite complex. It can be seen that the whole plot of the DOS along the *x* direction is completely shifted with respect to the DOS for *z* direction. The most pronounced changes are occurring at the Fermi level, caused by mostly the δ_d but also in some extent σ_d states. The shift also happens for the π_d states, however this is observed at the lower energies. These rapid changes that are predicted upon the reorientation of the magnetic moments could also be responsible for the giant magnetic anisotropy energy of the system.

However, the structures until now acquired an intrinsic magnetic moment that arises due the 2D confinement effects. The strong spin-orbit coupling for the 3d and 5d atoms together with the binding to the substrate led to a high magnetic anisotropy energy. However in this case, the spin-orbit coupling influences the structural stability as well. Similar results have already been observed in previous works [92, 93, 94]. Former investigations of structures based on 5d atoms show, that the change in the magnetization direction can lead to a complete change of the magnetic state [95]. That is why in this case the calculated giant magnetic anisotropy energy is in fact a de-magnetization energy.

Conclusion

In this thesis the $ab\ initio$ DFT calucutation were used to determine the magnetic properties of dimer, consisted of heavy 5d and strongly magnetic 3d atom, bonded onto free-standing defective graphene layer. Density functional calculations have been performed in the scalar-relativistic limit, self-consistent (including spin-orbit coupling) limit as well as the force theorem (non-self-consistent) calculations were used for different setup. The values of MAE in such configurations have been established, taking into account different initial configurations of the dimer. The interesting result of the studies show that the magnetic anisotropy energy remains similar for most of the variations in the computational setup. It has been demonstrated that for the dimer supported on the defective graphene, the strong binding of the TM atoms to the substrate stabilizes an out-of plane alignment for all cases.

In the first part of the calculations, the dimer/SVGraphene with Co atom bound to the substrate, complex showed consistent values of MAE of the order of 50 meV. The large values of MAE can be understood on a microscopic level, by considering the impact of the substrate (defective graphene) on the orbital/spin momentum and spin-orbit coupling of Ir and Co atoms forming the dimer. The spin and orbital moments of the Co atom are strongly quenched due to binding to the graphene layer. However, the adsorption is weakened by the binding within the dimer, which makes the Ir atom to behave like a free atom, leading to the strong anisotropy of the spin and orbital moment on the Ir atom. When the dimer position is switched and the Ir atom is bound to the SVGraphene layer, the system exhibits steady MAE of the value around 2 meV. This small number is explained by the non-collinear alignment of the spin and orbital moments of the dimer atoms as well as the almost non-existent spin and orbital anisotropies.

The second part involves the dimer to be adsorbed on the N-SVGraphene layer. For the case with Co atom bound to the substrate, the values of MAE differs more for different calculation setup. The MAE is in the order of 10 - 30 meV. This is explained by collinear alignment of the spin and orbital moments, together with the spin and orbital anisotropies. The important point also lies in the illustrated partial local densities of states for d orbitals of the dimer atoms. The σ_d state is more pronounced for the perpendicular magnetization direction. The variations of the values of MAE are also explained as a consequence of a discreet-like electronic density of states around the Fermi level. The more interesting results are for the Ir atom bound to the N-SVGraphene. The values differ by the order of hundreds of meV. This shows that the understanding of the magnetic anisotropy energy is more complex. The differences are caused by the fact, that the system in this configuration undergoes a structural stability. The change in the magnetization direction completely changes the magnetic state and causes de-magnetization of the system.

The results of theoretical studies described here are important for the understanding of magnetic properties of small system (TM dimers) interacting with monolayers of graphene substrates. They are relevant for design of structures displaying large MAE values and therefore appealing from the point of view of practical aspects requiring the possibility to manipulate the magnetic state at room temperature. Also, demonstration of a stable configuration of IrCo dimer attached to the graphene via vacancy may be stimulating for consideration of novel modulation techniques of 2D materials, introducing methods of inducing magnetic properties in intrinsically non-magnetic structures.

Nevertheless, further study is still needed. The free standing graphene, as a weakly reactive substrate, is still hard to obtain for further manipulation. The next step in the research of these systems should consider possible strong interaction between the dimer/graphene complex and metallic substrate.

Bibliography

[1] D. Sellmyer and R. Skomski, Advanced magnetic nanostructures, Springer, New York, 2006

[2] Gambardella, P., Rusponi, S., Veronese, M., Dhesi, S. S., Grazioli, C., Dallmeyer, A., ... & Carbone, C., Giant magnetic anisotropy of single cobalt atoms and nanoparticles, Science, 2003, 300(5622), 1130-1133.

[3] Chappert, Claude, Albert Fert, and Frédéric Nguyen Van Dau, The emergence of spin electronics in data storage, Nanoscience And Technology: A Collection of Reviews from Nature Journals, 2010, 147-157.

[4] Thompson, David A., and John S. Best, The future of magnetic data storage technology, IBM Journal of Research and Development 44.3, 2000, 311.

[5] Moser, A., Takano, K., Margulies, D. T., Albrecht, M., Sonobe, Y., Ikeda, Y., ... & Fullerton, E. E., Magnetic recording: advancing into the future, Journal of Physics D: Applied Physics, 2002, 35(19), R157.

[6] Brune, H. "H. Brune and P. Gambardella, Surf. Sci. 603, 1812, Surf. Sci. 603, 2009, 1812.

[7] Paulus, P. M., Luis, F., Kröll, M., Schmid, G., & De Jongh, L. J., Low-temperature study of the magnetization reversal and magnetic anisotropy of Fe, Ni, and Co nanowires, Journal of Magnetism and Magnetic Materials, 2001, 224(2), 180-196.

[8] Fritsch, D., Koepernik, K., Richter, M., & Eschrig, H., Transition metal dimers as potential molecular magnets: A challenge to computational chemistry, Journal of computational chemistry, 2008, 29(13), 2210-2219.

[9] Błoński, P., & Hafner, J., Magnetic anisotropy of transition-metal dimers: Density functional calculations, Physical Review B, 2009, 79(22), 224418.

[10] Strandberg, T. O., Canali, C. M., & MacDonald, A. H., Calculation of Chern number spin Hamiltonians for magnetic nano-clusters by DFT methods, Physical Review B, 2008, 77(17), 174416.

[11] Błoński, P., Lehnert, A., Dennler, S., Rusponi, S., Etzkorn, M., Moulas, G., ... & Hafner, J., Magnetocrystalline anisotropy energy of Co and Fe adatoms on the (111) surfaces of Pd and Rh, Physical Review B, 2010, 81(10), 104426.

[12] Lehnert, A., Dennler, S., Błoński, P., Rusponi, S., Etzkorn, M., Moulas, G., ... & Hafner, J., Magnetic anisotropy of Fe and Co ultrathin films deposited on Rh (111) and Pt (111) substrates: An experimental and first-principles investigation, Physical Review B, 2010, 82(9), 094409.

[13] Błoński, P., & Hafner, J., Magnetic anisotropy of heteronuclear dimers in the gas phase and supported on graphene: relativistic density-functional calculations, Journal of Physics: Condensed Matter, 2014, 26(14), 146002.

[14] Ostlund, N. S., & Szabo, A., Modern Quantum Chemistry: Introduction to advanced electronic structure theory, New edition edn: Dover Publications Inc., 1996.

[15] Griffiths, David J., Introduction to Quantum Mechanics, Upper Saddle River, NJ: Pearson Prentice Hall, 2005.

[16] Schrödinger, E., An undulatory theory of the mechanics of atoms and molecules, Physical review, 1926, 28(6), 1049.

[17] Born, Max., Quantum mechanics of collision processes, Zeit fur Phys, 1926, 38: 803.

[18] Pauli, Wolfgang, The connection between spin and statistics, Physical Review, 1940, 58.8: 716.

[19] Kohn, W., Nobel Lecture: Electronic structure of matter—wave functions and density functionals, Reviews of Modern Physics, 1999, 71(5), 1253.

[20] Thomas, L. H., The calculation of atomic fields. In Mathematical Proceedings of the Cambridge Philosophical Society, Cambridge University Press, 1927, Vol. 23, No. 5, pp. 542-548

[21] M. Born and R. Oppenheimer, On the quantum theory of molecules (german), Annalen der Physik, 1927, 389:457484.

[22] Fermi, Enrico, Statistical method to determine some properties of atoms, Rend. Accad. Naz. Lincei, 1927, 6.602-607: 5.

[23] Kittel, Charles, Paul McEuen, and Paul McEuen, Introduction to solid state physics, Vol. 8. New York: Wiley, 1996.

[24] Pavarini, Eva, Erik Koch, and Ulrich Schollwöck, eds, Emergent Phenomena in Correlated Matter: Autumn School Organized by the Forschungszentrum Jülich and the German Research School for Simulation Sciences at Forschungszentrum Jülich 23-27 September 2013, Lecture Notes of the Autumn School Correlated Electrons 2013. Vol. 3. Forschungszentrum Jülich, 2013.

[25] Dirac, Paul AM., Note on exchange phenomena in the Thomas atom, Mathematical Proceedings of the Cambridge Philosophical Society. Vol. 26. No. 3. Cambridge University Press, 1930.

[26] Perdew, J. P., & Zunger, A., Self-consistent equations including exchange and correlation effects Phys. Rev. B, 1981, 23, 5048-79.

[27] Perdew, J. P., & Schmidt, K., Density functional theory and its application to materials. Van Doren, 2001, V, 1-20.

[28] Capelle, K., A bird's-eye view of density-functional theory, arXiv preprint cond-mat/0211443, 2002.

[29] Hohenberg, P., & Kohn, W., Inhomogeneous electron gas, Physical review, 1964, 136(3B), B864.

[30] Kohn, W., & Sham, L. J., Self-consistent equations including exchange and correlation effects, Physical review, 1965, 140(4A), A1133.

[31] Perdew, J. P., & Kurth, S., Density functionals for non-relativistic Coulomb systems in the new century. In A primer in density functional theory (pp. 1-55), Springer, 2003, Berlin, Heidelberg.

[32] Fuentes-Cabrera, M., Baskes, M. I., Melechko, A. V., & Simpson, M. L., Bridge structure for the graphene/Ni (111) system: A first principles study, Physical Review B, 2008, 77(3), 035405.

[33] Kohn, W.; Sham, L. J., Quantum density oscillations in an inhomogeneous electron gas, Physical Review, 1965, 137.6A: A1697.

[34] Gross, E. K. U., & Kohn, W., Local density-functional theory of frequency-dependent linear response, Physical review letters, 1958, 55(26), 2850.

[35] Gell-Mann, Murray, and Keith A. Brueckner, Correlation energy of an electron gas at high density, Physical Review, 1957, 106.2, 364.

[36] Harmon, B. N., Antropov, V. P., Liechtenstein, A. I., Solovyev, I. V., & Anisimov, V. I., Calculation of magneto-optical properties for 4f systems: LSDA+ Hubbard U results, Journal of Physics and Chemistry of Solids, 1995, 56(11), 1521-1524.

[37] Dudarev, S. L., Botton, G. A., Savrasov, S. Y., Szotek, Z., Temmerman, W. M., & Sutton, A. P., Electronic structure and elastic properties of strongly correlated metal oxides from first principles: LSDA+ U, SIC-LSDA and EELS study of UO2 and NiO, Physica status solidi (a), 1998, 166(1), 429-443.

[38] Feibelman, P. J., Hammer, B., Nørskov, J. K., Wagner, F., Scheffler, M., Stumpf, R., ... & Dumesic, J., The CO/Pt (111) puzzle, The Journal of Physical Chemistry B, 2001, 105(18), 4018-4025.

[39] Tran, F., Laskowski, R., Blaha, P., & Schwarz, K., Performance on molecules, surfaces, and solids of the Wu-Cohen GGA exchange-correlation energy functional, Physical Review B, 2007, 75(11), 115131.

[40] Perdew, J. P., Burke, K., & Ernzerhof, M., Generalized gradient approximation made simple, Physical review letters, 1996, 77(18), 3865.

[41] Perdew, J. P., Chevary, J. A., Vosko, S. H., Jackson, K. A., Pederson, M. R., Singh, D. J., & Fiolhais, C., Atoms, molecules, solids, and surfaces: Applications of the generalized gradient approximation for exchange and correlation, Physical Review B, 1992, 46(11), 6671.

[42] Becke, A. D., Density-functional thermochemistry. III. The role of exact exchange. The Journal of chemical physics, 1993, 98(7), 5648-5652.

[43] Vosko, S. H., Wilk, L., & Nusair, M., Accurate spin-dependent electron liquid correlation energies for local spin density calculations: a critical analysis, Canadian Journal of physics, 1980, 58(8), 1200-1211.

[44] Giuliani, Gabriele, and Giovanni Vignale. Quantum theory of the electron liquid, Cambridge university press, 2005.

[45] Hamann, D. R., Schlüter, M., & Chiang, C., Norm-conserving pseudopotentials, Physical Review Letters, 1979, 43(20), 1494.

[46] Kerker, G. P., Non-singular atomic pseudopotentials for solid state applications, Journal of Physics C: Solid State Physics, 1980, 13(9), L189.

[47] Gross, Eberhard KU, and Reiner M. Dreizler, eds., Density functional theory, Vol. 337, Springer Science & Business Media, 2013.

[48] Hamann, D. R., Generalized norm-conserving pseudopotentials, Physical Review B, 1989, 40(5), 2980.

[49] Blöchl, Peter E., Generalized separable potentials for electronic-structure calculations, Physical Review B, 1990, 41.8, 5414.

[50] Blöchl, Peter E., Projector augmented-wave method, hysical review B, 1994, 50.24, 17953.

[51] Bjorken, J. D., & Drell, S. D., Relativistic quantum fields, McGraw-Hill, 1965

[52] Weinberg, S., The quantum theory of fields. Vol. 1: Foundations, Cambridge University Press, 1995.

[53] MacDonald, A. H., & Vosko, S. H., A relativistic density functional formalism, Journal of Physics C: Solid State Physics, 1979, 12(15), 2977.

[54] Ramana, M. V., Rajagopal, A. K., & Johnson, W. R., Effects of correlation and Breit and transverse interactions in the relativistic local-density theory for atoms, Physical Review A, 1982, 25(1), 96.

[55] Engel, Eberhard, and Seymour H. Vosko, Exact exchange-only potentials and the virial relation as microscopic criteria for generalized gradient approximations, Physical Review B, 1993, 47.20 (1993): 13164.

[56] Dyall, K. G., Grant, I. P., Johnson, C. T., Parpia, F. A., & Plummer, E. P., GRASP: A general-purpose relativistic atomic structure program, 1989, computer physics communications, 55(3), 425-456.

[57] Engel, E., Chevary, J. A., Macdonald, L. D., & Vosko, S. H., Asymptotic properties of the exchange energy density and the exchange potential of finite systems: relevance for generalized gradient approximations, Zeitschrift für Physik D Atoms, Molecules and Clusters, 1992, 23(1), 7-14.

[58] Engel, E., Keller, S., Bonetti, A. F., Müller, H., & Dreizler, R. M., Local and nonlocal relativistic exchange-correlation energy functionals: Comparison to relativistic optimized-potential-model results, Physical Review A, 1995, 52(4), 2750.

[59] Engel, E., & Dreizler, R. M., Density functional theory (p. 65), Springer-Verlag Berlin An., 2013

[60] Coey, John MD., Magnetism and magnetic materials, Cambridge University Press, 2010.

[61] Ibach, Harald, Physics of surfaces and interfaces, Vol. 12. Berlin: Springer, 2006.

[62] White, R. M., Quantum Theory of Magnetism, Magnetic Properties of Materials. ed., 2007.

[63] prof. RNDr. Jiří Vacík a kolektiv, Chemie - obecná a anorganická - pro gymnázia. SPN - pedgogické nakladatelství, a.s., 1995, p. 245.

[64] Tuček, J., Błoński, P., Ugolotti, J., Swain, A. K., Enoki, T., & Zbořil, R., Emerging chemical strategies for imprinting magnetism in graphene and related 2D materials for spintronic and biomedical applications, Chemical Society Reviews, 2018.

[65] Davis, S. D., Holland, S. D., Kingswell, M. S., Lavery, P. M., Smith, M. J., Thomas, C. M., ... & Hare, J. P., Exploring Carbon's Allotropy: A Pupil-Led Synthesis of Fullerenes from Graphite, Journal of Chemical Education, 2015, 92(7), 1263-1265.

[66] Makarova, T. L., Magnetic properties of carbon structures, Semiconductors, 2004, 38.6, 615-638.

[67] Yazyev, Oleg V., Emergence of magnetism in graphene materials and nanostructures, Reports on Progress in Physics 73.5, 2010, 056501.

[68] V. Georgakilas, J. A. Perman, J. Tucek, R. Zboril, Broad Family of Carbon Nanoallotropes: Classification, Chemistry, and Applications of Fullerenes, Carbon Dots, Nanotubes, Graphene, Nanodiamonds, and Combined Superstructures, Chem Rev., 2015, 115, 4744.

[69] Han, W., Kawakami, R. K., Gmitra, M., & Fabian, J., Graphene spintronics, Nature nanotechnology, 2014, 9(10), 794.

[70] Geim, Andre K., and Konstantin S. Novoselov, The rise of graphene, Nanoscience and Technology: A Collection of Reviews from Nature Journals, 2010, 11-19.

[71] Palacios, J. J., Fernández-Rossier, J., Brey, L., & Fertig, H. A., Electronic and magnetic structure of graphene nanoribbons, Semiconductor Science and Technology, 2010, 25(3), 033003.

[72] Novoselov, K. S., Fal, V. I., Colombo, L., Gellert, P. R., Schwab, M. G., & Kim, K., A roadmap for graphene, Nature, 2012, 490(7419), 192.

[73] Kan, Erjun, Zhenyu Li, and Jinlong Yang., Magnetism in graphene systems, Nano 3.06, 2008, 433-442.

[74] Singh, Ranber, Unexpected magnetism in nanomaterials, Journal of Magnetism and Magnetic Materials 346, 2013, 58-73.

[75] Błoński, P., Tucek, J., Sofer, Z., Mazánek, V., Petr, M., Pumera, M., ... & Zbořil, R., Doping with Graphitic Nitrogen Triggers Ferromagnetism in Graphene, Journal of the American Chemical Society, 2017, 139(8), 3171-3180.

[76] Kan, Erjun, Zhenyu Li, and Jinlong Yang, Graphene nanoribbons: Geometric, electronic, and magnetic properties, Physics and Applications of Graphene-theory - InTech, 2011.

[77] Galli, Giulia, Structure, stability and electronic properties of nanodiamonds, Computer-Based Modeling of Novel Carbon Systems and Their Properties, Springer, Dordrecht, 2010, 37-56.

[78] Son, Young-Woo, Marvin L. Cohen, and Steven G. Louie, Energy gaps in graphene nanoribbons, Physical review letters, 2006, 97.21, 216803.

[79] Tuček, J., Holá, K., Bourlinos, A. B., Błoński, P., Bakandritsos, A., Ugolotti, J., ... & Otyepka, M., Room temperature organic magnets derived from sp 3 functionalized graphene, Nature communications, 2017, 8, 14525.

[80] Saini, Deepshikha, Synthesis and functionalization of graphene and application in electrochemical biosensing, Nanotechnology Reviews, 2016, 5.4, 393-416.

[81] Błoński, Piotr, and Jürgen Hafner, Magneto-structural properties and magnetic anisotropy of small transition-metal clusters: a first-principles study, Journal of Physics: Condensed Matter, 2011, 23.13, 136001.

[82] Kresse, Georg, and Jürgen Furthmüller, Efficient iterative schemes for ab initio total-energy calculations using a plane-wave basis set, Physical review B, 1996, 54.16, 11169.

[83] Kresse, Georg, and D. Joubert, From ultrasoft pseudopotentials to the projector augmented-wave method, Physical Review B, 1999, 59.3, 1758.

[84] Vosko, Seymour H., Leslie Wilk, and Marwan Nusair, Accurate spin-dependent electron liquid correlation energies for local spin density calculations: a critical analysis, Canadian Journal of physics, 1980, 58.8, 1200-1211.

[85] KRESSE, G.; LEBACQ, O. VASP Manual, http://cms. mpi. univie. ac. at/vasp/vasp/vasp.

[86] Marsman, M., & Hafner, J., Broken symmetries in the crystalline and magnetic structures of γ-iron, Physical Review B, 2002, 66(22), 224409.

[87] Hu, Jun, and Ruqian Wu, Giant magnetic anisotropy of transition-metal dimers on defected graphene, Nano letters 14.4, 2014, 1853-1858.

[88] Ketabi, N., de Boer, T., Karakaya, M., Zhu, J., Podila, R., Rao, A. M., ... & Moewes, A., Tuning the electronic structure of graphene through nitrogen doping: experiment and theory, RSC Advances, 2016, 6(61), 56721-56727.

[89] Błoński, P., and J. Hafner, Cu (1 1 1) supported graphene as a substrate for magnetic dimers with a large magnetic anisotropy: relativistic density-functional calculations, Journal of Physics: Condensed Matter, 2014, 26.25, 256001.

[90] Chen, J. J., Wu, H. C., Yu, D. P., & Liao, Z. M., Magnetic moments in graphene with vacancies, Nanoscale, 2014, 6(15), 8814-8821.

[91] Błoński, P., & Hafner, J., Density-functional theory of the magnetic anisotropy of nanostructures: an assessment of different approximations, Journal of physics: Condensed matter, 2011, 21(42), 426001.

[92] Błoński, Piotr, and Jürgen Hafner, Geometric and magnetic properties of Pt clusters supported on graphene: Relativistic density-functional calculations, The Journal of chemical physics, 2011, 134.15, 154705.

[93] Huda, M. N., Niranjan, M. K., Sahu, B. R., & Kleinman, L., Effect of spin-orbit coupling on small platinum nanoclusters, Physical Review A, 2006, 73(5), 053201.

[94] Bruno, P., Tight-binding approach to the orbital magnetic moment and magnetocrystalline anisotropy of transition-metal monolayers, Physical Review B, 1989, 39(1), 865.

[95] Smogunov, A., Dal Corso, A., & Tosatti, E., Magnetic phenomena, spin-orbit effects, and Landauer conductance in Pt nanowire contacts: Density-functional theory calculations, Physical Review B, 2008, 78(1), 014423.

List of abbreviations

MAE	Magnetic Anisiotropy Energy
TM	Trantision Metal
DFT	Density Functional Theory
LDA	Local Density Approximation
LSDA	Local Spin Density Approximation
GGA	Generalised Gradient Approximation
ACM	Adiabatic Connection Method
PAW	Projector Augmented Wave
RDFT	Relativistic Density Functional Theory
QED	Quantum ElectroDynamics
RLDA	Relativistic Local Density Approximation
OPM	Optimized Potential Method
SOC	Spin-Orbit Coupling
GNRs	Graphene NanoRibbons
FM	Ferromagnetism
AFM	Anti-Ferromagnetism
VASP	Vienna Ab initio Simulation Package
SR	Scalar-Relativistic
SVGraphene	Single Vacancy Graphene
N-SVGraphene	Nitrogen doped Single Vacancy Grapehen
DOS	Density Of States
PDOS	Partial Density Of States

Supplementary information

Co down

Structure	SR	Perpendicular SOC			In-plane SOC			Anisotropies		MAE
	m_S	m_S	m_L	m_{tot}	m_S	m_L	m_{tot}	δm_S	δm_L	
Co down	1.59	1.46	1.7	3.15	1.3	0.7	2	0.15	0.99	51.41

Table S1 The spin (m_S) and orbital (m_L) moments and the spin (δm_S) and orbital (δm_L) anisotropies, together with the calculated magnetic anisotropy energy of the CoIr dimer on the SVGraphene layer. All magnetic moments are given in μ_B. The magnetic anisotropy energy is given in meV.

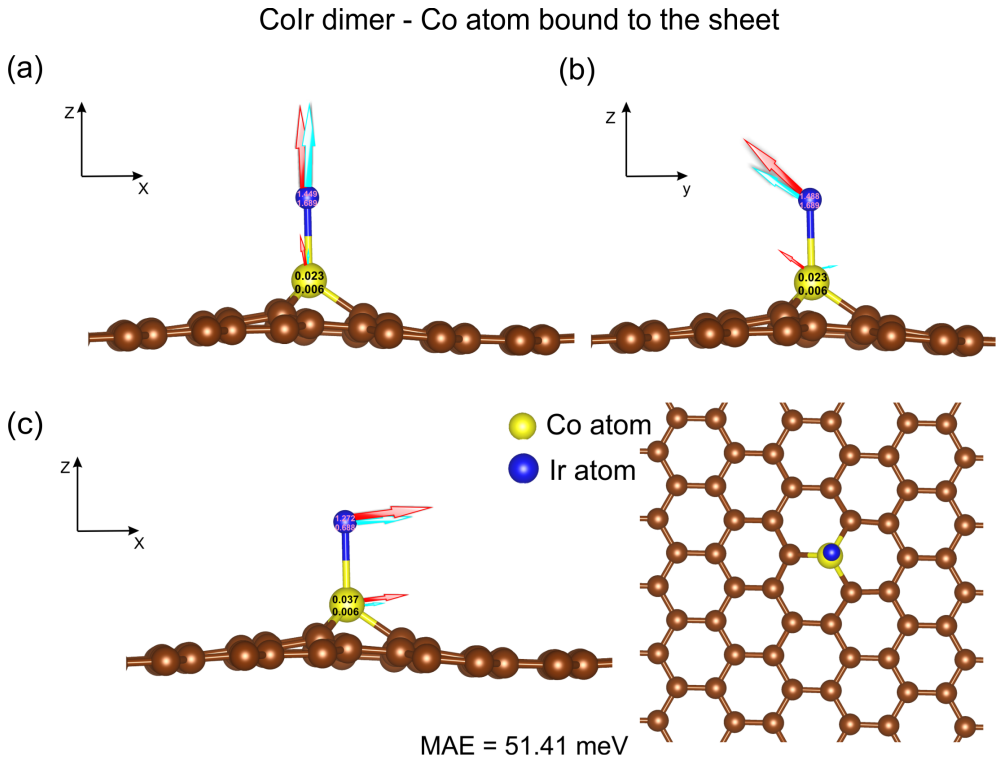

Figure S1 Magnetic structure of CoIr dimer supported on a graphene layer in the stable upright configuration. The different magnetization direction is displayed. The panels (a), (b), (c) demonstrate magnetisation along *x*, *y*, *z* directions, respectively. The magnetic anisotropy energy is listed underneath. Red (blue) arrows show the spin (orbital) magnetic moments. The numbers give the total spin (upper number), and orbital (lower number) magnetic moments in μ_B. Top view is shown in the inset in panel (c). The length of the arrows corresponding to the orbital momentum was multiplied by a factor of 10 for better visibility of vector orientation.

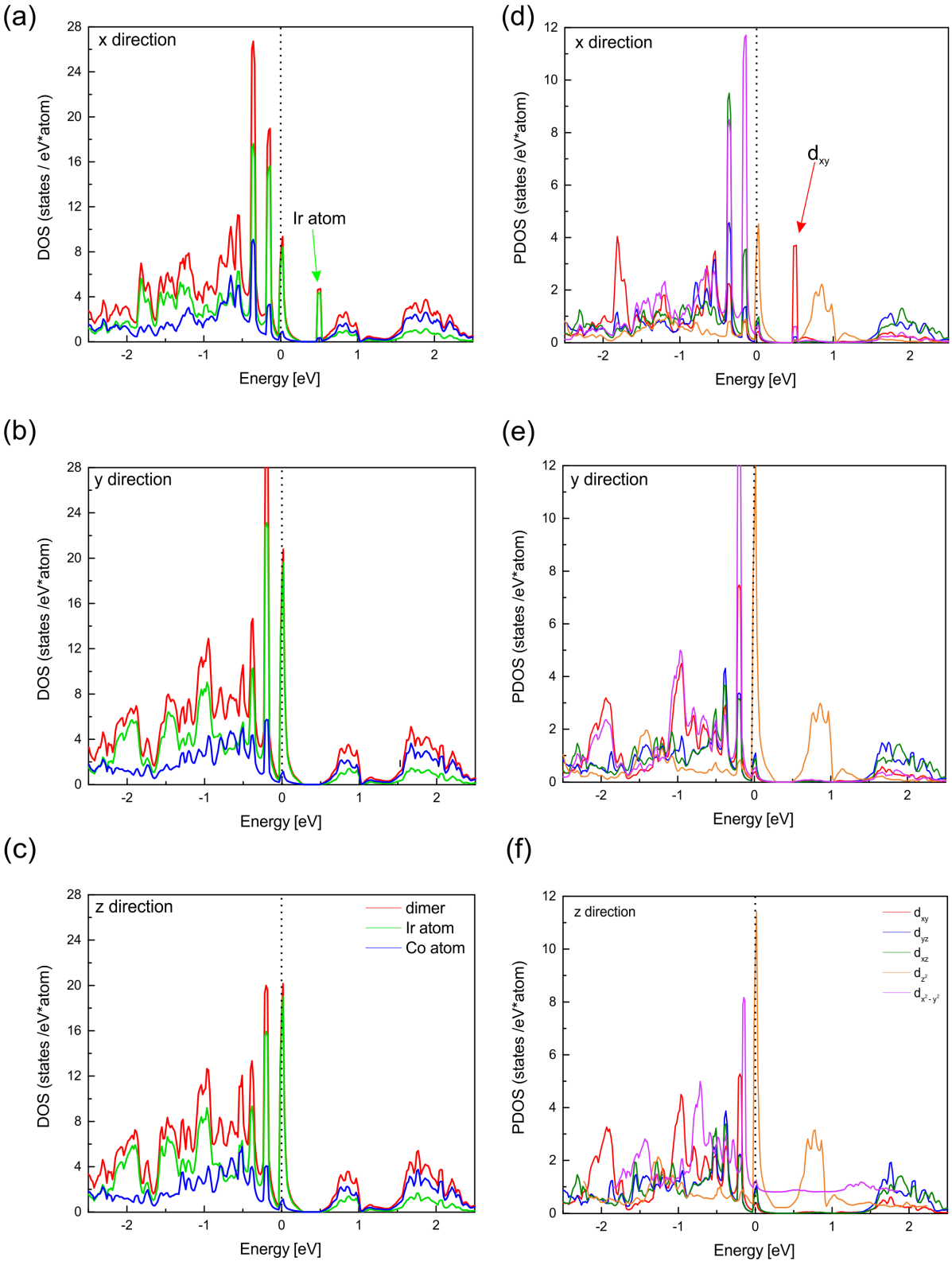

Figure S2 The Figure shows the total, side decomposed (panel (a), (b), (c)) and partial d-band (panel (d), (e), (f)) electronic DOS for CoIr dimer adsorbed on the SV-Graphene layer, calculated including SOC for different magnetization directions. For the magnetization parallel to the support and perpendicular to the dimer (along the *x* and *y* axis) the DOS are shown in the panels (a), (d), and (b),(e). For the magnetization perpendicular to the support and parallel to the dimer axis (along the *z* axis) are in the panels (c), (f). Dashed line shows the Fermi level.

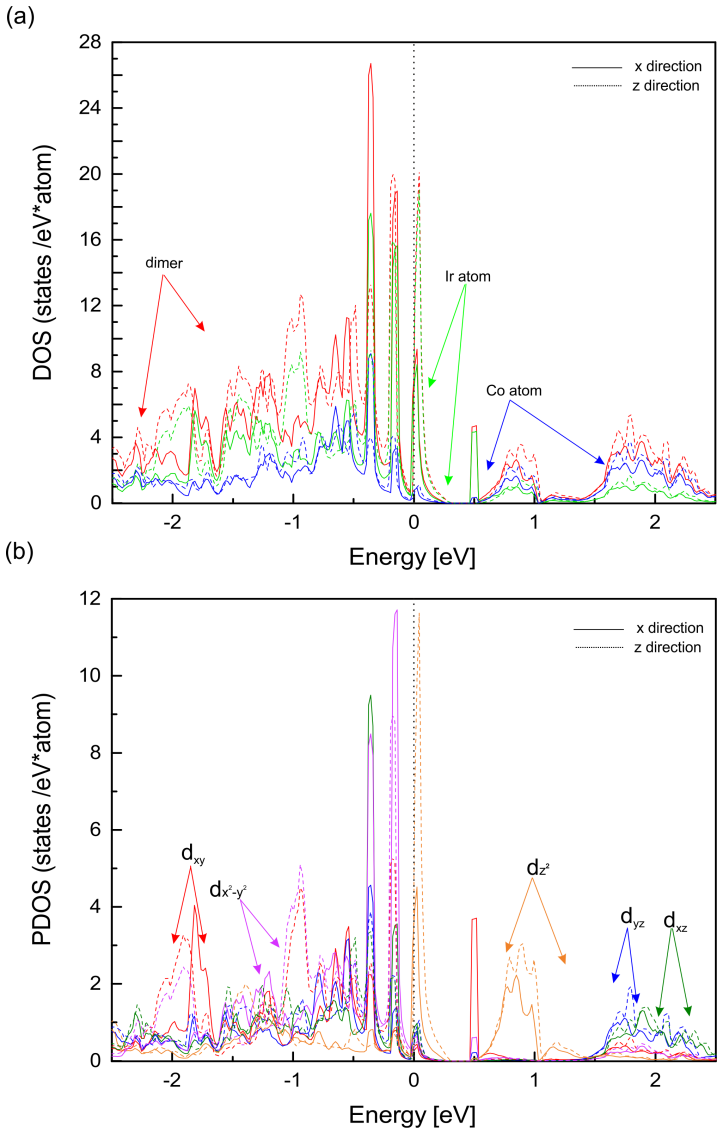

Figure S3 Comparison of the total, site decomposed (panel (a)) and partial d-band (panel (b)) electronic DOS for the CoIr dimer adsorbed on the defective graphene layer, for magnetization perpendicular to the support (*z*- direction, dash lines) and for magnetization parallel to the support (along the *x*-direction, full lines). Dashed perpendicular line shows the Fermi level.

Ir down

Structure	SR	Perpendicular SOC			In-plane SOC			Anisotropies		MAE
	m_S	m_S	m_L	m_{tot}	m_S	m_L	m_{tot}	δm_S	δm_L	
Co down	1.59	1.83	0.27	2.1	1.83	0.276	2.11	0	0	2.26

Table S2 The spin (m_S) and orbital (m_L) moments and the spin (δm_S) and orbital (δm_L) anisotropies, together with the calculated magnetic anisotropy energy of the CoIr dimer on the SVGraphene layer. All magnetic moments are given in μ_B. The magnetic anisotropy energy is given in meV.

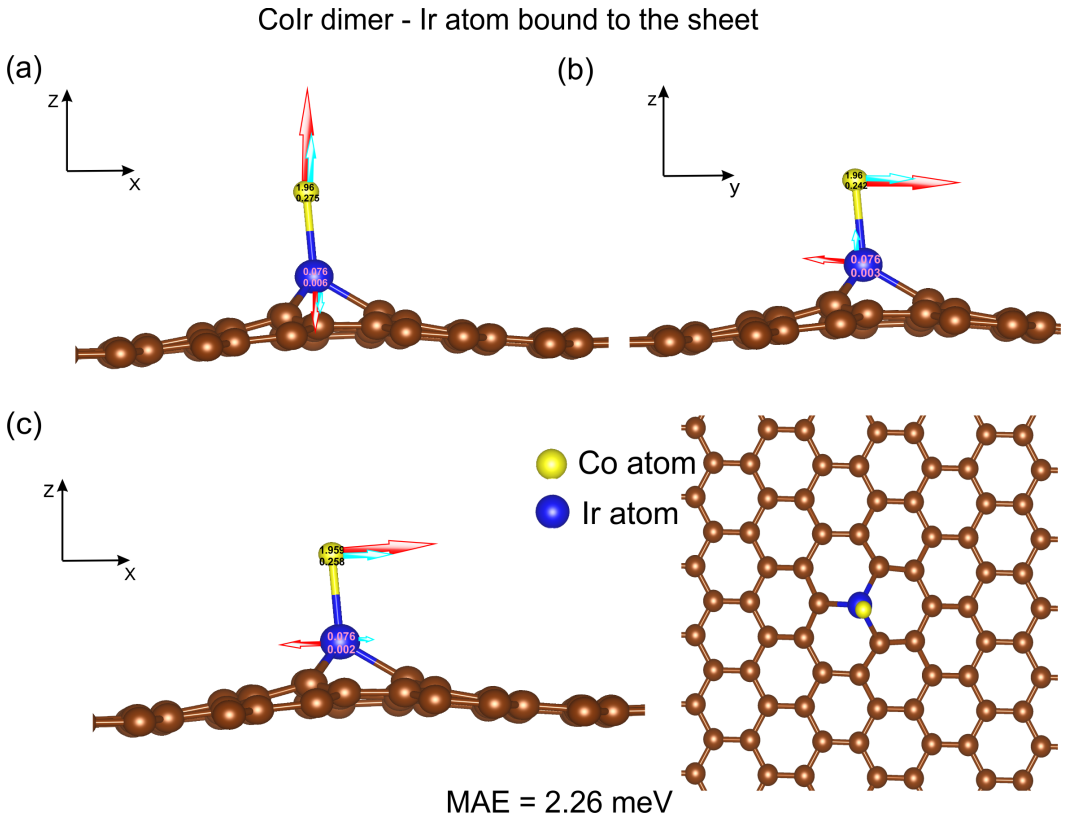

Figure S4 Magnetic structure of IrCo dimer supported on a graphene layer in the stable upright configuration. The different magnetization direction is displayed. The panels (a), (b), (c) demonstrate magnetisation along *x*, *y*, *z* directions, respectively. The magnetic anisotropy energy is listed underneath. Red (blue) arrows show the spin (orbital) magnetic moments. The numbers give the total spin (upper number), and orbital (lower number) magnetic moments in μ_B. Top view is shown in the inset in panel (c). The length of the arrows corresponding to the orbital momentum was multiplied by a factor of 10 for better visibility of vector orientation.

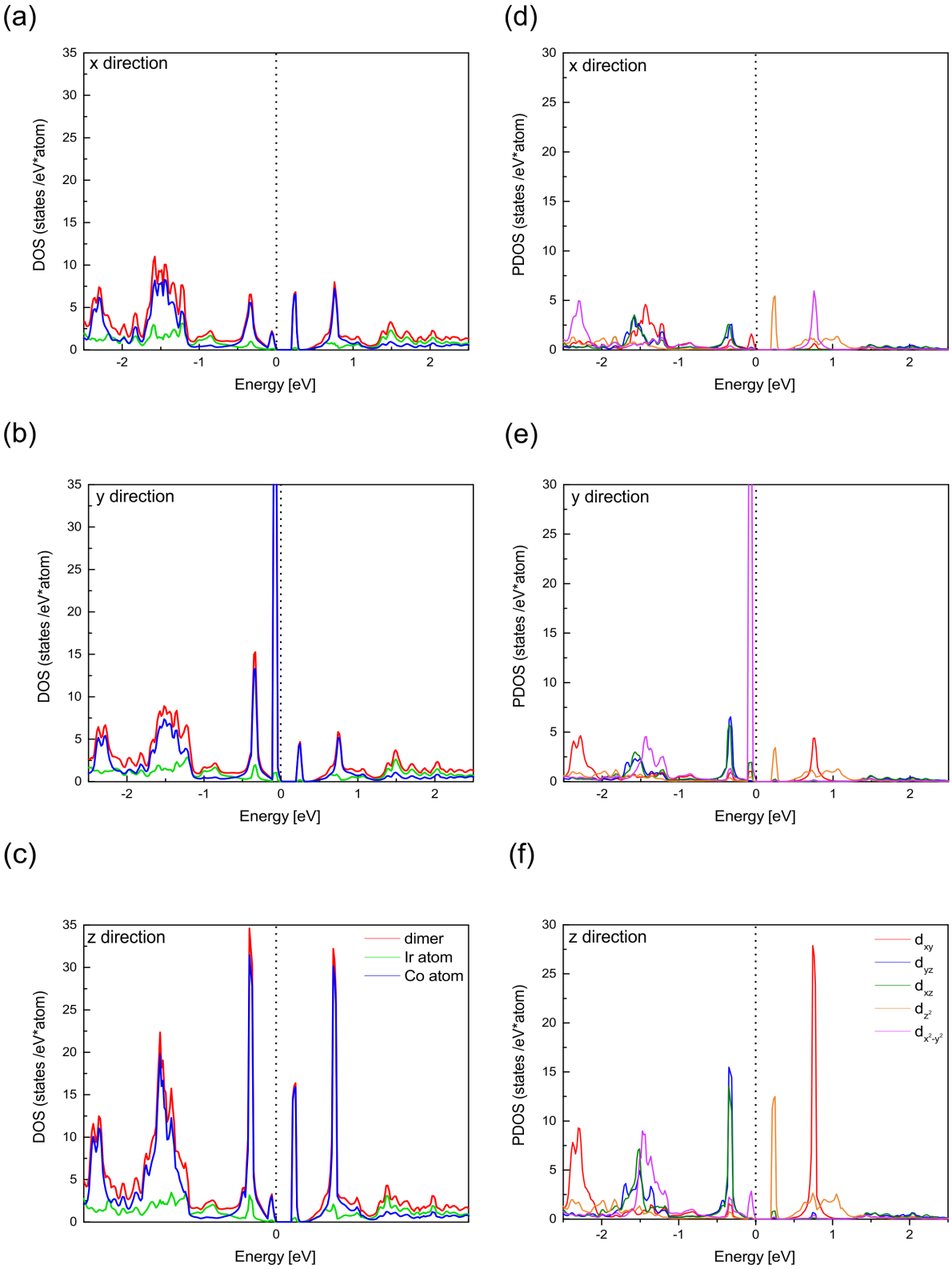

Figure S5 The Figure shows the total, side decomposed (panel (a), (b), (c)) and partial d-band (panel (d), (e), (f)) electronic DOS for IrCo dimer adsorbed on the SV-Graphene layer, calculated including SOC for different magnetization directions. For the magnetization parallel to the support and perpendicular to the dimer (along the *x* and *y* axis) the DOS are shown in the panels (a), (d), and (b),(e). For the magnetization perpendicular to the support and parallel to the dimer axis (along the *z* axis) are in the panels (c), (f). Dashed line shows the Fermi level.

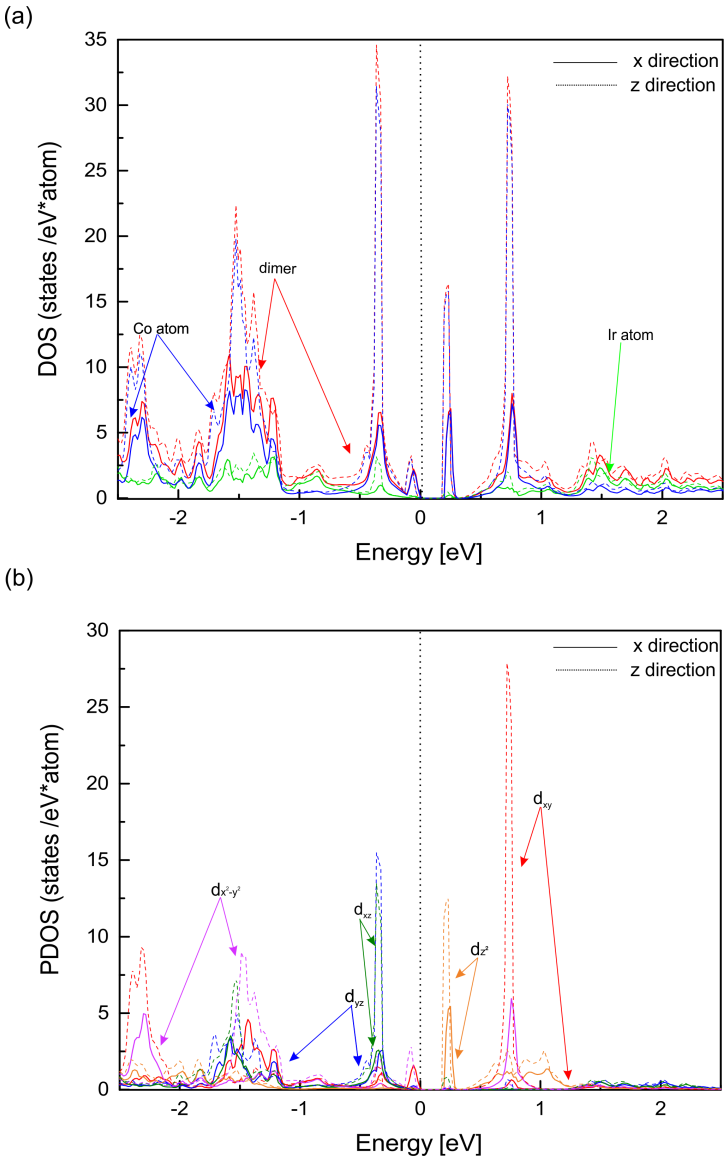

Figure S6 Comparison of the total, site decomposed (panel (a)) and partial d-band (panel (b)) electronic DOS for the IrCo dimer adsorbed on the defective graphene layer, for magnetization perpendicular to the support (*z*- direction, dash lines) and for magnetization parallel to the support (along the *x*-direction, full lines). Dashed perpendicular line shows the Fermi level.

Co down

Structure	SR	Perpendicular SOC			In-plane SOC			Anisotropies		MAE
	m_S	m_S	m_L	m_{tot}	m_S	m_L	m_{tot}	δm_S	δm_L	
Co down	1.59	1.36	0.91	2.27	0.70	0.12	0.82	0.45	0.79	11.03

Table S3 The spin (m_S) and orbital (m_L) moments and the spin (δm_S) and orbital (δm_L) anisotropies, together with the calculated magnetic anisotropy energy of the CoIr dimer on the N-SVGraphene layer. All magnetic moments are given in μ_B. The magnetic anisotropy energy is given in meV.

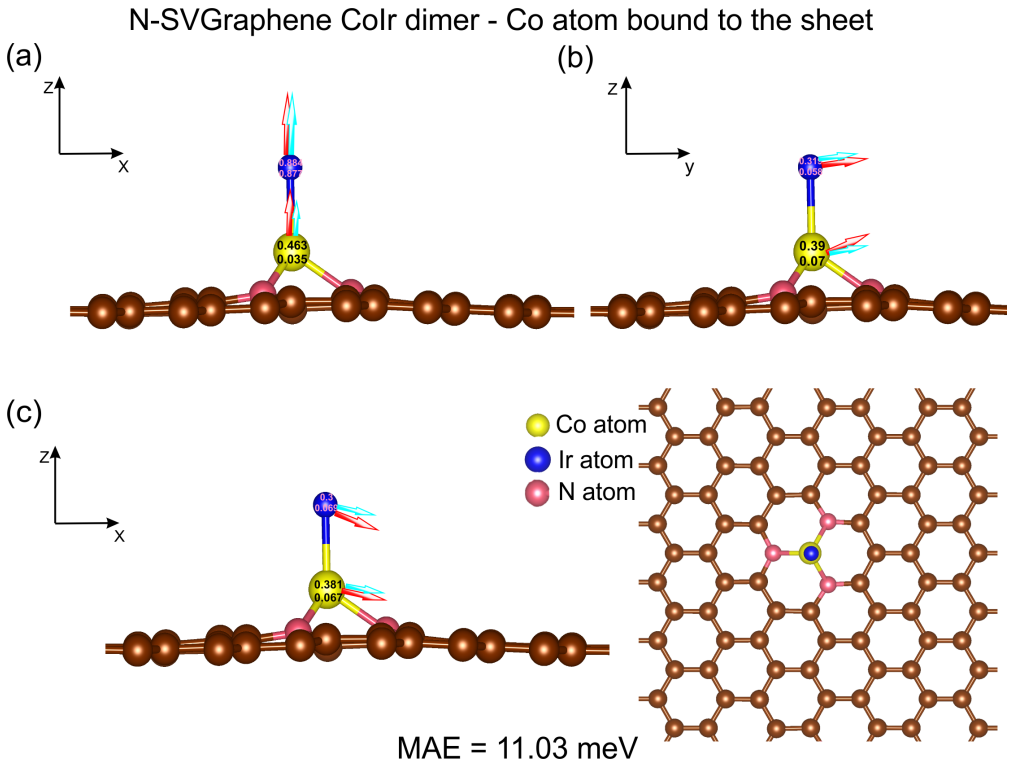

Figure S7 Magnetic structure of CoIr dimer supported on the N-SVGraphene layer in the stable upright configuration. The different magnetization direction is displayed. The panels (a), (b), (c) demonstrate magnetisation along *x*, *y*, *z* directions, respectively. The magnetic anisotropy energy is listed underneath. Red (blue) arrows show the spin (orbital) magnetic moments. The numbers give the total spin (upper number), and orbital (lower number) magnetic moments in μ_B. Top view is shown in the inset in panel (c). The length of the arrows corresponding to the orbital momentum was multiplied by a factor of 10 for better visibility of vector orientation.

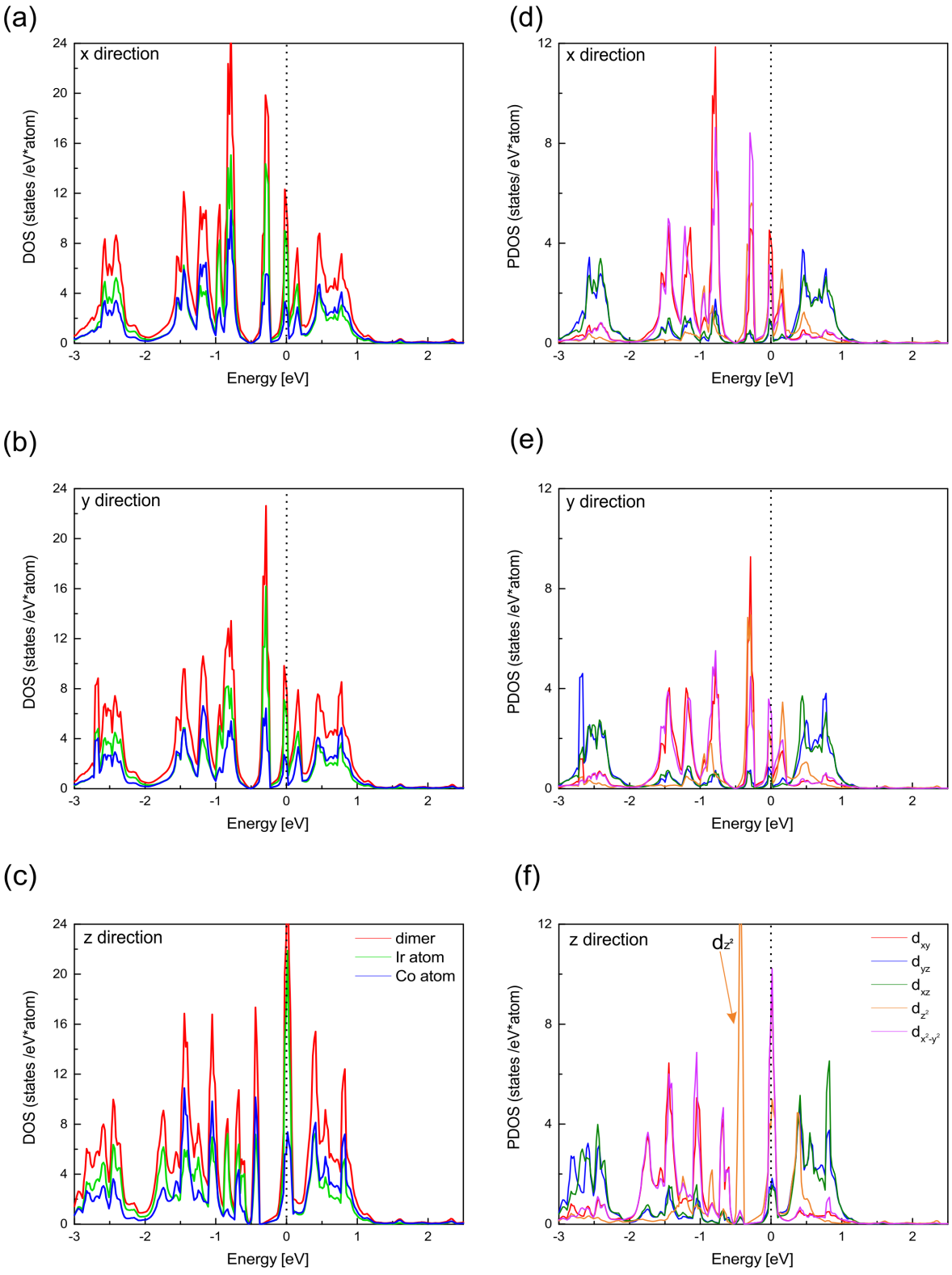

Figure S8 The Figure shows the total, side decomposed (panel (a), (b), (c)) and partial d-band (panel (d), (e), (f)) electronic DOS for CoIr dimer adsorbed on the N-SVGraphene layer, calculated including SOC for different magnetization directions. For the magnetization parallel to the support and perpendicular to the dimer (along the *x* and *y* axis) the DOS are shown in the panels (a), (d), and (b),(e). For the magnetization perpendicular to the support and parallel to the dimer axis (along the *z* axis) are in the panels (c), (f). Dashed line shows the Fermi level.

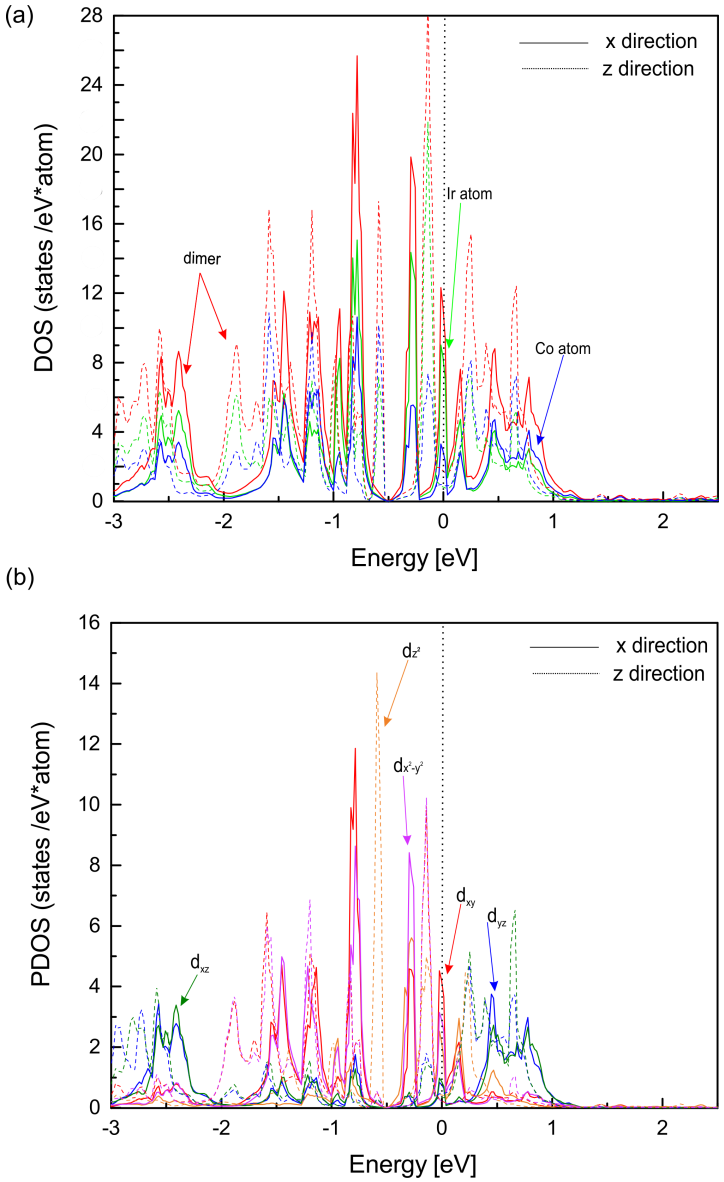

Figure S9 Comparison of the total, site decomposed (panel (a)) and partial d-band (panel (b)) electronic DOS for the CoIr dimer adsorbed on the N-SVGraphene layer, for magnetization perpendicular to the support (*z*- direction, dash lines) and for magnetization parallel to the support (along the *x*-direction, full lines). Dashed perpendicular line shows the Fermi level.

Ir down

Structure	SR	Perpendicular SOC			In-plane SOC			Anisotropies		MAE
	m_S	m_S	m_L	m_{tot}	m_S	m_L	m_{tot}	δm_S	δm_L	
Co down	1.59	1.66	1.22	2.86	1.60	0.12	1.72	0.06	1.10	33.11

Table S4 The spin (m_S) and orbital (m_L) moments and the spin (δm_S) and orbital (δm_L) anisotropies, together with the calculated magnetic anisotropy energy of the IrCo dimer on the N-SVGraphene layer. All magnetic moments are given in μ_B. The magnetic anisotropy energy is given in meV.

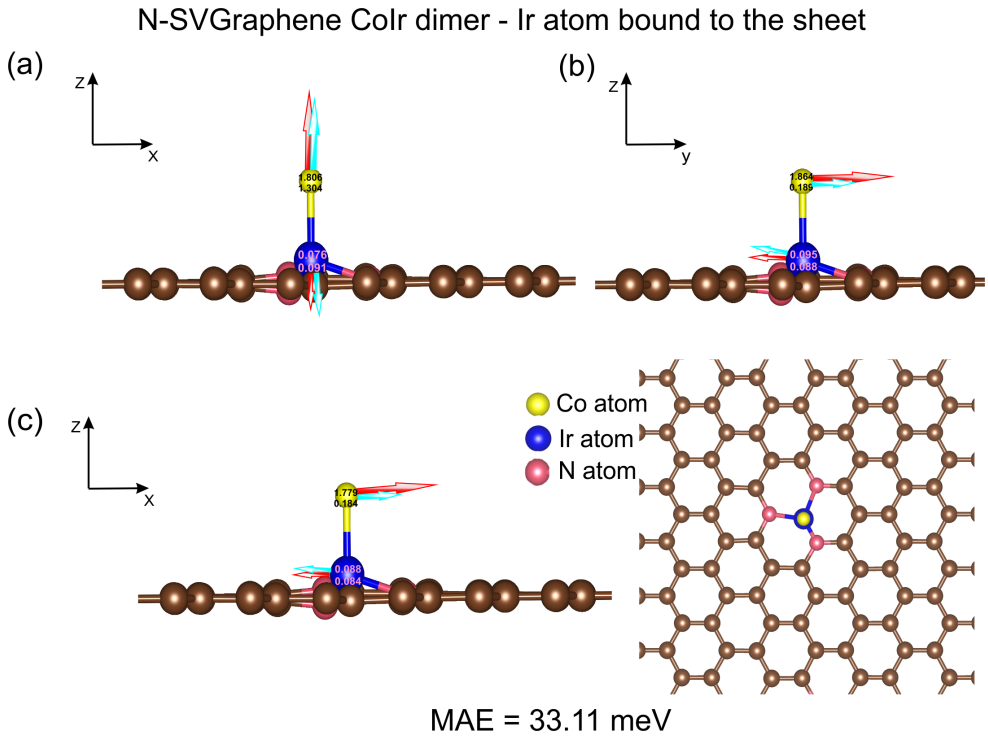

Figure S10 Magnetic structure of IrCo dimer supported on the N-SVGraphene layer in the stable upright configuration. The different magnetization direction is displayed. The panels (a), (b), (c) demonstrate magnetisation along *x*, *y*, *z* directions, respectively. The magnetic anisotropy energy is listed underneath. Red (blue) arrows show the spin (orbital) magnetic moments. The numbers give the total spin (upper number), and orbital (lower number) magnetic moments in μ_B. Top view is shown in the inset in panel (c). The length of the arrows corresponding to the orbital momentum was multiplied by a factor of 10 for better visibility of vector orientation.

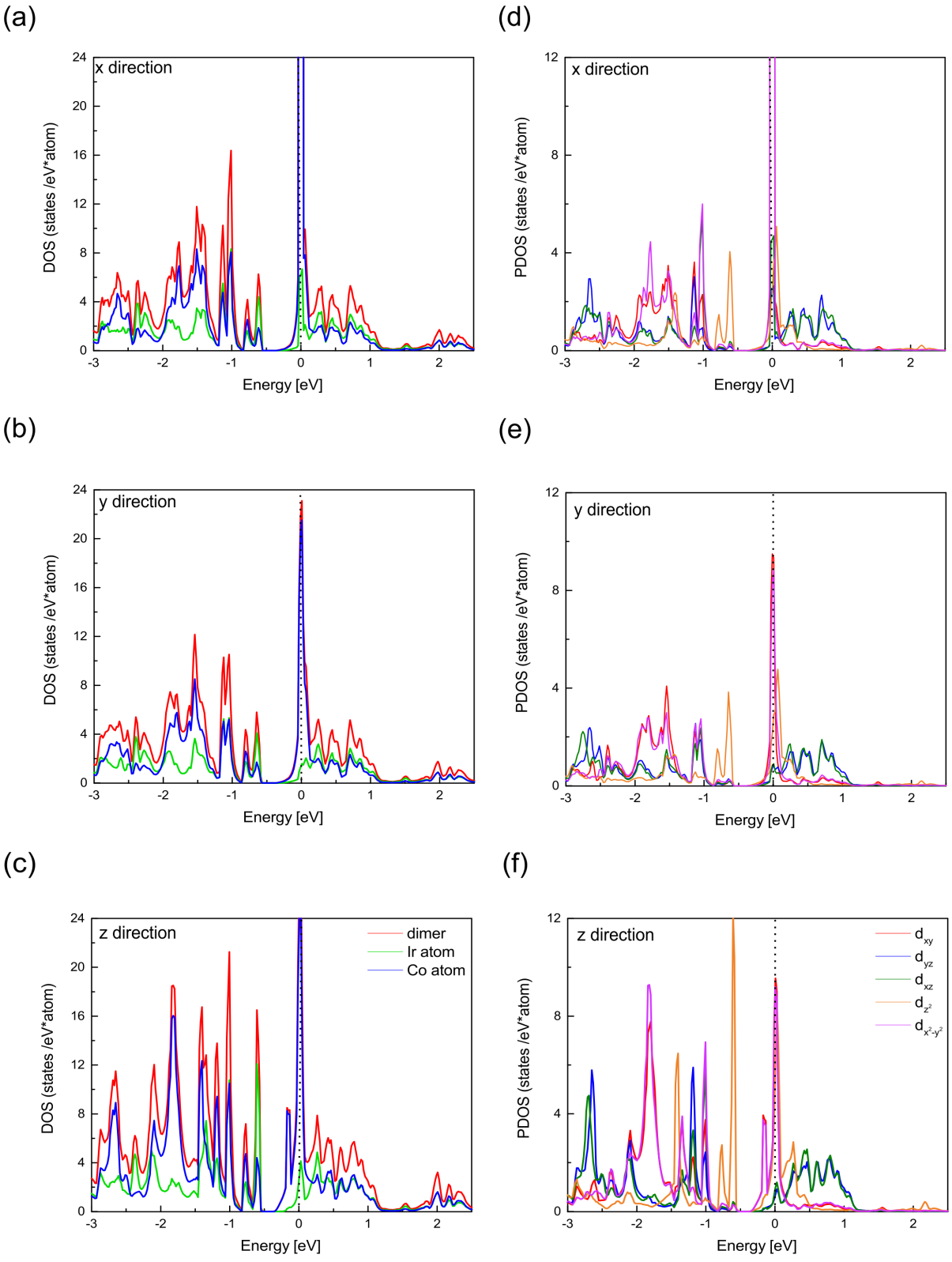

Figure S11 The Figure shows the total, side decomposed (panel (a), (b), (c)) and partial d-band (panel (d), (e), (f)) electronic DOS for IrCo dimer adsorbed on the N-SVGraphene layer, calculated including SOC for different magnetization directions. For the magnetization parallel to the support and perpendicular to the dimer (along the *x* and *y* axis) the DOS are shown in the panels (a), (d), and (b),(e). For the magnetization perpendicular to the support and parallel to the dimer axis (along the *z* axis) are in the panels (c), (f). Dashed line shows the Fermi level.

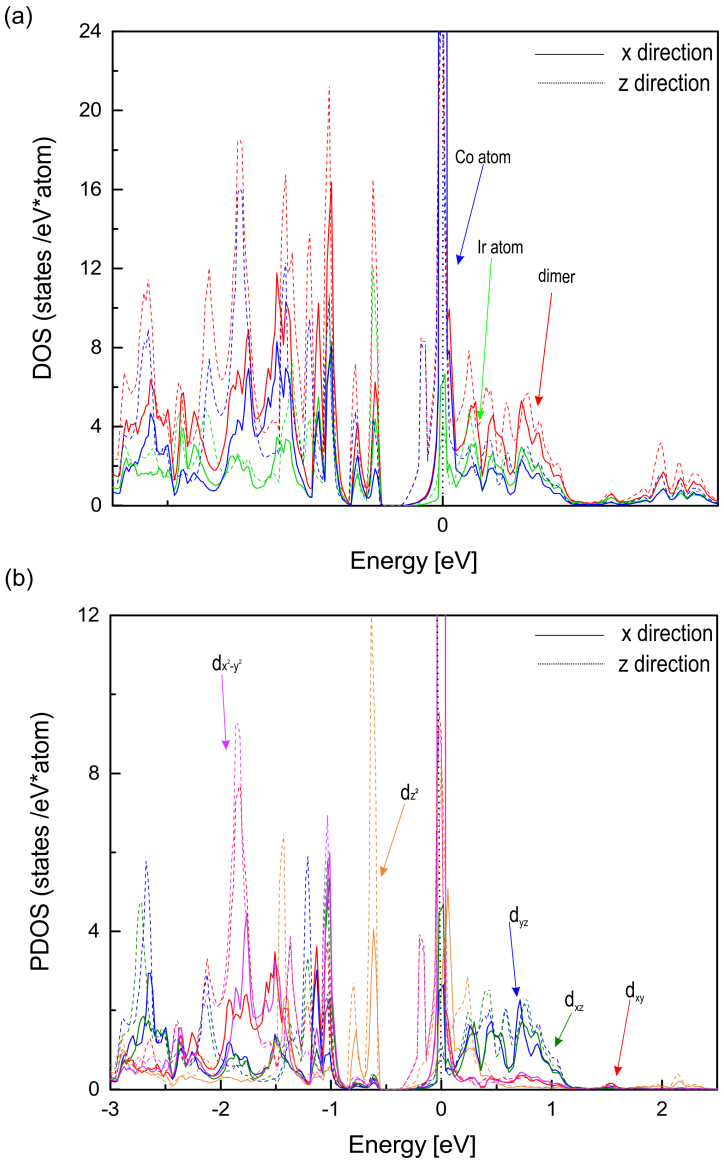

Figure S12 Comparison of the total, site decomposed (panel (a)) and partial d-band (panel (b)) electronic DOS for the IrCo dimer adsorbed on the N-SVGraphene layer, for magnetization perpendicular to the support (*z*- direction, dash lines) and for magnetization parallel to the support (along the *x*-direction, full lines). Dashed perpendicular line shows the Fermi level.